The Interaction of Kv1.3 with Dlg-like MAGUKs and its Impact on Calcium Signaling in Activated T Cells

zur Erlangung des akademischen Grades

Doctor rerum naturalium
(Dr. rer. nat.)

genehmigt durch die Fakultät für Naturwissenschaften
der Otto-von-Guericke-Universität Magdeburg

von   **Diplom-Biologin Juliane Handschuh**

geboren am   25. Oktober 1984 in Merseburg

Gutachter: Prof. Dr. rer. nat. Eckart D. Gundelfinger
                  Prof. Dr. rer. nat. Jürgen Wienands

eingereicht am: 21. Juni 2016
verteidigt am: 1. Februar 2017

" Nobody said it was easy,
oh it's such a shame for us to part

Nobody said it was easy,
no one ever said it would be this hard "

The Scientist
Coldplay, 2002

Contents

List of Tables

List of Figures

Abbreviations

% w/v	–	percent by mass
aa	–	amino acid
APC	–	Antigen-presenting cell
a.u.	–	arbitrary unit
BDP	–	Baseline-peak-difference
BiFC	–	Bimolecular fluorescent complementation
BSA	–	Bovine serum albumin
Ca^{2+}	–	Calcium ions
$[Ca^{2+}]_i$	–	Intracellular calcium concentration
cDNA	–	complementary DNA
CM	–	Conjugation medium
COS-7	–	African green monkey cell line
CRAC channels	–	Calcium-release activated calcium channels
C-terminal	–	Carboxy-terminal
D	–	Diffusion coefficient
DAG	–	Diacylglycerol
Dlg	–	Discs large
*d*Dlg	–	*Drosophila* Dlg
DMEM	–	Dulbecco's modified eagle medium
DNA	–	Deoxyribonucleid acid
E.coli	–	*Escherichia coli*
EDTA	–	Ethylenediaminetetraacetic acid
EGFP	–	Enhanced green fluorescent protein
EGTA	–	Ethylene glycol-bis(β-aminoethyl ether)-tetraacetic acid
FBS	–	Fetal bovine serum
FCS	–	Fetal calf serum
Fig.	–	Figure
FP	–	Fluorescent protein
FRET	–	Förster resonance energy transfer
GUK domain	–	guanylate kinase domain
h	–	Human
HBSS	–	Hank's balanced salt solution

HEK	–	Human embryonic kidney cell line
IgG	–	Immunoglobulin G
I_{max}	–	Maximum current
IP_3	–	Inositol-1,4,5-trisphosphate
IPTG	–	Isopropyl–β–D–thiogalactopyranoside
IRES	–	Internal ribosomal entry site
ITAM	–	Immunoreceptor tyrosine-based activation motifs
Itk	–	Interleukin-2-inducible T cell kinase
IS	–	Immune synapse
K^+	–	Potassium ions
KCa	–	Calcium-activated potassium channel
Kv	–	Voltage-gated potassium channel
kD	–	kilo Dalton
LAT^+	–	Linker for activation of T cells
LB	–	Lysogeny broth
Lck^+	–	$p56^{Lck}$ tyrosine kinase of the Src family
MAGUK	–	Membrane associated guanylate kinase
MCS	–	Multiple cloning site
MHC	–	Major histocompatibility complex
MAPK	–	Mitogen-activated protein kinase
mRFP	–	Monomeric red fluorescent protein
ms	–	Mouse
MS	–	Multiple sklerosis
MSD	–	Mean square displacement
NFAT	–	Nuclear factor of activated T cells
NF-κB	–	Nuclear factor 'kappa-light-chain-enhancer' of activated B-cells
NP-40	–	Nonyl phenoxypolyethoxylethanol 40
NMJ	–	Neuromuscular junction
N-terminal	–	Amino-terminal
PBS	–	Phosphate buffered saline
PFA	–	Paraformaldehyde
PVDF	–	Polyvinyliden fluoride
PLCγ	–	Phospholipase C γ
PI-3K	–	Phosphoinositide 3-kinase
PKC θ	–	Proteinkinase C θ

mhcP θ	–	Myosin heavy chain promoter
PEG	–	Polyethylene glycol
PMCA	–	Plasma membrane Ca^{2+} ATPase
PKAI	–	Protein kinase A I
PuroR	–	Puromycin resistance gene
PSD-95	–	Postsynaptic density-95
PDZ domain	–	PSD-95/Dlg/ZO-1 domain
QD®	–	Quantum Dot®
r	–	Rat
rb	–	Rabbit
RPMI	–	Roswell park memorial institute medium
RSL	–	Relative synapse localization
S.cerevisiae	–	*Saccharomyces cerevisiae*
SD	–	Synthetic defined
SDS	–	Sodium dodecyl sulfate
SDS-PAGE	–	Sodium dodecyl sulfate polyacrylamide gel electrophoresis
SEE	–	*Staphylococcus aureus* Enterotoxin E
SH3 domain	–	Src-homology-3
shRNA	–	Short hairpin RNA
siRNA	–	Short interfering RNA
SLE	–	Systemic lupus erythrematosis
SLP-76	–	SH2 domain-containing leukocyte protein of 76 kD
SMAC	–	Supramolecular activation cluster
SOC	–	Super optimal broth
SOCE	–	Store-operated calcium entry
SSR	–	Subsynaptic reticulum
STIM	–	Endoplasmic stromal interaction molecule
TAE	–	Tris-acetate-EDTA
TCA	–	T cell activation
T_{CM}	–	Central memory T cells
TCR	–	T cell receptor
TE	–	Tris-HCl-EDTA
T_{EM}	–	Effector memory T cells
TG	–	Tris-Glycine
TM	–	Transmembrane domains

Treg	–	Regulatory T cells
Tris	–	Tris(hydroxymethyl)-aminomethane
Tris-HCl	–	Tris(hydroxymethyl)-aminomethanhydrochloride
UAS	–	Upstream activated sequence
V_C	–	C-terminal part of Venus (Split-Venus)
V_F	–	Fragment of Venus (Split-Venus)
V_N	–	N-terminal part of Venus (Split-Venus)
WASP	–	Wiskott-Aldrich syndrome protein
Y2H	–	Yeast-two-hybrid
YFP	–	Yellow fluorescent protein
YPDA	–	Yeast peptone dextrose adenine
ZAP-70	–	ζ-chain-associated protein kinase 70
Δ	–	Deletion

Abstract

Alerting lymphocytes about the presence of pathogens is a key event of the adaptive immune response. Communication between cells is achieved by formation of an adhesive junction – called immunological synapse (IS) – between an antigen-presenting cell (APC) and lymphocytes. The IS is a highly dynamic but organized structure allowing for proper development of signaling events eventually leading to a cellular response of the receiving cell: migration, proliferation or secretion of cytokines or lytic granules. Cellular responses are regulated by relaying information via several intracellular signaling pathways that lead to activation of specific transcription factors like NFAT or NFκB. Signaling pathways include several protein kinase cascades that require calcium. Calcium signaling itself is tightly orchestrated by a number of players, amongst them potassium channels that provide the driving force for calcium ions to enter the cell. The voltage-gated potassium channel Kv1.3 controls baseline and activation-induced calcium levels in memory T cells, where it accumulates within the IS. Malfunctions in Kv1.3 accumulation are held accountable for generation of autoimmune diseases, like systemic lupus erythemathosus (SLE). Voltage-gated potassium channels are known to interact with PDZ domains of proteins of the Dlg-like MAGUK (membrane associated guanylate kinase) family, which may localize and cluster their binding partners to specific compartments of the cell. Moreover, Dlg1 has recently been linked to a role in development and signaling specifically of effector memory T cells.

In light of uncertainties relating to the mode of Kv1.3 movement and enrichment at the IS, I studied its presumed interaction with Dlg1, focussing on its importance at the IS for calcium signaling. In yeast-two-hybrid experiments, I validated and mapped the interaction of Kv1.3's C-terminal tail to the first two PDZ domains of Dlg1. Recruitment and localization studies in several cell types speak for a bilateral subcellular recruitment of both proteins. Notably, Kv1.3's binding to PDZ-containing proteins was responsible for its enrichment at synaptic sites, including the IS. The Dlg-like MAGUKs Dlg1 and PSD95 exerted a negative impact on lateral mobility of Kv1.3 in Quantum Dot® experiments, which was abrogated when Kv1.3's C-terminus was mutated. Most importantly, Fura-2 calcium imaging studies in Jurkat T cells demonstrated that Kv1.3's presence at the IS regulate the amplitude of calcium peaks. Higher abundance of Kv1.3 mediated calcium baseline levels and kinetics of activity induced calcium peaks.

In summary, I demonstrated that Kv1.3's interaction with Dlg-like MAGUKs is responsible for its enrichment at the IS and that this localization plays a major role in modifying the amplitude of calcium responses. Furthermore, I could show that a higher number of Kv1.3 molecules in T cells correlates with distinct calcium signaling, which may explain its role for effective signaling in memory T cells.

Zusammenfassung

Ein zentraler Bestandteil der adaptiven Immunantwort ist es, Lymphozyten auf die Anwesenheit von pathogenen Keimen aufmerksam zu machen. Dabei wird die Kommunikation zwischen den beteiligten Zellen durch die Herstellung eines Kontakts zwischen Antigen-präsentierenden Zellen und Lymphozyten, der sogenannten Immunsynapse (IS), gewährleistet. Die Struktur der IS ist zum einen hoch organisiert, erlaubt aber, durch dynamische Veränderungen die Signalübertragung zwischen Zellen zu regulieren und angemessene zelluläre Antworten einzuleiten. Diese Antworten variieren zwischen Migration, Proliferation oder Sekretion von Zytokinen oder lytischen Vesikeln.

Die Regulation verschiedener zellulärer Antworten wird mittels spezifischer intrazellulärer Signalkaskaden gesteuert, an deren Ende die entsprechende Aktivierung verschiedender Transkriptionsfaktoren wie NFAT oder NFκB steht. Diese Signalkaskaden sind gekennzeichnet durch sequentielle Aktivierung von Proteinkinasen oder Phosphatasen, die mitunter auch den second messenger Calcium benötigen. Calciumsignale selbst werden engmaschig durch verschiedene Akteure, wie z.B. Kaliumkanäle, moduliert. Deren Öffnung zieht einen Ausstrom von Kalium nach sich, welcher eine Triebkraft für den Einstrom von Calciumionen generiert. Der spannungsgesteuerte Kaliumkanal Kv1.3 reguliert das Basislevel und aktivierungsinduzierte Änderungen intrazellulären Calciums in Gedächtnis-T Zellen. Kv1.3 reichert sich nachgewiesenermaßen in der IS von T Zellen an und ist an den erläuterten regulativen Prozessen beteiligt. Unzulängliche IS-Akkumulierung des Kanals wird unter anderem in T Zellen von Patienten mit Autoimmunerkrankungen, wie z.B. Lupus erythematodes, beobachtet. Es wurde gezeigt, dass spannungsabhängige Kaliumkanäle mit PDZ–Domänen der Proteine aus der Familie der Dlg-ähnlichen MAGUKs interagieren. Mitglieder dieser Proteinfamilie werden in Bezug auf ihre Rolle bei der Entwicklung und Signalübertragung in Gedächtnis-T Zellen und regulatorischen T Zellen diskutiert. Weiterhin spielen Dlg-ähnliche MAGUKs eine entscheidende Rolle dabei, die von ihnen gebundenen Kanäle in spezifischen Zellkompartimenten anzureichern.

Derzeit ist nicht hinreichend bekannt, wie sich Kv1.3 tatsächlich in die Immunsynapse bewegt und seine dortige Anreicherung reguliert wird. Daher habe ich mich in meiner Arbeit mit der Interaktion von Kv1.3 und Dlg1 beschäftigt. Besonderen Fokus habe ich auf die Bedeutung der Interaktion für die laterale Mobilität des Kanals, dessen subzelluläre und immunsynaptische Lokalisierung und das an der IS initiierte Calciumsignal gelegt. In Hefe-2-Hybrid Experimenten konnte ich die Interaktion von Kv1.3 mit Dlg1 validieren und den Bereich Ihrer Interaktion auf den C-terminus des Kanals mit den ersten zwei PDZ Domänen von Dlg1 eingrenzen. Weiterhin deuteten Rekrutierungs- und Lokalisationsexperimente in verschiedenen Zelltypen aus

6

verschiedenen Spezies auf eine bilaterale Anbhängigkeit der subzellulären Verteilung beider Proteine hin. Insbesondere war die Bindung von Kv1.3 an PDZ-Proteine verantwortlich für dessen Anreicherung an synaptischen Kontakten wie der IS. Weiterhin konnte ich in Quantum Dot$^{®}$– Experimenten zeigen, dass die Dlg-ähnlichen MAGUKs Dlg1 und PSD95 die laterale Mobilität von Kv1.3 einschränken. Dieser Effekt konnte durch Mutation des C-terminalen Bereichs des Kanals aufgehoben werden. Eine zentrale Beobachtung war ein Einfluss der IS-Lokalisation des Kanals auf die Amplitude der Calciumantwort nach Stimulation von Jurkat T Zellen. Weiterhin hatte die generelle Anwesenheit von Kv1.3 in T Zellen Effekte sowohl auf das Basislevel als auch die Kinetik des Calciumsignals, welches nach Aktivierung der T Zellen entsteht.

Zusammengefasst konnte ich zeigen, dass die Interaktion von Kv1.3 mit Dlg-ähnlichen MAGUKs verantwortlich für dessen Anreicherung an der IS ist. Weiterhin konnte gezeigt werden, dass die von Dlg-ähnlichen MAGUKs abhängige Anreicherung von Kv1.3 eine wichtige Rolle bei der Modifizierung der Amplitude von Calciumantworten spielt.

1 Introduction

1.1 The Immunological Synapse

The immune system comprises several organs and biological processes that protect the human body against pathogens like bacteria, viruses or parasites. It is classified into two principal subsystems jointly operating, the innate and the adaptive immune system. The innate immune system acts rather unspecific but immediate, recognizing and responding to pathogens in a generic way. On the other hand, the adaptive immune system is highly specialized, containing specific cells and processes that are able to generate long-lasting immunity against once encountered pathogens. Besides protecting the body against outside threats, the immune system manages to discriminate foreign agents from the organism's own healthy tissue. Failures in discrimination lead to manifestation of autoimmune diseases like multiple sklerosis (MS) or systemic lupus erythematosus (SLE).

The adaptive immune system is initiated by responses of the innate immune system, e.g. antigen presentation by specific cells of the latter. Recognition of antigens by lymphocytes that express receptors or membrane-associated antibodies against a specific antigen causes secretion of antibodies against that antigen by B lymphocytes (B cells) or activation of T lymphocytes (T cells). Binding of antibody exerts two functions: inactivation of viruses and microbial toxins by blocking their ability to bind to receptors on host cells and marking of pathogens for destruction by phagocytic cells of the innate immune system [Delves et al., 2011]. Activation of T cells is initiated by antigen recognition by the T cell receptor (TCR) complex along with initiation of co-stimulatory factors [Wülfing and Davis, 1998]. Activated TCRs entail the transient formation of a highly dynamic immunological synapse (IS) [Norcross, 1984].

The IS, similar to the well-studied neuronal synapse, constitutes a site of active information propagation between cells. It is characterized by receptor-based recognition of an extracellular ligand followed by intracellular signaling, which leads to a change in the activation state of the T cell. The extracellular ligand, i.e. the antigen, is presented to the T cell by an antigen presenting cell (APC) with the use of major histocompatibility gene complex (MHC class I or II), thus ensuring recognition of only foreign antigens. Self tolerance is aquired in the thymus by a process called negative selection. During negative selection, cells that bind to MHC complexes coupled with self-peptides with high affinity undergo apoptosis or are otherwise suppressed. Those that do not bind too avidly to any such MHC complex complete development and become T helper cells (CD4$^+$) or mature cytotoxic T cells (CD8$^+$) [Berg et al., 2002]. CD4$^+$ T cells, activated when presented with antigen by MHC class II molecules, assist other cells of the immune system

in their function. For example, they may induce maturation of B cells into antibody-producing plasma cells and memory B cells or help activate CD8+ T cells by secretion of cytokines. CD8+ T cells, activated when presented with antigen by MHC class I molecules, destroy virus-infected and tumor cells via secretion of lytic granules. Both types of T cells may transform into memory cells that sustain after an infection has resolved, providing the immune system with memories of past infections. Upon re-exposure to their cognate antigen, they quickly expand into large numbers of effector T cells. Yet another population, the regulatory T cells (Tregs), represses the action of other T cells (CD4+ as well as CD8+) in order to end an ongoing immune reaction as well as to suppress autoreactive T cells [Delves et al., 2011].

Following recognition of antigen, the IS forms via recruitment of numerous signaling and scaffolding molecules to the contact site [Weikl and Lipowsky, 2004, Singleton et al., 2009]. This highly organized but dynamic structure ensures ordered and efficient propagation of information to the nucleus, launching several cell-type-specific programs, like migration, proliferation or secretion of cytokines.

The mature IS features a bull's eye arrangement of supramolecular activation clusters (SMACs) that form within a few minutes after antigen-recognition (Fig. 1). Observing the IS with fluorescent microscopy, SMACs occur as increased densities of specific molecules [Grakoui et al., 1999, Monks et al., 1998]. The central part of the SMAC (cSMAC) is enriched for the TCR complex and MHC molecules along with signaling molecules, surrounded by a peripheral ring – the pSMAC – which harbors cell adhesion molecules and their cytoskeletal anchors. A more distal ring, containing the phosphatase CD45 and dense actin cytoskeleton, has later been defined as dSMAC [Freiberg et al., 2002].

It has been a matter of debate whether the formation of signaling clusters is mediated by their incorporation into lipid rafts or co-clustering by protein-protein interactions.

Figure 1: Depiction of the bull's eye arrangement of the IS with prominent transmembrane proteins in black and associated cytoplasmic proteins in grey. Modified from [Roufaiel et al., 2015].

Lipid rafts are ordered membrane domains, characterized by a specific lipid composition of the plasma membrane, e.g. high concentrations of cholesterol and gangliosides, leaving molecules that are located to these structures detergent-insoluble. Lipid rafts have been correlated with the presence of signaling molecules, like Src family and receptor tyrosine kinases or the co-stimulatory molecule CD154 [Cinek and Hořejší, 1992, Bohuslav et al., 1993, Benslimane et al., 2012]. Importantly, effective TCR signal transduction depends on raft integrity of the receptor and other proteins important for structural preservation of signaling complexes [Xavier et al.,

1998, Round et al., 2005]. Nevertheless, it has been proposed that co-clustering within the IS also requires protein-protein interactions that is not entirely maintained by inclusion into lipid rafts. Protein-protein interactions trap molecules at the IS and create microdomains that concentrate or exclude cell surface proteins to facilitate T cell signaling [Douglass and Vale, 2005]. Most likely, both processes cooperate in the formation of a functional IS.

1.2   Signaling at the IS

A variety of TCR-induced processes act synergistically to transmit information to the nucleus (Fig. 2). These processes initially require the reorganization of the actin-cytoskeleton, a stepwise assembly of signaling molecules as well as initiation of calcium signaling.

The primary event following TCR-MHC/peptide interaction constitutes the Lck-mediated phosphorylation of tyrosine residues within the immunoreceptor tyrosine-based activation motifs (ITAMs) of CD3- and ζ-chains of the TCR complex [Kane et al., 2000]. Subsequently, ζ-chain-associated protein kinase 70 (ZAP-70) – a critical docking molecule for a number of TCR effectors – translocates to the contact site [Kane et al., 2000, Wang et al., 2010]. Translocation of ZAP-70 has been proposed to rely on recruitment via the Lck-associated scaffolding protein Dlg1 that forms a Lck–Dlg1–Zap-70–Wiskott-Aldrich syndrome protein (WASP) complex [Hanada et al., 1997, Round et al., 2005]. This complex locally couples signal transduction and actin-reorganization [Dupré et al., 2002, Badour et al., 2004].
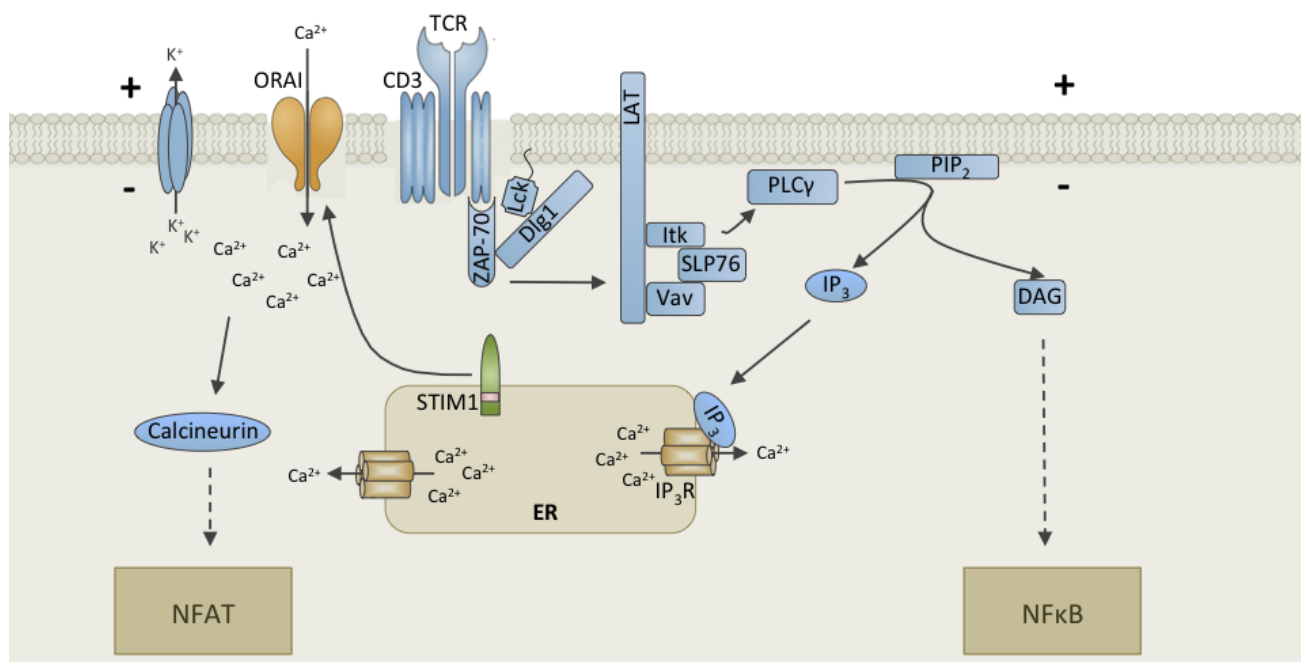
Figure 2: **TCR-Proximal Signaling of the IS.** For explanation, refer to text. Modified from [Feske, 2007]

Once ZAP-70 is activated, it phosphorylates a series of adaptor proteins, including Linker for activation of T cells (LAT), which in turn recruits Vav, SH2 domain-containing leukocyte protein of 76 kD (SLP-76), phosphoinositide 3-kinase (PI-3K), interleukin-2-inducible T cell kinase (Itk), phospholipase C γ (PLC-γ) and Ras to the activated TCR complex [Zhang et al., 1998, Zhang et al., 1999]. At this stage in T cell activation, pathways for signaling (via G-protein activated PLC-γ and Ras) and cytoskeletal reorganization (via Vav and SLP-76 [Fischer et al., 1998]) emerge.

PLC-γ, generating inositol-1,4,5-trisphosphate (IP$_3$) and diacylglycerol (DAG) by hydrolysing phosphatidylinositol-4,5-bisphosphate, further guides signaling towards two directions. DAG activates proteinkinase C θ (PKCθ) and the Ras/Raf-1/MEK/ERK pathway that leads to the canonical activation of p38 mitogen-activated protein kinase (MAPK), promoting nuclear translocation of activated nuclear factor 'kappa-light-chain-enhancer' of activated B-cells (NF-κB). IP$_3$ triggers calcium (Ca^{2+}) signaling within the T cell [Berridge, 1993], which in turn may both induce and repress gene transcription via nuclear factor of activated T cells (NFAT) or NF-κB [Feske et al., 2001, Feske, 2007].

In general, integration of the aforementioned pathways leads to the functional outcome of T cell activation, which may manifest in various responses, depending on T cell subset and the nature and strength of the stimulus.

1.3 Calcium Signaling Mechanisms of the T Cell

1.3.1 Translation of Calcium Signals into Cellular Responses

Elevated intracellular levels in Ca^{2+} ([Ca^{2+}]$_i$) entail both, short term and long term consequences. Short term consequences involve the support of the formation of the IS by reducing cell mobility and sustaining the interaction between the T cell and APC [Negulescu et al., 1996, Bhakta et al., 2005]. Long term consequences, identified by transcriptional responses, entail a variety of responses within cells, including secretion of lytic granules or cytokines, motility, growth and differentiation [Feske et al., 2001, Cristillo and Bierer, 2002, Diehn et al., 2002, Macián et al., 2002].

One of the main challenges in optimizing the information capacity of a calcium signal is to ensure signal specificity by regulating its amplitude and kinetics. For example, NFAT translocation to the nucleus requires prolonged elevation of calcium levels, whereas transient increase is sufficient for NF-κB activation [Dolmetsch et al., 1997, Conley et al., 2016]. Therefore, calcium signals can occur in several patterns: single transients, oscillations or sustained plateaus [Berridge, 1993, Clapham, 1995]. Different calcium signals are decoded by generic calcium sen-

sors, consecutively activating calcium transducers, e.g. calcineurin, a phosphatase that actively dephosphorylates NFAT, prompting its accumulation within the nucleus [Feske, 2007, Conley et al., 2016]. Given the diversity of T cell subsets along with varying modes of activation, many details relating to the translation of [Ca^{2+}] signals into gene expression or suppression remains to be disclosed.

1.3.2 Generation, Regulation and Maintenance of Calcium Signals

IP$_3$ binds to receptors that reside within the membrane of the endoplasmic reticulum (ER), triggering efflux of calcium ions from intracellular stores. When depletion of these stores is detected by the endoplasmic stromal interaction molecule 1 (STIM1), store-operated calcium entry (SOCE) from the extracellular space is elicited, boosting the [Ca^{2+}]$_i$ rise in the cytoplasm [Zweifach and Lewis, 1993, Zhang et al., 2005, Liou et al., 2005]. The existence of a calcium-release activated calcium (CRAC) channel has been under debate, but a molecular basis was long undetected [Fanger et al., 1995]. Identification of the ORAI gene by mutation analysis advanced the generation of the concept of the CRAC channel [Yeromin et al., 2006, Zhang et al., 2006, Feske et al., 2006]. Upon detection of intracellular store-depletion, STIM1 accumulates in close proximity to the plasma membrane [Luik et al., 2006, Wu et al., 2006, Hauser and Tsien, 2006], allowing it to interact with Orai, which resembles the pore-forming unit the the channel [Zhang et al., 2006, Vig et al., 2006]. Together, STIM1 and Orai are found at the IS [Lioudyno et al., 2007].

Once CRAC channels are open, Ca^{2+} ions enter the cell according to their electrochemical gradient. To ensure sufficient and highly regulated influx, several mechanisms are employed by the cell. Plasma membrane Ca^{2+} ATPase (PMCA) operates in eventual clearance of Ca^{2+} ions from the cytoplasm [Bautista et al., 2002, Dadsetan et al., 2008]. Mitochondria act as buffers for intracellular calcium entry through CRAC channels, which are otherwise inactivated by [Ca^{2+}]$_i$ [Hoth et al., 1997, Quintana and Hoth, 2004]. Therefore, mitochondria help to maintain elevated [Ca^{2+}]$_i$ levels over sustained periods of time [Quintana et al., 2011]. Yet another important player in the regulation of Ca^{2+} signals are potassium channels, leading to exit of positive charge in the form of potassium ions (K$^+$), which in turn generates a driving force for the entrance of Ca^{2+} ions through CRAC channels (reviewed in[Cahalan and Chandy, 2009]).

1.4 Potassium Channels in T Cells

An influential role of K$^+$ currents in the initial steps of TCA has been reported early on in the history of studying the IS [Matteson and Deutsch, 1984, Cahalan and Lewis, 1990]. First

accounts of these currents in human T cells described them to be solely attributed to voltage-gated channels of the delayed rectifier type [Chandy et al., 1984, DeCoursey et al., 1984]. These channels, identified as Kv1.3, play a significant role in TCA-mediated gene transcription and were implicated in controlling either protein synthesis itself or events leading there [Chandy et al., 1984, Attali et al., 1992]. However, another, Ca^{2+}-activated type of K^+ current was later shown to be similarly important in T cells [Cahalan and Lewis, 1990]. The molecular basis of this additional channel was identified to be KCa3.1 [Ishii et al., 1997, Joiner et al., 1997, Logsdon et al., 1997]. Today, a role for both channels in human T cells is generally acknowledged, with each channel having distinct expression patterns and resulting functions in the different T cell subsets (reviewed in [Cahalan and Chandy, 2009]).

The Ca^{2+}-activated K^+ channel KCa3.1 consists of a tetrameric pore of α-subunits that display a six-transmembrane segment architecture. The pore-forming unit is located between transmembrane regions 5 and 6 [Joiner et al., 1997]. The channel is closed under resting conditions with low basal cytosolic Ca^{2+} and opens rapidly as Ca^{2+} increases, mediated by the Ca^{2+}–sensing subunit CaM located within its C-terminus [Fanger et al., 1999]. KCa3.1 displays low numbers in resting $CD4^+$ and $CD8^+$ T cells, being outnumbered by Kv1.3 (Fig. 3). Channel numbers are relatively higher in activated naïve and central memory $CD4^+$ and $CD8^+$ T_{CMS} [Wulff et al., 2003]. Localization experiments at the IS of activated primary human $CD4^+$ T cells overexpressing functional YFP-tagged

Figure 3: Chart of average Kv1.3 and KCa3.1 channel numbers per cell in the three $CD4^+$ and four $CD8^+$ CCR7/CD45RA-distinguished T cell subsets, naïve, central memory (T_{CM}) and effector memory (T_{EM}) T cells in the resting and the activated state. $CD4^+$: T helper cells, $CD8^+$: cytotoxic T cells. Modified from [Wulff et al., 2003].

KCa3.1 demonstrated channel translocalization into the IS upon stimulation with CD3/CD28-coated beads or virus-infected B cells [Nicolaou et al., 2007a]. Furthermore, these channels contributed to the generation of $[Ca^{2+}]_i$ signals in overexpressing cells, indicated by lack thereof when channels were blocked pharmacologically. It is therefore likely that KCa3.1 is the main contributor to the Ca^{2+} driving force during TCA in KCa3.1^{high} T cells, whereas Kv1.3 takes over that function in the remaining populations (see below).

The voltage-gated K^+ channel Kv1.3 is a *Shaker*-type potassium channel, whose mutational depletion in *Drosophila melanogaster* has been linked to a leg-shaking phenotype [Kaplan and Trout, 1968, Tempel et al., 1987].

In the nervous system, Kv1.3 is prominently expressed in neurons of the olfactory bulb [Fadool, 1998]. Olfactory glomeruli of mice with a gene-targeted deletion of the Kv1.3 channel are smaller and more numerous than those of wild type controls. Furthermore, potassium currents in olfactory bulb cells from Kv1.3 null mice display slow inactivation kinetics and modified voltage dependence. Kv1.3 knock-out mice are described to detect and discriminate odors much more easily than wild type controls [Fadool et al., 2004].

Similar to KCa3.1, Kv1.3 exhibits a tetrameric α-subunit structure, each consisting of six transmembrane segments with the K^+-selective pore formed by the loops between segment 5 and 6 [Matteson and Deutsch, 1984, Doyle et al., 1998] (see Fig. 8 (B)). Contrary to murine T cells, where other Kvs are expressed and able to form heterotetramers with Kv1.3 [Freedman et al., 1995, Liu et al., 2002], it is the only Kv in human T cells. Therefore, its particular function is best studied in human T cells, where it has been shown to sustain the resting membrane potential. Channel current is elicited by a positive change in membrane potential that arises when positively charged Ca^{2+} ions accumulate in the cytoplasm, thereby counteracting depolarization. Unlike typical *Shaker*-type channels (e.g. Kv1.4), Kv1.3 does not comprise a ball-and-chain inactivation mechanism [Hoshi et al., 1990], but rather undergoes rapid cumulative inactivation involving phosphorylation or its association with the intracellular β-subunit [Rettig et al., 1994, Heinemann et al., 1994, Fadool et al., 2004].

Initial functional studies on the channel revealed its role in hypoxia-induced inhibition of human T cells. Acute long-term hypoxia induces inhibition of Kv1.3 currents leading to a selective decrease in channel expression [Conforti et al., 2003], entailing the depression of $[Ca^{2+}]_i$ signals after stimulation of T cells [Robbins et al., 2005]. Kv1.3 current inhibition has repeatedly been demonstrated to be mediated by phosphorylation of the channel via cytosolic kinases of the src-family [Payet and Dupuis, 1992, Fadool et al., 1997, Tóth et al., 2009, Szigligeti et al., 2006, Matsushita et al., 2008]. A recent study, however, suggested protein kinase A I (PKAI) to be solely responsible for Kv1.3 current modulation by direct phosphorylation. Its modulating action depends on the presence of Lck and the scaffold protein Dlg1 [Kuras et al., 2012]. Dlg1 has previously been shown to interact with both Lck and Kv1.3 in T cells [Hanada et al., 1997]. Hence, it is likely that this protein is responsible for mediating close proximity between Lck, PKAI and Kv1.3.

Though displaying moderate numbers itself, Kv1.3 outnumbers KCa3.1 in resting $CD4^+$ and $CD8^+$ T cells. Relatively high numbers of Kv1.3 are observed in activated $CD4^+$ and $CD8^+$

T_{EM}s [Wulff et al., 2003] (Fig. 3). Interestingly, activated myelin-reactive reactive T cells from patients with MS displayed Kv1.3^{high}KCa3.1^{low} expression [Wulff et al., 2003]. Hence, it has been speculated that targeting of Kv1.3 in T_{EM} cells may be employed for therapeutic purposes in MS and other T cell-mediated autoimmune diseases by application of selective inhibitors while leaving other T cell types unaffected [Wulff et al., 2003, Rangaraju et al., 2009]. For example, a recent study in rats could substantiate the role of T_{EM}s, displaying high numbers of Kv1.3, in ear infections. By applying the specific Kv1.3 blocker Shk-186, inflammatory responses were abrogated along with suppression of T_{EM} cell enlargement and motility, which is otherwise observed in infections. Furthermore, Shk-186 effectively treated disease in a rat model of multiple sklerosis [Matheu et al., 2008].

The implication of T cells expressing high numbers of Kv1.3 in the generation of autoimmune phenotypes has motivated more recent studies to focus mainly on the role of Kv1.3 in the IS. Kv1.3 is evenly distributed along the plasma membrane of resting T cells [Panyi et al., 2003, Nicolaou et al., 2010] but becomes highly enriched within the IS until signaling is arrested [Panyi et al., 2004, Szílagyi et al., 2013]. The kinetics of channel localization at the IS in patients suffering from SLE is altered, as its accumulation is only transient [Nicolaou et al., 2007b], leading to sustained elevated $[Ca^{2+}]_i$ [Nicolaou et al., 2010]. Consistently, preventing Kv1.3 recruitment to the IS by cross-linking channel molecules on the surface of T cells results in a significant increase of the Ca^{2+} amplitude [Nicolaou et al., 2009]. This implies that channel movement along the plasma membrane accounts for accumulation at the IS. It further suggests that the localization of Kv1.3 at the IS appears to be indispensable for tight regulation of its currents, e.g. by local kinases, which in turn modifies Ca^{2+} influx and downstream signaling processes.

How Kv1.3 moves to and is kept within the IS remains mostly elusive. The channel may either be actively transported along the membrane or stochastically diffuse to the IS and be trapped within. Intracellular interaction partners may in part be responsible for the channel's movements, localization and accumulation [Szílagyi et al., 2013, Hajdu et al., 2015].

1.5 Dlg-like MAGUKs

Mammalian Dlg-like MAGUKs constitute a family of four scaffolding proteins: Discs large homolog 1 / Synapse associated protein 97 (Dlg1 / SAP97)), Postsynaptic density-93 (PSD-93/ Dlg2), Synapse associated protein 102 (SAP102/ Dlg3) and Postsynaptic density-95 (PSD-95/Dlg4). Dlg, their *Drosophila melanogaster* homolog, has initially been classified as a tumor suppressor protein due to neoplastic overgrowth of imaginal disc epithelia in larvae harboring mutations in the *dlg*-gene [Stewart et al., 1972, Perrimon, 1988]. Dlg-like MAGUKs have further

been implicated in maintaining the polarity of epithelial cells and the integrity of epithelial junctions [Bryant et al., 1993, Woods et al., 1996]. Most prominently, Dlg-like MAGUKs play important roles in defining the molecular architecture and hence the function and plasticity of neuronal synapses [Oliva et al., 2012, Zhou et al., 2008].

Most of their function can be attributed to their domain structure. By definition, MAGUKs in general display a tripartite core consisting of one N-terminal PDZ (PSD-95/Dlg/ZO-1) , one SH3 (Src-homology-3) and one C-terminal GUK (guanylate kinase-like) domain, all of them serving in protein-protein interactions [Funke et al., 2005]. They are able to interact with transmembrane proteins like receptors, cell adhesion molecules or ion channels [Funke et al., 2005], signaling molecules [Hanada et al., 1997], members of the intracellular transport system [Hanada et al., 2000] and the cytoskeletal machinery of the cell [Hanada et al., 2003]. Thereby, they are able to organize macromolecular protein complexes to integrate their respective functions.

PDZ domains show compact and modular structures, harboring a binding groove for peptide ligands [Fanning and Anderson, 1996, Doyle et al., 1996]. They typically bind C-terminal sequences in target proteins [Kim et al., 1995, Niethammer et al., 1996]. Dlg-like MAGUKs usually contain three consecutive PDZ domains.

SH3 domains occur in proteins with diverging functions [Kuriyan and Cowburn, 1997]. They typically bind polyproline motifs (PXXP), which however does not apply to MAGUK SH3 domains. Here, the polyproline binding helix is replaced by part of the so-called Hook–region, which originally was shown to mediate membrane association of the MAGUK Dlg in Drosophila [Hough et al., 1997, Thomas et al., 2000]. A subsequence of the Hook region, the I3 segment, binds to protein 4.1R, which is involved in linking junctional proteins to the spectrin–actin network that in turn underlies the plasma membrane [Hanada et al., 2003].

GUK domains share sequence homology (40 %) with the guanylate kinase (Guk1) of *Saccharomyces cerevisiae*, an enzyme catalyzing GMP phosphorylation to GDP. Yet, the MAGUK GUK domain remains inactive. However, it constitutes a protein-protein interaction unit. For example, it can interact with the SH3 domain intramolecularly , which may block the binding ability of the GUK domain with other partners [Wu et al., 2000]. It is further implicated in the targeting of MAGUKs to synaptic sites via association to the transport machinery of the cell [Thomas et al., 2000, Hanada et al., 2000]. In addition to the core domains, supplementary domains may occur N-terminally of PDZ domains [Doerks et al., 2000].

Dlg-MAGUKs are enriched at the IS of different cell types to various degrees and durations. In murine CD8$^+$ T cells, Dlg-like MAGUKs were shown to maintain cell polarity as a part of the Scribble protein complex, being localized at the distal pole of the resting cell and transiently redistributed to the IS upon stimulation [Ludford-Menting et al., 2005]. In these cells, MAGUKs

stay within the IS for the first 10 minutes after its formation. Notably, the time course of Dlg1 enrichment in the IS varies considerably with the T cell subtype. For example, Dlg1 remains within synapses of Tregs for at least 20 minutes after synapse formation to a degree that exceeds that of other CD4$^+$ cells 4-fold [Zanin-Zhorov et al., 2012].

Such differences may account in part, but not exclusively, for the divergence of various reports on Dlg's function in the immune system. Dlg1 was repeatedly found to exert a role in NFAT-mediated gene transcription in different murine and human T cell populations. The actual impact on NFAT, however, varied considerably between the individual approaches, ranging from upregulating to abrogating effects on T cell signaling. In studies from the Miceli group, Dlg1 was shown to reside within lipids rafts of murine CD8$^+$ T cells upon stimulation and to be required for antigen-induced actin polymerization. In these cells, it was found to be associated with a protein complex comprising Lck, ZAP-70 and WASP. This complex specifically activates NFAT, but not NF-κB, via an alternative activation of the MAP kinase p38. Overexpression of Dlg1 augmented NFAT activation. Conversely, siRNA-mediated knock-down of Dlg1 led to downregulation of p38 and NFAT activity, as well as diminished cytokine production [Round et al., 2005, Round et al., 2007]. Moreover, phosphorylation of p38 via an association with Dlg1 appears to be present only upon stimulation of experienced but not naïve primary human CD4$^+$ and CD8$^+$ T cells [Adachi and Davis, 2011]. Consistent with these findings, yet in CD4$^+$ Tregs, abrogated T cell function due to impaired NFAT activation was monitored upon silencing endogenous Dlg1 expression, possibly mimicking reduced Treg function in patients suffering from rheumatoid arthritis [Zanin-Zhorov et al., 2012]. Oppositely, data from the human Jurkat T cell line detected downregulation of NFAT activity upon Dlg-overexpression and upregulated NFAT when endogenous expression of Dlg1 was diminished [Xavier et al., 2004]. Studies in chimeric Dlg1 knock-out mice reported on hyperproliferative T cells without observing cellular changes, e.g. regarding calcium signaling [Stephenson et al., 2007]. Being in line with [Adachi and Davis, 2011], Dlg1 was shown to be required for the generation of T$_{EM}$s but not for the development of normal CD8$^+$ or CD4$^+$ T cell types [Gmyrek et al., 2013]. A comprehensive study, comparing results from different Dlg1 knock-out animal models and knock-down in Jurkat T cells, concluded that Dlg1 is indeed able to facilitate or attenuate discrete TCR signals in different T cell subsets [Humphries et al., 2012]. The authors further discussed that widely missing cellular phenotypes in Dlg knock-out animals may be due to compensatory upregulation of other members of the Dlg-like MAGUK family. However, while redundancy among Dlg-like MAGUKs has indeed been documented in neurons (e.g.[Schlüter et al., 2006]), upregulation of other isoforms in Dlg1 knock-out T cells was not observed by [Gmyrek et al., 2013].

1.6 Interaction of Dlg-like MAGUKs with Transmembrane Proteins

PDZ domains of Dlg-like MAGUKs recognize the C-termini, specifically the last four amino acids, of their target proteins. However, recent studies suggest for more than the canonical four amino acid binding motif to be involved by actively interfering with interaction [Tonikian et al., 2008]. Numerous interactions have been reported, mostly involving transmembrane proteins like neuronal receptors [Niethammer et al., 1996], cell adhesion molcecules [Thomas et al., 1997b] or ion channels [Kim et al., 1995, Marks and Fadool, 2007]. Dlg-like MAGUKs have been implicated in clustering *Shaker*-type potassium channels to specific sub-cellular compartments, including synapses or the axon initial segment of neurons [Kim et al., 1995, Tejedor et al., 1997, Ogawa et al., 2008]. Moreover, different Dlg-like MAGUKs are shown to localize their binding partners to distinct compartments of the cell [Kim and Sheng, 1996, Tiffany et al., 2000].

Few reports have studied the interaction of the PDZ domains of Dlg-like MAGUKs in T cells. Dlg has has been found in pull down fractions of overexpressed Kv1.3 [Hanada et al., 1997]. Nevertheless, IS localization of Kv1.3 has been implicated to solely rely on another family member, PSD-95 [Szílagyi et al., 2013].

1.7 Aims of this work

While both Kv1.3 and Dlg1 have been implicated in T cell signaling, the role of their presumed interaction in this context has remained elusive. The aims of my work therefore were to:

- validate the physical interaction and its impact on the subcellular distribution of either protein with particular emphasis on the immune synapse

- assess Kv1.3 surface mobility and its modulation by Dlg1

- evaluate the Dlg1-Kv1.3 interaction for its role in the control of Ca^{2+} signaling during T cell activation

2 Material and Methods

2.1 Material

2.1.1 Chemicals

The employed chemicals were, unless noted differently, obtained from: Roche, Clontech, Invitrogen, Roth, Serva, Merck and Sigma. Diverging chemicals are mentioned when relevant. Each solution was prepared with double deionized and autoclaved water (H_2O).

2.1.2 Kits, Enzymes, Molecular Biology and Biochemistry Reagents

Table 1: Molecular Biology Reagents

Item	Company
Endonucleases	New England Biolabs
	Fermentas, Finnzymes
Phusion DNA Polymerase	Thermo Scientific
Alkaline Phosphatase from calf intestine (CIP)	New England Biolabs
Deoxynucleotide Triphosphate Set (dNTPs)	Fermentas
T4 DNA Ligase	Fermentas
T4 Polynucleotide Kinase (PNK)	Fermentas
Cold Fusion™ Cloning Kit	System Biosciences
Klenow Fragment	New England Biolabs
Nucleospin® PCR cleanup gel extraction Kit	Macherey-Nagel
NucleoBond® Xtra Midi / Maxi Kit	Macherey-Nagel
Lipofectamine®2000	Thermo Scientific
Fura-2-AM	Thermo Scientific
Polybrene (94% titration)	Sigma
Dynabeads® Human T-Activator CD3/CD28 - for physiological activation of human T cells	Thermo Scientific
Staphylococcal Enterotoxin E (SEE)	Toxin Technology
Ionomycin	Thermo Scientific
Goat anti-Mouse IgG Magnetic Beads	New England Biolabs
F(ab')2-Goat anti-Mouse IgG (H+L) Secondary Antibody, Qdot® 655 conjugate	Thermo Scientific
F(ab')2-Goat anti-Mouse IgG (H+L) Secondary Antibody, Qdot® 605 conjugate	Thermo Scientific
5x Roti®-Nanoquant	Roth
EMD Millipore Immobilon Western Chemiluminescent HRP Substrate (ECL)™	Millipore

2.1.3 Cells

2.1.3.1 Bacteria and Yeast Cell Strains

Table 2: List of Bacteria Cell Strains used in this work.

Bacterial Strain	Company
E.coli BL21-CodonPlus®(DE3)-RIPL	Stratagene
E.coli XL10 Gold Bacteria	Stratagene

Table 3: List of Yeast Cell Strains used in this work.

Yeast Strain	Genotype	Transformation Marker	Reporter Gene	Company
S.cerevisiae AH109	MATa, trp 1-901, leu2-3, 112,ura-3-52, his3-200, gal4Δ, gal80Δ, LYS::GAL1$_{UAS}$-Gal1$_{TATA}$-HIS3, GAL2$_{UAS}$-GAL2$_{TATA}$-ADE2, URA3::MEL1$_{UAS}$-MEL1$_{TATA}$-*lacZ*	trp1, leu2	LacZ, HIS3	Clontech

2.1.3.2 Mammalian Cells

Table 4: List of Mammalian Cell Lines used in this work.

Mammalian Cell Line	Company / Supplied by
Kidney fibroblast cells from african green monkey (COS-7 cells)	Clontech
Human embryonic kidney cells (HEK293-T)	ATCC®
Lenti-X 293T	Clontech
Human Jurkat T cells	ATCC®
Human Raji B cells	ATCC®

2.1.4 Buffers and Cell Culture Media

2.1.4.1 Buffers used in Biomolecular or Biochemical Work

Table 5: Buffers used in Biochemical and Molecular Biological Assays.

Buffer / Solution	Composition
1x PBS	2.7 mM KCl, 1.5 mM KH2PO4, 137 mM NaCl, 8 mM Na2HPO4, pH 7.4
6x DNA Orange loading dye	15% Ficoll®-400, 66mM EDTA, 19.8mM Tris-HCl, 0.102% SDS, 0.9% Orange G, pH 8.0

---

[1]Fetal Calf Serum

Buffer / Solution	Composition
Cell Lysis Buffer	1% NP-40, 0.16M NaCl, 10mM EDTA, 50mM Tris-HCl, Protease-Inhibitor-Cocktail Complete Mini Ultra (Roche)
Fly Squishing Buffer	10mM Tris-HCl, 1mM EDTA, 25mM NaCl, $200\mu g$/ml freshly added Proteinase K, pH 8.2
Calcium-free Saline	(128 mM NaCl, 2 mM KCl, 4 mM $MgCl_2$ x 6 H_2O, 35.5 mM sucrose, 5 mM HEPES, 1 mM EGTA, pH 7.2)
PBT	0.05 mMNa_2HPO_4, 0.05 M NaH_2PO_4, 0.1% Triton X-100, pH 7.2
Fixative for *Drosophila*	0.05 M Na_2HPO_4, 0.05 M NaH_2PO_4, 4% PFA, pH 7.2
10x Annealing Buffer	100mM Tris, 500mM KCl, 10mM EDTA, pH7.5
1x TAE Buffer	40mM Tris acetate, 1mM EDTA, pH 8.2 - 8.4
1x TG Electrophoresis Buffer	25 mM Tris, 192 mM Glycin, 0.2% SDS
1x TG Blotting Buffer	25 mM Tris, 192 mM Glycin, 0.02% SDS, 20% MetOH
10x LiAc	1 M LiAc in H_2O, pH 7.5
10x TE	0.1 M Tris-HCl, 10 mM EDTA, pH 7.5
PEG	50 % (v/v) polyethylenteglycol 4000 (PEG) in H_2O
PEG/TE/LiAc	8 ml PEG, 1 ml 10x TE, 1 ml 10x LiAc
Live Imaging Buffer for Immune Cells	1% FCS[1], 1% L-Glutamine in RPMI
Live Imaging Buffer for COS-7 Cells	1% FCS, 1% L-Glutamine in DMEM

2.1.4.2   Cell Culture Media and Reagents for Mammalian Cell Lines

Table 6: Media for Mammalian Cell Lines.

Item	Composition
COS-7 and HEK293-T cell culture medium	DMEM (Invitrogen), 10% FCS, 1% L-Glutamine, 100 U/ml Penicillin, 100 μg/ml Streptomycin
Opti-MEM Reduced Serum Medium	Gibco
Trypsin	0.5% Stock solution, diluted 1:10 in HBSS (Invitrogen)
Poly-D-Lysin	100mg/ml Poly-D-Lysin in 100mM Boric Acid, pH 8.5, sterile filtered
Poly-L-Lysin	0.01%, sterile-filtered, supplied by Sigma
HBSS	Ca^{2+} and Mg^{2+} free (Invitrogen)
Jurkat T-Cell culture medium	RPMI-1640 (Gibco), 10% FBS (Pan Biotech, origin: South America), 1% L-Glutamine (Gibco), 1% Penicilllin / Streptavidin (Gibco)
Conjugation Medium (CM) for Jurkat T cells	RPMI-1640 without Phenolred (Gibco), 1% FBS (Pan Biotech, origin: South America), 1% L-Glutamine (Gibco), no antibiotics
Raji B cell culture medium	RPMI-1640 (Gibco), 10% FBS (Pan Biotech, origin: South America), 1% L-Glutamine (Gibco)
Puromycin	Gibco

2.1.4.3 Culture Media and additives for Bacterial and Yeast Cells

Table 7: Media and Reagents for Yeast and Bacterial Cell Culture.

Species	Culture Medium	Composition
E. coli	LB-Medium	20 g LB Broth Base (Invitrogen) / 1000 ml H_2O
	SOC-Medium	15 g Select Agar (Invitrogen) / 1000 ml LB-medium
	YPDA-medium	50 Broth (Gibco) / 1000 ml H2O; plus 10 ml 0.3% Adeninehemisulfate
S. cerevisiae	Minimal SD-medium	20 g Glucose; 1.7 g Yeast-Nitrogen Base (Gibco), 5 g $(NH_4)_2SO_4$/ 1000 ml H_2O; pH 7.0.
	-LW-medium	0.64g -Leu/-Trp DO Supplement (Clontech) per 1l Minimal SD-Medium
	-LWAH-medium	0.60g -Ade/-Leu/-Trp/-His DO Supplement (Clontech) per 1l Minimal-SD-medium; 1 mM 3-amino-1,2,4-triazole

2.1.5 Antibodies

2.1.5.1 Primary Antibodies

Table 8: List of Primary Antibodies used in this work.

Primary Antibody	Antigen	WB dilution	ICC/IHC dilution	Company/ Cat.-No.
ms[2]-α Dlg	*Drosophila* Dlg		1:300	Developmental Studies Hybridoma Bank 4F3
ms-α HA (12CA5)	Human influenza hemagglutinin		fix 1:1000 live 1:200	Sigma 000000011583816001
rb[3]-α RFP	Red Fluorescent Protein		1:200	Rockland 600-401-379
rb-α Dlg	h[4]-, ms- and r[5]Dlg1	1:500	1:200	Santa Cruz sc-25661
rb-αPSD-95	h, ms- and rPSD-95	1:200	1:500	Synaptic Systems 124 012
ms-αPSD-95	h, ms- and rPSD-95	1:200	1:500	NeuroMab 75 348
ms-α CD3 (UCHT1)	hCD3		1:1000	eBioscience 14-0038-82
rb-α Kv1.3	hKv1.3	1:200	1:200	Sigma P4497
ms-α CD3 Biotin (UCHT1)	hCD3			eBioscience 13-0038
ms-α CD28Biotin (CD28.2)	hCD28			eBioscience 13-0289

2.1.5.2 Secondary Antibodies

Table 9: List of Secondary Antibodies used in this Work

Antibody	Antigen	WB dilution	ICC dilution	Company
donkey or goat Alexa Fluor^{TM}488	rb or m IgG		1:1000	Invitrogen
donkey or goat Cy3	rb or m IgG		1:1000	Jackson ImmunoResearch
donkey or goat Cy5	rb or m IgG		1:1000	Jackson ImmunoResearch
goat IgG, peroxidase-conjugated	rb or m IgG	1:10 000		Jackson ImmunoResearch

2.1.6 Oligodeoxyribonucleotides

Oligodeoxyribonucleotides (Primers) were used for Polymerase Chain Reaction (2.3.2, shRNA- and HA-oligonucleotide annealing (2.3.3) as well as analyzing DNA constructs (2.3.6). The Primers were purchased from Biomers. A list of the utilized Primers in this work is to be found in Tables 12 and 13.

2.2 Working with *Drosophila melanogaster*

Table 10: List of Fly Strains Used in this Work

Stock	Remark	Source/ Reference
w^{118}	wild type control	Bloomington Stock Center
y w sn dlg^{XI-2} / Basc;; C57-Gal4	*dlg*-mutant allele combined with muscle-specific Gal4 transcription activator	[Thomas et al., 1997b]
w1118;; mhcP-hCD8-GFP-Kv1.3[3-1]	Kv1.3 reporter under control of the myosin heavy chain promoter	this work
w1118; UAS–SAP97[194.17]; mhcP-hCD8-GFP-Kv1.3[3-1]	SAP97 (rat Dlg1) under control of the upstream activation sequence (UAS) for Gal4, Kv1.3 reporter (see above)	SAP97: [Thomas et al., 1997a]

----

[2]mouse
[3]rabbit

[4]human
[5]rat

2.2.1 Storage

Animals were kept in vials with nutrient pulp-covered bottoms (3 liter formula: 25 g Agar-Agar, 120 g raisins, 180 g bakers yeast, 115 g semolina, 80 g sugar-beet sirup, 15 ml Nipagin, 10 ml propionic acid, ad 3 litre H_2O). Established fly stocks were stored at 18 °C. Only for analysis reasons, crosses were kept in a 25 °C chamber.

2.2.2 Generating Transgene Flies

Drosophila-specific vector-constructs (e.g. hCD8-GFP-Kv1.3$_{FTDV}$-pmhcP) were used for germline transformation, which was done by BestGene. After generating fly strains that stably express the construct through balancing the chromosomes, the strain expressing the reporter construct at desired levels at the larval NMJ was determined through screening several obtained fly strains.

2.2.3 Driven Expression in *Drosophila* Larvae

One advantage of working with *Drosohila melanogaster* is the possibility of employing the bipartite Gal4/UAS system. In this system, an UAS upstream of a gene is recognized by a (tissue-speciffcally expressed) Gal4 transcriptional activator, in turn permitting the expression of the gene in a tissue of interest. In this work, I mainly used the Gal4 activator stock C57 (Table 10) that drives muscle-specifc expression when crossed to a UAS-binding site–carrying genotype.

2.2.4 Preparation of 3rd Instar Larvae

All *Drosophila*-larvae (for a detailed description of the Drosophila larval development,see [Ashburner et al., 2005]) were prepared at larval stage 3 according to the magnet-chamber method [Budnik et al., 2006]. In this procedure, larvae were pinned down with magnetic clips at their anterior and posterior ends and dissected along their dorsal midline. After removing the viscera, the sides of the body walls were also pinned with magnetic clips. All steps were conducted in Calcium-free saline, which was exchanged several times throughout preparation. The obtained body wall, consisting of cuticle, epidermis, muscles and nervous system were further employed for immunohistochemistry (2.6).

2.3 Biomolecular Methods

2.3.1 Single Fly DNA Preparation

One fly of the desired genotype was placed in a 0.5 ml tube and mashed for 5-10 sec with a pipette tip containing 50 μl of squishing buffer, which was added when the fly was smashed and incubated for 30 min at 37 °C. Then, the mixture was heated to 95 °C for 2 min for inactivation of the Proteinase K. The DNA preparation could be stored at 4 °C for months, 1 μl of it being sufficient for PCR (2.3.2).

2.3.2 Polymerase Chain Reaction

The polymerase chain reaction is a technique for amplification of genes or parts of genes, but also for introduction of point mutations into a DNA sequence. For PCR, 20-50 ng template DNA, 50 pM of each Primer (see Table 13), 200 μM of each deoxynucleotide triphosphate (dNTP), 10 μl 5x Phusion^{TM} HF buffer, 0.5 Units of Phusion TM Polymerase (Finnzymes) and H$_2$O ad 50 μl were mixed in a thin wall PCR tube (Thermo Scientifc) on ice. The tube was placed in a PCR thermal cycler (Eppendorf) that was programmed as follows:

I	98 °C	120 seconds	initial denaturation	
II	98 °C	30 seconds	denaturation	
III	x^6 °C	25 seconds	annealing	30-32 cycles
IV	72 °C	x^7 seconds	elongation	
V	72 °C	30 seconds	final elongation	

2.3.3 Oligonucleotide Annealing

715 pmol of each complementary oligonucleotide was mixed with 1x Annealing Buffer (see Table 5) and H$_2$O to a total volume of 60 μl. After a 5 minute incubation in boiling water on a hotplate, the hotplate was turned off and the tube left in the beaker to slowly cool to room temperature in order for hybridization to occur. The resulting annealed oligonucleotides were further diluted to a final concentration of 0.250 pmol/μl for further purposes.

2.3.4 DNA Agarose Gel Electrophoresis

DNA fragments obtained by PCR (2.3.2) or restriction digestion (2.3.5) were separated according to their size by one-dimensional agarose gel electrophoresis. Agarose gels (0.75-1.5 % w/v)

---

[6]unique for each primer pair and adjusted for each PCR according to the instructions of the producing company (Biomers)

[7]dependent on the length of the amplified fragment: 2kbp/min.

were prepared by melting the agarose (UltraPure, Gibco) in the appropriate amount of 1x TAE buffer (5). To visualize the DNA under UV light, 5 -10 μl Ethidium bromide solution (10 mg/ml in H2O) were added before gel polymerization. DNA samples were diluted in 6x loading buffer and loaded onto the gel, which was run at 80 V in 1x TAE buffer in an electrophoresis chamber (Biorad). DNA fragments were visualized under UV-light and photographed with an Eagle-Eye (Stratagene) using the gel documentation system Gel Doc (Biorad).

2.3.5   Restriction Enzyme Digestion of Plasmid DNA

Plasmid DNA underwent restriction either for analyzing matters or preparative restriction for subsequent ligation. Restriction enzymes from Invitrogen, NEB or Fermentas hold 10 units/μl and are provided with the appropriate reaction buffer. For analyzing purposes, 1.5 units/μg plasmid DNA were used and incubated with the provided reaction buffer in an appropriate reaction volume for 1h at 37 °C. 4 units/μg plasmid DNA were used for preparative restriction for 2hrs at 37 °C.

2.3.6   Analyzing DNA Constructs

DNA constructs (Mini or Midi preparations) were first analyzed by test-cleavages (2.3.5) and a subsequent separation of the resulting DNA-fragments in a 0.7 % agarose TAE gel (2.3.4). If constructs proved to be correct, indicated by the observation of expected fragment, they were further checked by sequencing with the appropriate primer (Table 13)

2.3.7   Dephosphorylation of Vector DNA

After linearizing vectors with a single restriction enzyme, the 5'-phosphoryl was removed with Antarctic Phosphatase, the protocol followed as specified by the producing company (NEB).

2.3.8   cDNA Cloning into Expression Vectors

T4 DNA Ligase based cloning procedure. DNA fragments were amplified by PCR (2.3.2). Following agarose gel electrophoresis (2.3.4), fragments were purified with the PCR cleanup gel extraction kit (Table 1) and subsequently ligated into the pJET1.2/blunt positive selection vector. Following DNA isolation, positive analytic enzyme restriction and sequencing, the fragment of interest was obtained by preparative restriction (2.3.5) and ligated to the linearized vector of interest with 2.5 units of T4 DNA ligase. The employed DNA fragment/vector ratio was 3:1. Ligations were performed at 22 °C for 2 hours. The ligated fragment-vectors were transformed into *E. coli* XL10-Gold competent cells (2.3.9).

Cold Fusion$^{\text{TM}}$-based cloning procedures. Cold Fusion$^{\text{TM}}$ (see Table 1) allows for direct cloning of any PCR product into any linearized expression vector, at any site. PCR fragments, carrying a ~15 bp homology to the destined site within the expression vector at their linear ends, were generated (2.3.2). 2 μl of the supplied 5x Cold Fusion$^{\text{TM}}$ master mix were mixed with each 1 μl of PCR product and linearized destination vector and 7 μl H$_2$O, followed by a 5 min incubation at RT. Constructs were transformed into *E. coli* XL10-Gold competent cells (2.3.9).

2.3.9 Transformation of Heat Shock Competent XL10-Gold *E.coli* Cells

An aliquot of *E.coli* XL10-Gold cells (Table 2) was slowly thawed on ice. An appropriate amount of DNA of already existing constructs or the whole reaction batch of new ligations was added to the cells, which were left on ice for 10 min. The cells were heat shocked for 40 sec at 42 °C and 200 μl liquid LB medium (2.1.4.3) were added. The solution was shaken for at least 30 min at 37 °C and thereupon 100 μl were plated onto LB agar plates containing the appropriate antibiotic for positive selection and DNA mini preparation (2.3.10). The plates were kept at 37 °C over night to ensure growth of single cultures.

2.3.10 Isolation of Plasmid DNA by Means of Alkaline Lysis

Isolation of plasmid DNA from *E.coli* XL10-Gold cells (Table 2) was done for small (0.3 μg/μl, usage of Mini Kit) or medium yield (up to 1.5 μg/ μl, usage of Midi or Maxi Kit). The procedure was followed as specified in the protocol provided by the producer (Table 1), only aberrations noted here. For Mini preparation, overnight cultures of 1.3 ml of LB fluid medium containing the appropriate antibiotic and one culture of previously transformed and positively selected XL10-Gold *E.coli* (2.3.9) were inoculated in the 37 °C shaker overnight. Bacterial cells were harvested by centrifugation for 2 min at 13 000 rpm Resuspension (50 mM Tris/HCl, 10 mM EDTA, 10 μg/ml RNAse A, pH 8.0), lysis (200 mM NaOH, 1% SDS) and neutralization (3 M potassium acetate, pH 5.5) buffer were added according to the suppliers protocol. Following 10 min centrifugation, the supernatant was transferred to a new tube containing 600 μl isopropanol to precipitate the plasmid DNA. After 10 min centrifugation at 13 000 rpm, the pellet washed with 400 μl ice-cold 70 %ethanol and spun down for 4 min at 13 000 rpm. The derived DNA pellet was dried and then redissolved in 40 μl H$_2$O. For medium and maximum yield preparation of DNA, an overnight culture of 100 or 500 ml of LB fluid medium was prepared, respectively, and processed according to the companies' protocol.

2.3.11   Custom-Made DNA Constructs: Cloning Procedures and Listing

Table 14 summarizes all constructs used in this work. A detailed description of the constructs' cloning is outlined here. The primers used for amplification of DNA fragments are listed and defined in Table 13.

hCD8-GFP-Kv1.3cyto-pmhcP reporter construct. A fly strain carrying a reporter construct for the C-terminus of the *D.melanogaster* Shaker Kv channel (corresponding to mammalian Kv1.4) was used to perform single fly PCR for amplification of the hCD8-GFP-portion (see 2.3.1). Recognition sites for NheI and EcoRI were introduced at its 3' and 5' ends, respectively. The C-terminal cytoplasmic tail of Kv1.3 was obtained by PCR on the template cDNA KCNA3, introducing EcoRI- and SalI restriction sites at the corresponding ends. The fragments hCD8-GFP, Kv1.3$_{FTDV}$ and the NheI/SalI linearized *Drosophila* expression vector pmhcP were fused in a three-factor-ligation (see Fig. 5).

Yeast-two-Hybrid constructs. PCRs were conducted on the template EGFP-Dlg1 for generating PCR-fragments of the Dlg1 PDZ1/2-tandem or PDZ3-domain, introducing EcoRI- and SalI sites. C-terminal fragments of Kv1.4 and Kv1.3 were generated from the corresponding template cDNAs KCNA4 and KCNA3, respectively, introducing EcoRI- and SalI restriction sites. The fragments were cloned into both, linearized pGBKT7 (EcoRI/SalI) and pGADT7 (EcoRI/XhoI) vectors.

Kv1.3-EGFP. For Kv1.3-EGFP$_{485}$, a PCR fragment of the Kv1.3 cytoplasmic N-terminus and transmembrane α–helices (TM) was generated from the KCNA3 template. The fragment, carrying NheI restriction enzyme sites at both ends, was cloned into the NheI linearized pEGFP-C2 vector. This lead to the N-terminal fraction of Kv1.3 to be located upstream of EGFP. As for the C-terminal cytoplasmic tail, a PCR introduced EcoRI- and SalI sites. The fragment was cloned into into the EcoRI-/SalI linearized Kv1.3-EGFP-C2, creating a Kv1.3 construct that is internally tagged with EGFP. Similar cloning procedures were implemented for the generation Kv1.3-EGFP$_{1545}$ and Kv1.3-EGFP$_{1670}$, differences lying within the use of restriction enzyme sites (see Fig. 6(A)). For Kv1.3-mRFP, the EGFP of Kv1.3-EGFP$_{555}$ was exchanged for mRFP via the restriction sites NheI/BglII. Along with the cloning of FP-tagged Kv1.3, a construct carrying the full length Kv1.3 was cloned in the pCDNA3.1 mammalian expression vector via ERI/SalI sites (Kv1.3-pCDNA3.1).

Kv1.3^{HA}. An EcoRI recognition sequence was introduced within the desired tagging sites via PCR of a front and a back part on Kv1.3-EGFP$_{555}$. After cloning both segments into a mammalian expression vector, the channel construct carried the EcoRI site, which was subsequently used to insert annealed oligonucleotides carrying the DNA sequence of HA, flanked by

an EcoRI site, into the construct (Fig. 5).

Kv1.3-EGFP-$_{\text{WSGG}}$. To realize this mutation, I employed a construct encoding rat Kv1.3 with an altered C-terminus (FTDV > WSGG; gift from Dr. L. Conforti, University of Cincinnati, Ohio). Due to identity of the C-termini of rKv1.3 and human Kv1.3 (TNNNPNSCVNIKKIF TDV), the rKv1.3 construct is a valid source for the mutant C-terminus. Hence, The C-terminus of the wild type (FTDV-containing) Kv1.3 was exchanged for rKv1.3$_{\text{WSGG}}$. A PCR fragment of the C-terminus of rKv1.3$_{\text{WSGG}}$ was created, introducing a BglII site at its 5' end. The BglII site is also located between EGFP and the Kv1.3 C-terminus within the Kv1.3-EGFP construct as a residue of previous subcloning. This site, along with the SalI site present at the 3' end of the Kv1.3-EGFP construct, was used to exchange the wild type (FTDV-containing) against the mutant (WSGG-containing) C-terminus.

Dlg1/PSD-95 shRNA-cloning shRNA oligonucleotides for the designated target sites were designed with linker sites for the H1 promoter MCS (BglII, HindIII) and a central loop (according to [Moore et al., 2010]; see Table 12). Annealed shRNA oligonucleotides were cloned into the H1 promoter-based vectors pZoff-EGFP (Dlg1, gift from Dr. D. Ivanova, LIN Magdeburg) and pCMS4-EGFP (PSD-95, gift from Dr. S. Kliche, IMKI Magdeburg), whereby EGFP serves as transfection control. The Dlg1-shRNA-containing pZoff constructs were further modified by replacing EGFP with mRFP for confirmation of knock-down of Dlg1-EGFP in COS-7 cells. For assessment of knock-down efficiency in Jurkat T cells, Dlg1 shRNA$_{2575}$ annealed oligonucleotides were subcloned into the pCMS4, a vector suitable for transfection and expression in Jurkat T cells.

BiFC. I received constructs of the fragments of the FP Venus (V$_{\text{F}}$: Venus fragment) from the group of Dr. Michael Kreutz [Hradsky et al., 2011]. Dlg1 and Kv1.3 were to be intrinsically fused with each of the V$_{\text{F}}$. Before the actual tagging process, the Dlg1 template (EGFP-Dlg1; gift from Dr. Toshihiko Hanada, Tufts University, Massachusetts) needed to be voided of an existing NheI site and the N-terminal EGFP, which was realized by enzyme restriction, subsequent Klenow blunting and re-ligation of the construct. NheI restriction sites were introduced at positions [825] and [1460] – right before or after PDZ1-2 tandem – PCR of the N-terminal front part and C-terminal back part of the CDS (Fig.8 (B) and (D); for deeper explanation of the basic principle, please refer to the generation of Kv1.3$^{\text{HA}}$). For Kv1.3-V$_{\text{F}}$-cloning, I used the Kv1.3-EGFP construct (3.2.1) to exchange EGFP for V$_{\text{F}}$ (Fig.8 (D)). The V$_{\text{F}}$ constructs contained Start- and Stop codons and were surrounded by NheI- and BamHI sites. For the them to fit my purposes, PCRs were conducted on each V$_{\text{F}}$ construct to eliminate the Stop codon, induce new restriction enzyme sites (NheI/NheI and NheI/BglII for Dlg1- and Kv1.3 tagging, respectively) and adjust the reading frame (Fig. 8 (C)). The resulting fragments were cloned into their target constructs, namely Dlg1$^{\text{Nhe[852]}}$, Dlg1$^{\text{Nhe[1460]}}$ and Kv1.3-EGFP.

Viral Kv1.3^{HA}-mRFP$_{(WSGG)}$-[IRES-Puromycin]-FUGW. PCR fragments of Kv1.3^{HA}-mRFP or Kv1.3^{HA}-mRFP-$_{WSGG}$ were generated from the respective EGFP-vector-based template constructs (see Table 14), introducing a BamHI- and SalI site. After subcloning, the fragments were ligated into the BamHI/SalI linearized FUGW vector. Subsequently, a PCR fragment harboring the IRES-Puromycin expression cassette was generated from the template vector pGIPZ. It contained an overlap of ∼15 bp that was homologous to the area surrounding the BspEI recognition site of Kv1.3^{HA}-mRFP$_{(WSGG)}$-FUGW and used for cloning into its linearized destination vector via Cold Fusion^{TM} cloning.

Viral Kv1.3^{HA}-mRFP$_{WSGG}$-[H1-shRNA]-FUGW. A PCR fragment of Kv1.3^{HA}-mRFP-$_{WSGG}$ was generated from its EGFP-vector-based template construct (see Table 14), introducing a BamHI- and SalI site. After subcloning, the fragment was ligated into the BamHI/SalI linearized FUGW vector. PCR fragments consisting of the H1-promoter/shRNA expression cassettes for Dlg1 or PSD-95 and a ∼15 bp overlap homologous to its destination site were generated from the respective template vectors (see Table 14). The fragments, containing an additional overlap of ∼15 bp homologous to the area surrounding the BspEI-recognition site of Kv1.3^{HA}-mRFP$_{WSGG}$-FUGW, were cloned into linearized Kv1.3^{HA}-mRFP$_{WSGG}$-FUGW via Cold Fusion^{TM}. For a simplified scheme of all viral constructs, see Fig. 14 (A).

2.4 Yeast-Two-Hybrid Assay

The yeast-two-hybrid (Y2H) assay is a valuable approach to study in vivo protein-protein interactions by taking advantage of the Gal4 protein of the yeast *S.cerevisiae*. The Gal4 protein is a transcriptional activator required for the expression of genes encoding enzymes of galactose metabolism. It consists of two separable, yet functional domains, the DNA-binding- and activating domain (DNA-BD and -AD, respectively) [Fields and Song, 1989]. I used the Gal4-based Matchmaker^{TM} Yeast Two-Hybrid System 3 by Clontech, wherein a bait protein is fused to the Gal4 DNA-BD, while the suspected interaction partner (the prey) is linked to the Gal4-AD. Upon bait and prey protein interaction, both Gal4 domains are brought into vicinity, activating transcription of independent nutritional reporter genes (HIS3, ADE2) in the host genome of the yeast strains by binding to their upstream activating sequence (UAS). The double transformation protocol used in the present work was kindly provided by W.Altrock:

One colony of the AH109 yeast strain in 25 ml fluid YPDA medium (2.1.4.3) was inoculated over night at 30 °C while shaking. On the next day, the OD600[8] was adjusted to a value of 0.2 - 0.3 by dilution in a total volume of 50ml. The fresh culture was shaken at 30 °C for 3-5 hours until an OD600 of 0.9 - 1.0 was reached. The cells were harvested by centrifugation at 500 x g

---

[8]optical density at 600 nm

for 2 min at RT, washed for 2 min with 50 ml 1 x TE (see Table 5) and centrifuged at 500 x g for 2 min. Hereafter, the pellet was washed with 40 ml 1xTE/LiAc for 510 min, centrifuged at 500 x g for 2 min, and resuspended in 1 ml of 1 x TE/LiAc. 10 μl hering carrier DNA, 1 μl plasmid (pGBKT7 prey- and pGADT7 bait-construct, 1 - 1.5 μg each) and 50 μl competent yeast cells were mixed in a 2 ml tube. Subsequently, 300 μl of 40% PEG were added and mixed by shaking vigorously. The mixture was placed in a 42 °C water bath for 40 min and put on ice for 2 min. After harvesting the cells by centrifugation at 500 x g for 2 min, the pellet was resuspended in 200 μl H$_2$O. 100 μl each were plated on appropriate SD medium agar plates. Cotransformed cells were reported by growth on –LW-medium. The interaction of co-expressed proteins activating expression of reporter genes was monitored as growth on –LWAH-medium after 4 to 7 days at 30 °C. Potential self-activation of constructs was always tested in parallel by co-transformation with empty prey or bait vectors. Co-expression of pGBKT7-53 and pGADT7-T, as provided by Clontech, served as a positive control for interaction.

2.5 Cell Culture Techniques

2.5.1 Adherent Cell Cultures (HEK293-T, Lenti-X 293 and COS-7)

2.5.1.1 Poly-D-Lysine Coating of Glass Cover Slips

Coverslips were transferred into Corning® Costar® cell culture plates, coated with 200 μl of poly-D-lysine working solution (Table 6) per coverslip and incubated for 10 min at RT. After removal of the working solution, ultra pure water was added to each plate. Before usage of the coverslips the water was removed.

2.5.1.2 Splitting of Cells into Culture Plates

Cells were washed with pre-warmed HBSS for 5 min and subsequently incubated with 1 ml of 1x Trypsin per 75 cm^2 flask for 5 min at 37 °C. Upon dissociation of the cells from the plate, degradation of extracellular proteins by the protease trypsin was blocked by adding 9 ml of fresh, pre-warmed DMEM (10% FCS). The cells were then transferred into plates with additional medium in order to reach a suitable concentration.

2.5.1.3 Transfection of COS-7 or HEK293-T Cells

Transfection with Liposomes. COS-7 or HEK293-T cells were grown on poly-D-lysine coated glass coverslips to 50–70 % confluency in 24-well plates. Prior to transfection, antibiototic-containing DMEM was exchanged for antibiotic-lacking DMEM. 0.5-1.0 μg DNA / construct was

used, depending on the efficacy of the construct. The appropriate amount of DNA was mixed with 50 μl Opti-MEM. Another 50 μl of Opti-MEM were mixed with 1.5 μl Lipofectamine®2000 Reagent in another tube. Both volumes were then joined and mixed vigorously. The resulting transfection mix was incubated at RT for 20 min in order for the DNA-containing liposomes to be formed. After incubation, the entire transfection mix was added to one well. If more cover slips were to be transfected, the amounts of the respective mixtures were increased and distributed accordingly. After leaving the cells with the mixture for 2 hours in the 37 °C incubator, the medium was exchanged for an appropriate amount of fresh DMEM.

Transfection with the Calcium-Phosphate Method. When producing viral particles, Lenti-X 293-T cells were transfected with the CaPO$_4$ method. Confluent cells were split the day before transfection in a 1:3 ratio and grown in a 150 cm^2 flask. On the day of transfection, medium was exchanged for 20 ml of fresh DMEM. The appropriate amount of DNA (see 3.5.2) was mixed with 1 ml solution A (500 mM CaCl$_2$), then the same amount of solution B (140 mM NaCl, 50mM HEPES, 1.5 mM Na$_2$PO$_4$, pH 7.5) was added. The resulting transfection mixture was incubated for 1 min at RT and then added to the cells. After 4 - 6 hours, the cell medium was exchanged for fresh DMEM.

Successful transfection, indicated by expression of the protein of interest, could be detected after 18 - 24 hours.

2.5.1.4 Virus Poduction

Viral particles were produced in Lenti-X 293-T cells via transfection of the viral vectors pVSVG, psPAX2 and FUGW with the CaPO$_4$ method (see 2.5.1.3). For a 150 cm^2 flask, 5 μg of pVSVG, 7.5 μg psPAX2 and 10 μg of the respective FUGW-construct were applied. 24 hours post transfection, DMEM was exchanged for modified RPMI1640 (4 % FBS, 0.9 mM CaCl$_2$, penicillin / streptavidin, L-glutamine). Viral particles were harvested with the cultures' supernatant 48h and 72h after transfection. After centrifugation of the supernatant (2 000 x g, 5 min), it was sterile-filtrated (PVDF, 0.45 μm pore-size, Millipore), aliquoted in 2 ml tubes and stored at -80 °C. Once thawed, the viral supernatant could not be used again since infection efficiency would be considerably lower.

2.5.2 Immune Cell Lines (Jurkat T- and Raji B cells)

2.5.2.1 Poly-L-Lysine Coating of Glass Cover Slips

Sufficient drops of poly-L-lysine (see Table 6) were placed in a paraffin-film-coated plastic dish and covered by Ø 12 mm coverslips, which were incubated for 30 min at RT. The coverslips

were then transferred into Corning® Costar® cell culture plates, washed with ultra pure water three times and completely dried. The coverslips could be stored at 4 °C for 1-2 weeks.

2.5.2.2 Maintenance of Cultures

The non-adherent immune cell lines were kept at a density of $\sim$ 0.1 - 0.5 x 10^6 in RPMI1640 cell culture medium (see Table 6). Cells were transferred to new medium every 2 - 3 days by centrifugation for 4 min at 1 200 rpm and 4 °C, followed by resuspending the pellet.

2.5.2.3 Electroporation of Jurkat T Cells

20 x 10^6 cells were harvested via centrifugation for 4 min at 1 200 rpm and 21 °C. 12.5 ml of the supernatant were kept for later use, the rest discarded. The remaining pellet was washed with 1 x PBS (Dulbecco, with Ca^{2+} and Mg^{2+}), spun down (see above) and resuspended in 350 μl 1 x PBS. In an electroporation cuvette, the cell suspension was mixed with 15 μg of DNA and electroporated at 230 V and 950 μF in the Bio Rad Gene Pulser II Electroporation System. Afterwards, cells were taken up in 1 ml of pre-warmed RPMI1640 and the debris of dead cells was removed. The surviving cells were transferred into a new 75 cm² flask, were they were suspended in 25 ml RPMI, which consisted of the harvest supernatant (see above) and fresh medium at a 1:1 ratio. Successful electroporation, indicated by expression of the protein of interest, could be detected after approximately 24 hours.

2.5.2.4 Viral Infection of Jurkat T Cells via Spinoculation

0.5 x 10^6 cells were spun down for 4 min at 1 200 rpm and RT. 1 ml virus-containing medium (see 3.5.2) was thawed, pre-warmed at 37 °C and added to the cells. For infection with Kv1.3-FUGW-constructs, 100 % of viral supernatant, for the GFP-control construct, a 20 % viral supernatant – RPMI1640 dilution were employed. 0.8 μg/ml Polybrene (Table 1) was added and gently mixed. The infection batches were centrifuged (Eppendorf 5424 R) at 0.1 x g and 32 - 37 °C for 30 min. The resulting pellet was resuspended in 1 ml of fresh RPMI and kept in a Corning® Costar® cell culture well over night. Successful infection, indicated by expression of the protein of interest, could be detected after approximately 24 hours. The Kv1.3-infected cultures usually showed an infection efficacy of $\sim$10 % and were used for generation of stably expressing cell lines.

2.5.2.5 Generation of Stably Expressing Jurkat T Cell Lines

Selection via Magnetic Bead Separation. Cells expressing Kv1.3$^{\text{HA}}$-mRFP$_{\text{WSGG}}$-[H1-shRNA]-FUGW were selected for their extracellular HA-epitope. 5 x 10^6 cells of a previously infected culture (2.5.2.4) were employed. The HA-epitope was labeled with ms α-HA primary antibody (Roche) in a 1:200 dilution in 1 ml 5 % RPMI (5 % FBS, 1 % L-glutamine, 1 % penicillin/streptavidin) for 5 min at 4 °C. After three washing steps in 5 % RPMI, cells were resuspended in 1 ml. 0.15 μl of goat-α ms magnetic beads (Table 1) were washed in a tube magnet, resuspended in 10 μl 1x PBS and subsequently added to the cells. After 1 hour incubation at 4 °C, the HA / magnetic bead–labeled cells were magnetically separated to the side of the tube for 10 - 20 min. The bead-cell pellet was resuspended in 2 ml fresh RPMI medium. Cells were further grown until the size of a maintenance culture was achieved. Magnetic separation was repeated every 4-6 weeks in order to ensure the stability of the expressing cell line.

Selection via Puromycin-Resistance. Puromycin selection was employed for cells expressing Kv1.3$^{\text{HA}}$-mRFP$_{\text{(WSGG)}}$-[IRES-Puromycin]-FUGW constructs. 1 μg/ml puromycin was added to a maintained culture for at least one week. Introducing puromycin to the cultures every 8-10 weeks ensured the stability of the expressing cell line.

Positive mRFP signal in all cells proved an effective generation of a stably expressing cell line.

2.5.2.6 Stimulation of Jurkat T Cells

Stimulation of Jurkat T Cells with *Staphylococcus aureus* enterotoxin E (SEE)-loaded Raji B Cells. Jurkat T cells were stimulated with SEE-loaded Raji B cells for generating immune-synapse forming cell pairs. 0.5 x 10^6 Raji B-Cells were collected via centrifugation for 4 min at 1 200 rpm and 21 °C and resuspended in 1.5 ml RPMI. After adding and mixing SEE (final concentration: 2 μg/ml, see Table 1), the cell suspension was incubated in the 37 °C incubator over night. The following day, the cells were spun down (see above), washed in fresh RPMI1640 and resuspended in 1 ml conjugation medium (CM, see Table 6). 0.5 x 10^6 Jurkat T cells were spun down and taken up in 1 ml CM. Both, Raji and Jurkat cells were habituated in CM for at least 1 hour, then spun down and redissolved in 200 μl CM. 20 μl of each cell suspension was placed onto pre-warmed, poly-L-lysine-coated Ø 12mm glass cover slips in cell culture plates. After a quick pipetting step for mixing both cell types, the conjugation batches were moved to the 37 °C incubator for 10 min. Conjugation reactions were arrested by adding 2% PFA in PBS for 5 min. The obtained T-B cell pairs on cover slips were further subjected to immunocytochemistry (2.7.1)

Stimulation of Jurkat T Cells CD3/CD28-coupled Dynabeads®. Jurkat T cells activated by CD3/CD28-coupled Dynabeads® were employed for Ca^{2+}-flux measurements. For the exact procedure, see section 2.8.

2.6 Immunohistochemistry – Antibody Staining of Larval Body Walls

To the calcium-free saline in which the body wall (2.2.4) was rested, 2-3 drops of fixative (Table 5) was added for 1 min. The solution was then exchanged for fixative and the body wall was incubated for 20 min. After fixation, the body wall was washed with PBT (Table 5), removed from the preparation chamber and placed into a small bowl. After three 15 min washing steps with PBT, the body walls were incubated with primary antibody (Table 8) in 150-200 μl PBT at 4 °C overnight while shaking. After three 15 min washing steps with PBT, secondary antibodies (Table 9) were incubated for 1h at RT. Hereafter, the body walls were washed three times each 15min in PBT, placed on a object slide (76 x 26mm, Roth), mounted with Vectashield® Mounting Medium H1000 and topped with a cover slide (18 x 18mm, Roth). Finally, specimen was sealed with clear nailpolish and was kept at -20 °C.

2.7 Immunocytochemistry

2.7.1 Immunostaining

HEK 293-T- / COS-7 cells. Cells on Ø 12mm glass cover slips were fixed for 3 - 5 min with 37 °C pre-warmed 4% PFA in PBS. If required, cell were permeabilized by 15 min incubation in 5% BSA, 0.1% Triton X-100 in PBS. Antibodies were diluted in 30 μl 5% BSA in PBS per coverslip, placed on a paraffin film in a wet chamber (antibody list and corresponding dilutions, see Table 8) and covered by coverslips with cells facing the antibody solution. Over night incubation at 4 °C was followed by three PBS washing steps. The secondary antibody was applied at RT for one hour. After washing three times in PBS, coverslips were mounted on object slides in Mowiol. Mounted coverslips were stored at 4 °C until usage.

Jurkat T and Raji B cell pairs. The staining protocol for immune cells was similar to that of HEK 293-T and COS-7 cells, with the following deviations. Cells were fixed in 2% PFA in PBS and permeabilized in 5% horse serum, 0.1% Triton X-100 in PBS for 5 min. Instead of BSA as an agent to prevent unspecific binding of antibodies, horse serum was used.

2.7.2 Quantum Dot® (QD®) Experiments

QD® Experiments on COS-7 Cells. Previously Kv1.3^{HA}-transfected cells on poly-D-lysine–coated cover slips were surface-labeled with primary ms α-HA antibody. Therefore, 100

μl of a 1:200 antibody dilution in 5% DMEM medium (5% FCS, 1% L-glutamine, no phenolred) were placed on Parafilm in a petri dish with the cover slip being placed on the drop facing down. The cells were incubated for 5 min at 4 °C. After three quick washing steps with 5% DMEM medium in a 6-well cell culture plate, the cells were incubated with αms–QD®-655 at a final concentration of 1:4000 for 15 min at 4 °C. A 1:10 QD® labeling solution, which was used for dilution, was prepared as follows: 1 μl of QD®-655 (Table 1) were mixed with 8 μl 1x PBS and 1 μl 10 x Casein for 10 min while gently shaken. Following three washing steps, the cover slip was placed in a Low Profile Open Bath Chamber (Warner Instruments) and filled with warmed 1% DMEM medium (5% FCS, 1% L-glutamine, no phenolred) and imaged employing fluorescence microscopy (see below).

QD® Experiments on Jurkat T Cells. The general labeling-strategy of Jurkat T cells stably expressing Kv1.3^{HA}-constructs with QD®–566 against the extracellular HA-epitope was kept. Living Jurkat T cells are generally not adherent and will not properly stay on poly-L-lysine–coated cover slips during elaborated labeling and washing steps. Hence, the labeling-protocol was adjusted by performing careful washing steps in a tube via 2 min spinning at 2 000 rpm in a tabletop centrifuge. For each washing step, 200 μl CM medium were employed. 0.3 x 10^6 cells were used per labeling. Since Jurkat T cells are rather small and round, fluorescent imaging of single QD®-labeled molecules of Kv1.3^{HA} was proven to be impractical. For overcoming this obstacle, QD®-labeled Jurkat T cells were imaged using Total Internal Reflection Fluorescence (TIRF) microscopy, which allows for steady imaging of the portion of cells contacting the glass cover slip. Baseline movement of QD®®-labeled Kv1.3 molecules was monitored on poly-L-lysin–coated cover slips. In order to observe possible changes in movement or numbers of QD®-labeled Kv1.3 molecules when an immune synapse is formed, experiments were performed on poly-L-lysin–coated cover slips that were additionally layered with ms α-hCD3 (5 μg/ml) and ms α-hCD28 (2 μg/ml) over night. In both cases, 300 μl of labeled cells were added to a an imaging chamber containing a cover slip that was already located in the in the microscope. Live acquisition was initiated as soon as a cell was about to settle on the cover slip, as followed in light microscopy.

Imaging was performed at 37 °C using an 63 x (COS-7) or 100 x TIRF (Jurkat T cells). The employed microscope (Olympus) was able to be switched between normal fluorescence and TIRF mode and controlled by MetaMorph Imaging (Molecular Devices). Live streams were acquired at 33Hz for at least 1 min for baseline surface mobility and up to 5 min on α-hCD3/α-hCD28-layered cover slips.

Data analysis was performed with a custom-made software [Groc et al., 2007]. Two parameters were analyzed: the Mean Square Displacement (MSD) and the Instantaneous Diffusion Coefficient (D). The MSD is calculated by the distance that a QD$^{®}$ moves in between two images, for example between the 1th and 2th and the 2th and 3th image. The second MSD point is based on the covered distance between the 1th and 3th and the 2th and 4th image. The MSD provides information about the area a QD$^{®}$ explores within a defined time window. D describes the general velocity of a QD$^{®}$ calculated from the first 4 images of the stream.

2.8 Single Cell Ca^{2+}–flux Measurement

Ca^{2+}–flux Measurement 0.2×10^2 Jurkat T cells were loaded with 2 μM Fura-2 AM in 1 ml CM (Table 6) for 30 min at 37 °C. The incubation volume was then exchanged for 300 μl of fresh CM. Cells were allowed to settle on a poly-L-lysine–coated Ø 18mm coverslip, which was inserted into an quick change imaging chamber (RC-41LP, Warner Instruments), for ∼5 min. Imaging was performed with the MetaMorph Program (Molecular Devices) under a fluorescence microscope (Olympus) in 40x magnification. Every 6 seconds for a total of 900 seconds (150 frames), the probes were excited with 360 and 380nm, emission was acquired at 510nm. The relative Ca^{2+}-flux was determined by plotting the ratio of the 360 and 380 nm values in Excel. Cells were stimulated with CD3/CD28 coated Dynabeads$^{®}$ (Table 1). At frame 140, 2 μM ionomycine were added (Table 1).

Stimulation of Jurkat T Cells CD3/CD28-coupled Dynabeads$^{®}$. After ∼10 frames of imaging, 2 μl of Dynabeads$^{®}$ Human T-Activator CD3/CD28 stock solution diluted in 20 μl CM were added carefully to the cells.

2.9 Biochemical Methods

2.9.1 Isolation of Whole Cell Proteins from Jurkat T Cells

2×10^6 cells were harvested at 1 200 rpm for 4 min at 21 °C and 1 200 rpm in a Eppendorf 5810 R centrifuge and the supernatant was discarded. The remaining pellet was redissolved in 60 μl Lysis Buffer (see Table 5), put on ice for 15 min and subsequently centrifuged for 30 min at 4 °C and 13 000 rpm in a Eppendorf 5427 R. The supernatant was then collected into a new tube and stored at -21 °C until it was further used.

2.9.2 Protein Concentration Determination employing the Bradford Method

The Roti®-Nanoquandt (Table 1) modification of Bradford's protein assay was carried out in cuvettes as specified in the provided protocol from Roth. Acquired values of known BSA standard solutions were used to calculate a calibration curve, which could then be used for determination of protein concentration of samples produced in 2.9.1.

2.9.3 Sodium Dodecyl Sulfate Polyacrylamide Gel Electrophoresis (SDS–PAGE)

Proteins were separated using one-dimensional sodium dodecyl sulphate polyacrylamide gel electrophoresis (SDS-PAGE) under fully denaturating conditions [Laemmli, 1970]. Gradient gels which had an acrylamide concentration ranging from 5% on top to 20% on the bottom were used. Additionally, a stacking gel covered the separating gel to focus the proteins (Table 11). Samples were first incubated with SDS-sample buffer at 95 °C for 5 min and loaded onto the gel afterwards. Gels were allowed to run at a current strength of 8 mA within the stacking gel and 10 mA during the separation phase in an electrophoresis chamber (Hoefer Mighty Small System SE 250 from Amersham Biosciences) filled with 1x electrophoresis buffer. Subsequently, the gels were used for Western Blot.

Table 11: Buffers for Tris-Glycine SDS-PAGE

Buffer	Composition
4x SDS sample buffer	250 mM Tris/HCl, pH 6.8, 1% (w/v) SDS, 40% (v/v), glycerol, 4% β-mercaptoethanol, 0.02% bromophenol blue
Tris-glycine Electrophoresis Buffer	192 mM glycine, 0.1% (w/v) SDS, 25 mM Tris-base, pH 8.3
Separation Buffer	1.5 mM Tris, pH 8.8
Stacking Buffer	0.5 mM Tris, pH 6.8
Separation gel (20%)	8.25 ml separation buffer, 7.5 ml 87%Glycerol, 16.5 ml 40% Acrylamyde, 330 μl EDTA (0.2 M), 22 μl TEMED, 120 μl 0.5% Bromophenol blue and 75 μl 10% APS
Separation gel (5%)	8.25 ml separation buffer, 17.94 ml dH2O, 1.89 ml 87% Glycerol, 4.12 ml 40% Acrylamide, 330 μl EDTA (0.2 M), 22 μl TEMED and 118 μl APS
Stacking gel (5%)	6 ml stacking buffer, 7.95 ml dH2O, 5.52 ml 87% Glycerol, 3.90 ml 30% Acrylamyde, 240 μl EDTA (0.2 M), 240 μl 10% SDS, 17.2 μl TEMED, 30 μl Phenol red and 137 μl 10% APS

2.9.4 Western Blotting

Proteins were electrotransferred from polyacrylamide gels to Millipore Immobilon-FL transfer membranes (polyvinylidene fluoride [PVDF] membrane). Prior to transfer, the membrane

was activated in methanol for 30 sec. The transfer was performed in a Western Blot chamber (Mighty Small Transfer Tank, Hoefer) filled with Blotting buffer at 4 C for 1.45 h with 200 mA. After the transfer the membrane was rinsed again with methanol and air dried.

2.9.5 Immunodetection

The PVDF membrane was blocked in 5% BSA containing PBS-Tween for 30 min at RT. Primary antibodies were diluted in 2% BSA containing PBS-Tween and probed for 90 min at RT or overnight at 4 C. After three washing steps with PBS-Tween, secondary, peroxidase-conjugated antibodies diluted in PBS-Tween were incubated for 45 min at RT. After three final washing steps with PBS-Tween, the membrane was subjected to immunodetection with chemiluminescent HRP substrate (Millipore, Table 1). Chemiluminescent signal was detected in an INTAS ECL ChemoCam Imager.

2.10 Statistical Analysis

Data are given as mean values $\pm$ standard error of the mean (SEM) for data displaying Gaussian distribution, median values alone, with tukey or 10-90 percentile whiskers if Gaussian distribution was not given. ANOVA tests (one-way analysis of variance and Bonferoni's multiple comparison test for values following Gaussian distribution, Kruskall-Wallis test and Dunn's multiple comparison test for values not following Gaussian distribution) were employed for testing for significant differences. Statistical calculations were performed in GraphPad Prism 5.04B. Statistical significance was set as [*] : $p < 0.05$; [**] : $p < 0.01$; [***] : $p < 0.001$.

3   Results

3.1   Kv1.3-Dlg-like MAGUK Interaction Revisited

The binding of NMDA-receptor subunits 2A and B and Shaker-type channel Kv1.4 to PSD-95-like MAGUKs [Kim et al., 1995, Kornau et al., 1995] constitute the prototypical interactions between C-terminal S/T-X-V motifs and PDZ domains. In their original yeast-two-hybrid (YTH) assays, Kim et al.[1995] also found a strong interaction between the C-terminus of Kv1.3 with PDZ domains 1 and 2 of PSD-95 and a slightly weaker interaction with a construct comprising all three PDZ domains of Dlg1. Furthermore, PSD-95 has been shown to interact *in vivo* with Kv1.3, with marked co-localization of both proteins in neurons of the olfactory bulb [Marks and Fadool, 2007]. Subsequent studies, however, pointed to a crucial impact of the glutamate residue (E) at the -3 position of the PDZ binding motif, where Kv1.3 carries a phenylalanine (F) [Lim et al., 2002, Tonikian et al., 2008]. Other reports on the interaction between Kv1.3 and Dlg1 and/or PSD-95 [Hanada et al., 1997, Szílagyi et al., 2013] did not specify the interface between the two and even left open the possibility that the interaction is indirect.

3.1.1   Validation of the Interaction of Kv1.3 and Dlg1

In light of the aforementioned uncertainties, I pursued a comparative binding study involving the PDZ domains of Dlg1 and the C-termini of Kv1.3 and Kv1.4 by YTH. Co-transformants expressing baits with the last 89 or 93 aa of Kv1.3 (KCNA3) or Kv1.4 (KCNA4), respectively, and a prey containing the PDZ1-2-tandem of Dlg1 grew equally well and only slightly less than positive controls on selective agar plates (-LWAH) (Fig4). In contrast, co-expressing the same baits with a PDZ3-encoding prey yielded no growth. This finding implies robust and selective interaction between the C-terminus of Kv1.3 and the PDZ1-2 tandem and is thus basically consistent with the original finding by [Kim et al., 1995]

3.1.2   Dlg-dependent Recruitment of a Kv1.3 Reporter to a Heterologous Synaptic Junction

To further evaluate the interaction in regard to Dlg-dependent localization of Kv1.3 to specific subcellular compartments *in vivo*, I exploited the availability of *Drosophila* as a model. Specifically, I established flies stably expressing a reporter construct under the control of the muscle-specific myosin heavy chain (mhc) promoter. The construct, which was designed according to a previously described reporter for Kv1.4 (Shaker) [Zito et al., 1997], comprises the last

	Dlg1	
	PDZ1-2	PDZ 3
Kv1.3 GAL4 DNA-BD F483 - 81aa - C V N I K K I F T D V	++	-
Kv1.4 GAL4 DNA-BD F566 - 76aa - C S N A K A V E T D V	++	-

Figure 4: **Summary of the Y2H Results for Kv1.3-Dlg1-Interaction.** Mapping of the interaction site for Kv1.3 within Dlg1, whereas [+] expresses a presence of interaction with the number of [+] (1-3) corresponding to the strength of interaction compared to positive p53-T-interaction control, which was set to [+++], whereas [-] indicates an absence of interaction.

93 amino acids of the Kv1.3 C-terminus downstream of human CD8 and GFP (hCD8-GFP-Kv1.3$_{\text{FTDV}}$, Fig.5 (A)). *Drosophila Dlg* (*d*Dlg) is highly enriched on the postsynaptic site of larval neuromuscular junctions (NMJs), which covers only about 2-5% of the muscle surface. NMJ-recruitment of the Kv1.4 reporter is highly dependent on the presence of *d*Dlg [Zito et al., 1997]. Localization of the Kv1.3 reporter was assessed at NMJs of wild type and *dlg*-mutant
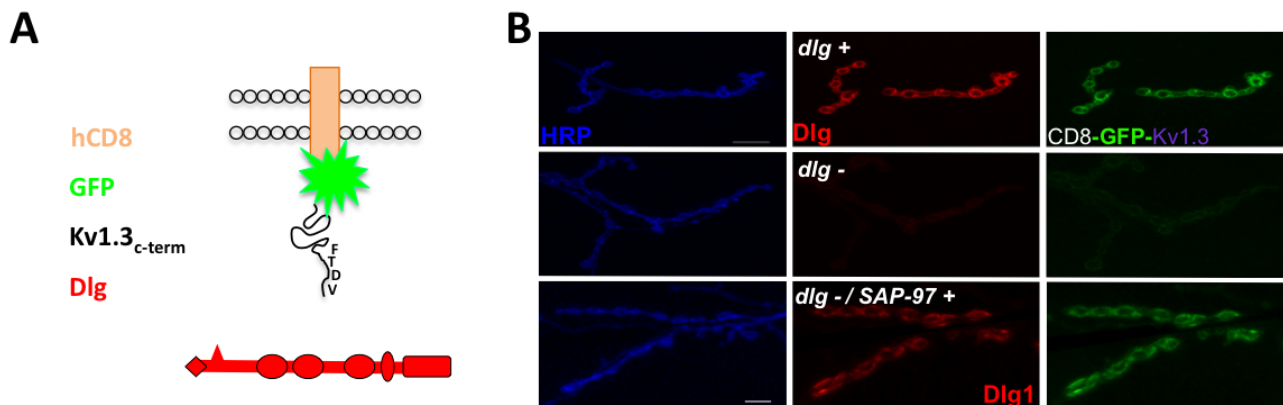
Figure 5: **Validation of *in vivo* Interaction Between Kv1.3 and Dlg. (A)** Structure of the Kv1.3-reporter construct, which is inserted into the plasma membrane due to its hCD8-domain. **(B)** Exemplary confocal pictures for the Dlg-like MAGUK-dependent localization of the Kv1.3-reporter construct. The upper panel depicts a *dlg*-wild type background, the middle panel a *dlg*-mutant and the lower panel a re-expression of Dlg1 (rat SAP97) in a *dlg*-mutant background. Horseradish peroxidase staining represents a control for pre-synaptic neurons of the larval NMJ, Dlg1-staining the Dlg-like MAGUKs and GFP-signal the reporter construct. Scale bar 50μm.

D. melanogaster larvae by confocal microscopy. The reporter construct clearly localized at the larval NMJ together with *d*Dlg (Fig. 5(B), upper panel). Strongly diminished Dlg expression led to a severe reduction of the Kv1.3-reporter recruitment to NMJs (Fig.5 (B), middle panel). Since the genetic background used in this experiment does not constitute a null-mutant

for *dlg*, some residual portion of the protein is present along with remnant localization of the reporter construct. The extent of residual *d*Dlg at the NMJ vaguely matches the amount of reporter construct still present at the synapses. A previous report revealed that mammalian MAGUKs can restore viability of otherwise lethal *D. melanogaster dlg* mutants [Thomas et al., 1997b]. Consistently, rat Dlg1 (SAP97) is able to restore reporter recruitment in a *dlg*-mutant background. This was clearly the case (Fig. 5 (B), lower panel).

Thus, I was able to demonstrate *in vivo* interaction between the Kv1.3 reporter construct, i.e. Kv1.3's C-terminus, and DLG-like MAGUKs. Recruitment of the reporter construct was largely dependent on the presence of *D.melanogaster* Dlg, which could be replaced by its mammalian homologue Dlg1. This finding points toward a possible role for Dlg-like MAGUKs in localizing Kv1.3 to specific subcellular domains, like synapses.

3.2 Establishing Functional GFP- and HA-tagged Kv1.3 Constructs

3.2.1 Internal Tagging with a Fluorescent Protein

In order to visualize Kv1.3 in both living and fixed cells independent of antibody labeling, I generated constructs encoding the Kv1.3 α-subunit internally tagged with Enhanced Green Fluorescent Protein (EGFP). Additionally, this type of construct was designed envisaging the assessment of its binding to Dlg1 by Förster Resonance Energy Transfer (FRET) studies. Therefore, the EGFP needed to be positioned as close to the C-terminus as possible, while maintaining channel function and MAGUK binding (3.1.1). I generated three constructs with EGFP inserted at Kv1.3 amino acid positions '485', '510' and '555' within the cytoplasmic tail (see Section 2.3.11).

For expression and membrane localization studies of these constructs, I used the african green monkey kidney fibroblast-like cell line COS-7. Due to its flat and wide appearance, this cell line allows for monitoring the localization of proteins at the plasma membrane. According to the online expression profile tool The Human Protein Atlas (`www.proteinatlas.org`), kidney cells do not endogenously express Kv1.3. Considering that the EGFP-tagging of all four α-subunits might interfere with proper channel tetramerization, function and/or localization, I co-expressed the constructs with untagged Kv1.3 (Kv1.3-pCDNA3.1). In addition, I co-expressed the beta-subunit of the Kv-channel family (Kvβ2-pCMVSPORT6), which has been shown to promote channel localization to the cell membrane as well as to modulate its physiological properties [Gulbis et al., 1999, McCormack et al., 1999].

In general, expression of the Kv1.3-EGFP-constructs led to enriched EGFP-signal in the area surrounding the nucleus, herein referred to as the perinuclear region (Fig 6(B)). This localization

pattern was routinely observed in expression experiments with Kv1.3 constructs (Fig 6(C)). The variant of Kv1.3 harboring EGFP closest to the PDZ-binding site (Kv1.3-EGFP$_{555}$) localized to cell membranes efficiently without extensive enrichment within the cell body in COS-7 cells (Figure 6(B)). Thus, this variant was employed for further experiments and served as a template for cloning and will hereupon be referred to as Kv1.3-EGFP. From this template, I also cloned a Kv1.3 channel internally tagged with mRFP, in which the EGFP is exchanged for mRFP. Along with the cloning of FP-tagged Kv1.3 constructs, a construct of the full length wild type Kv1.3 in the pCDNA3.1 mammalian expression vector was generated (Kv1.3-pCDNA3.1).

3.2.2   Internal Tagging with a HA-epitope

One major aim of this work included tracking the mobility of single Quantum Dot$^{\circledR}$-labeled Kv1.3 molecules on the cell surface. Hence, specific antibody-labeling of the channel was required. Attempts to use a commercially available polyclonal antibody (Sigma) directed against an epitope within the first extracellular loop of the α-subunit resulted in poor labeling, even when published protocols were followed carefully [Nicolaou et al., 2009]. Thus, I pursued a strategy for tagging the extracellular portion of the channel with a well-described epitope of Human influenza hemagglutinin (HA) [Pati, 1992].

Three positions for insertion of the tag were selected, two within the first extracellular loop (Kv1.3^{L253}, Kv1.3^{Q271}), the third in the last (Kv1.3^{A421}). These positions were picked based on current knowledge of Kv1.3 and/or comparable ion channel proteins: Kv1.3^{L253} and Kv1.3^{Q271} lie within or are close to the epitope recognized by the abovementioned antibody, binding of which reportedly did neither interfere with the channel's cellular distribution nor its electrophysiological properties [Nicolaou et al., 2007a, Nicolaou et al., 2009]. Kv1.3^{A421} is analogous to a site of the L-type voltage-gated calcium channel, which has successfully been tagged with the HA-epitope [Altier et al., 2002]. The HA-epitope was inserted into both, non-tagged and FP-tagged variants (see Section 2.3.11).

Living (i.e. non-fixed, non-permeabilized) COS-7 cells expressing variants of Kv1.3^{HA}-EGFP were subjected to ms-α-HA antibody staining (Fig. 6(C)). A membrane-confined labeling with the antibody in cells that display EGFP-signal throughout the soma indicates HA-tagging of Kv1.3$^{HA(Q271)}$-EGFP and successful display thereof on the cell surface.

Hence, I was able to generate a construct of Kv1.3 extracellularly tagged with an epitope for Human influenza hemagglutinin (HA).
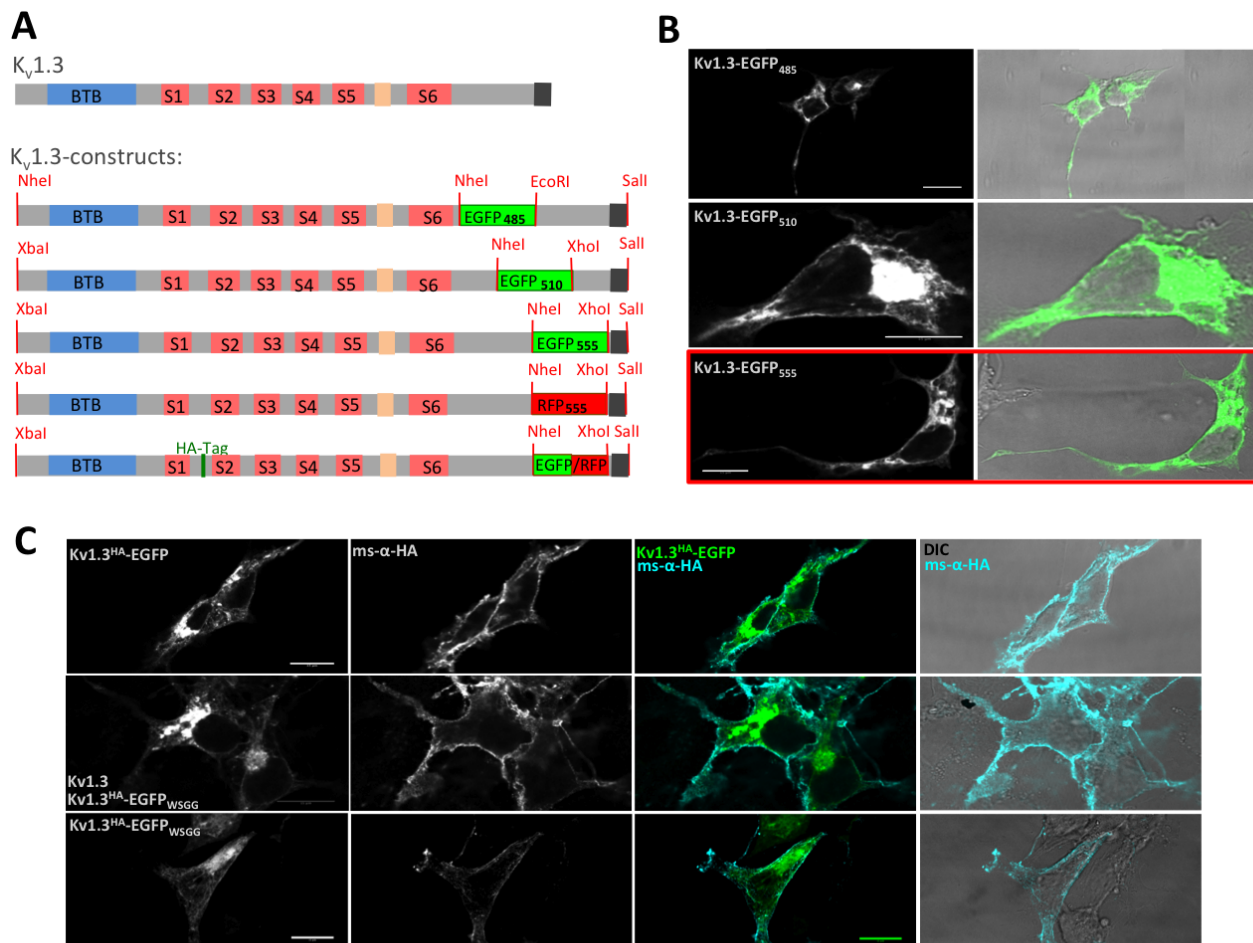
Figure 6: **Establishing Functional Kv1.3 Constructs – Expression and Localization Tests. (A)** Scheme of DNA with encoded protein domains of the main Kv1.3-FP-constructs cloned in this work. Structure: BTB-domain, a multimerizing domain thought to be crucial for homotetramerization of the α–subunits. S1-S6, transmembrane spanning domains, with the selective K^+ ion filter being formed by S5 and S6. The four C-terminal amino acids FTDV are presumed to be bound by the PDZ domain of scaffolding proteins, such as MAGUKs. Red lines and letters indicate restriction sites used for cloning of the DNA constructs. EGFP, enhanced green fluorescent protein, inserted into the C-terminus of Kv1.3 at several positions (tagging positions on protein level implied by lowerscript numbers). mRFP, monomeric red fluorescent protein inserted into the Kv1.3 C-terminus at position 555, as tested by expression studies with EGFP–tagged versions of Kv1.3. HA–epitope for labeling of the extracellular entity of the channel protein. All fluorescence/HA–tagged versions of Kv1.3 are also available as C-terminal PDZ-binding mutant carrying the four C-terminal amino acids WSGG instead of FTDV. **(B)** Expression of the three respective Kv1.3 constructs carrying EGFP at different sites within its C-terminus, corresponding to schemes in (A). EGFP-tagged constructs were co-expressed with Kvβ2 and full length Kv1.3-pCDNA3.1 to ensure its localization at the plasma membrane. **(C)** Expression of Kv1.3^{HA}–EGFP and the respective WSGG-binding mutant in COS-7 cells. Cells expressing Kv1.3^{HA}–EGFP were labeled with ms-α-HA antibody before fixation. Hence, antibody labeling of the membrane indicates surface expression of an HA-tagged channel. Scale bars 50μm.

3.2.3 Establishing Kv1.3 Lacking a PDZ-binding Motif

Examining the impact of the interaction between Kv1.3 and MAGUKs on Kv1.3 was to be assessed through several strategies. One approach was to mutate the channel's C-terminal PDZ-binding motif (see Section 2.3.11).

Expression studies in COS-7 cells were performed for the mutated channel co-expressed with or without wild type subunits. Kv1.3$^{\text{HA}}$-EGFP$_{\text{WSGG}}$ (binding mutant Kv1.3) combined with untagged wild type channel displayed a subcellular distribution indistinguishable from that of Kv1.3$^{\text{HA}}$-EGFP, i.e. recruitment to the plasma membrane, as indicated by successful live HA-staining next to retainment in perinuclear regions (Fig. 6(C), mid panel)

3.2.4 Electrophysiological Testing of Previously established Kv1.3-constructs

In order to check for functional integrity of the Kv1.3 constructs, electrophysiological properties thereof were assessed. The experiments and analyses shown here were conducted by Carina Fürst in the lab of Dr. Martin Heine. Since the results of these measurements were crucial for the continuation of the project, the data are included in this work.

Wild type control Kv1.3 (Kv1.3) or Kv1.3$^{\text{HA}}$-EGFP was cotransfected with Kvβ2 into HEK293T cells. An EGFP expression vector served as transfection control for Kv1.3. To test if antibody labeling of living cells interferes with channel function, cells expressing Kv1.3$^{\text{HA}}$-EGFP were additionally labeled with msα-HA (1:200) for 5 min at 37 °C.

Transfected cells were subjected to whole cell patch clamp potassium measurements. The I-V relationship displays no change in activation kinetics of Kv1.3$^{\text{HA}}$-EGFP or antibody labeled Kv1.3$^{\text{HA}}$-EGFP when compared to control (Fig. 7(A)). Furthermore, no change in average potassium current passing through the membrane, indicated by the current density, were observed for both experimental setups compared to control (Fig. 7 (B); Kv1.3$^{\text{HA}}$-EGFP: 762.2 pA/pF $\pm$ 267.6 pA/pF; Kv1.3$^{\text{HA}}$-EGFP + msα-HA: 848.2 pA/pF $\pm$ 255.9 pA/pF; Kv1.3: 805.4 pA/pF $\pm$ 261.6 pA/pF) . Determining the inactivation kinetics, i.e. the mean time constant τ and steady state current, the tagged or tagged and antibody-labeled versions of Kv1.3 displayed no differences when compared to control (Fig. 7 (C): Kv1.3 $\tau = 0.3228$ s $\pm$ 0.0437 s; Kv1.3$^{\text{HA}}$-EGFP $\tau = 0.3775$ s $\pm$ 0.05 s, Kv1.3$^{\text{HA}}$-EGFP + msα-HA $\tau = 0.2670$ s $\pm$ 0.048 s / Fig. 7 (D); Kv1.3: 8.138 % $\pm$ 1.283 %; Kv1.3$^{\text{HA}}$-EGFP: 10.18 % $\pm$ 1.889 %; Kv1.3$^{\text{HA}}$-EGFP + msα-HA: 9.503 % $\pm$ 3.414 %).

In summary, no differences in activation kinetics (Fig. 7(A)), inactivation kinetics (Fig. 7(C), (D)) or standardized currents were found for the constructs generated in this work. Ergo, they can be used to study the cellular function of Kv1.3.
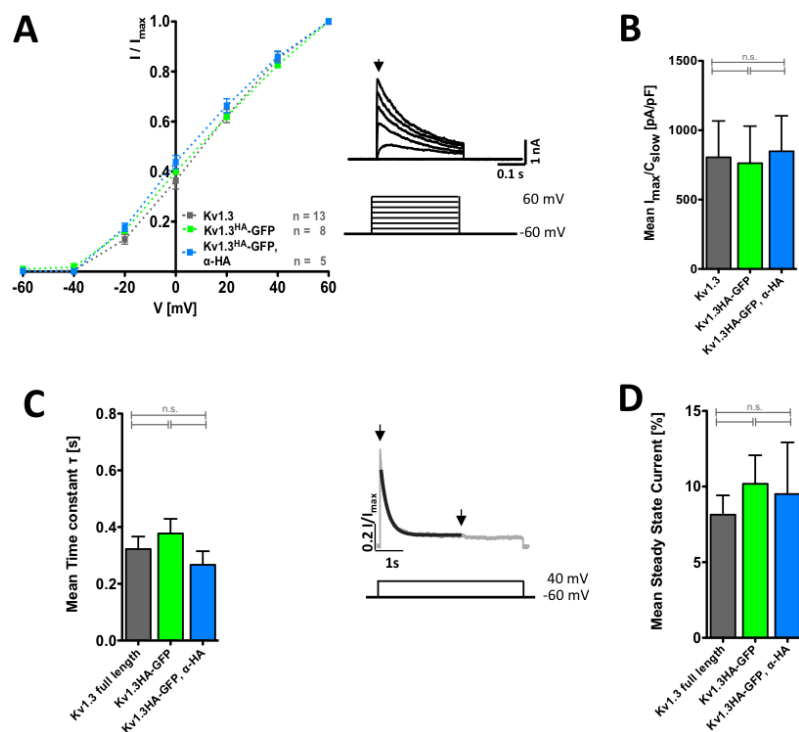
Figure 7: **Generation of Functional Kv1.3 Constructs – Electrophysiological Properties.** **(A)** Current(I)-voltage(V)-relationship for relative currents (I/I_{max}) at membrane potentials ranging from -60 mV to +60 mV (20 mV steps), delineating opening kinetics of the examined channel constructs. The arrow in the inset represents maximum current I_{max}. **(B)** Mean current density [pA/pF], calculated as I_{max} divided by capacitance c_{slow}, describing standardization of the current to cell size. **(C)** Mean time constant τ, defining the point in time when I_{max} is decreased by $^2/_3$, describes inactivation kinetics. Arrows in inset represent I_{Max} and the steady state current. **(D)** Mean steady state current as % of I_{max}

3.3 Interaction and Localization of Kv1.3 and Dlg1 in Mammalian In Vivo Systems

3.3.1 Bimolecular Fluorescence Complementation (BiFC) Assay

Bimolecular fluorescence complementation may be utilized for *in vivo* protein interaction studies, in which two non-fluorescent fragments of a fluorescent protein (FP) associate when they are brought in proximity to each other by an interaction between proteins fused to the fragments [Kerppola, 2008]. Thus, two proteins, each fused to a non-fluorescent fragment of a fluorescent protein, will yield fluorescence signal once they interact within the cell (Figure 8 (A)). The FP-fragments must have sufficient freedom of motion in the interaction complex to allow for frequent collision with each other to facilitate bimolecular fluorescent complex formation. Since it is difficult to predict the arrangement of the fluorescent protein fragments that will produce maximal signal, fusion proteins that produce optimal signal must be identified by empirical testing of several combinations thereof [Kerppola, 2008].

I used this method to (I) monitor the *in vivo* interaction of full length Kv1.3 with Dlg1 in a mammalian system and, (II) thereby rule out that the internal FP tag of Kv1.3 would interfere with binding to PDZ domains.

Based on two N-terminal (V_N155 and V_N173) fragments and one C-terminal (V_C156) fragment of the FP Venus (which has an emission-/excitation spectrum close to that of Yellow Flu-

46
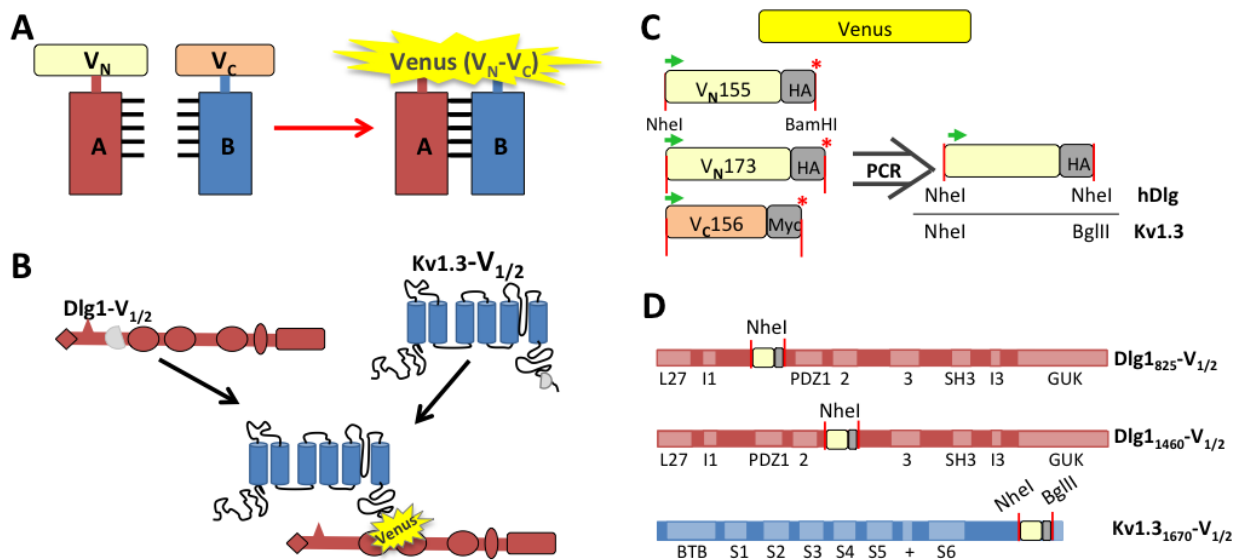
Figure 8: **Schematic Illustration of the Employment of BiFC for the Interaction of Dlg1 and Kv1.3.(A)** Explanatory sketch for BiFC. **(B)** Basic model of the BiFc used for Kv1.3 together with Dlg1 with the fluorescent protein Venus-YFP. **(C)** Overview of the fragments of Venus used as templates for PCRs in order to achieve the required reading-frames and enzyme sites for cloning into Dlg1 and Kv1.3, respectively. Two different N-terminal fragments of Venus (V_N) and one C-terminal fragment (V_C) were made available to us. Each fragment was C-terminally tagged with a HA- (V_N) or Myc- (V_C) tag, followed by a STOP codon (red asterisk) and surrounded by recognition sites for NheI and BamHIII. For my purposes, the STOP codon was eliminated along with changing restriction enzyme recognition sites. Via PCR and subcloning, I generated suitable V_N-HA and V_C-Myc fragments with the desired restriction enzyme sites (noted below the PCR-fragment depiction for each target gene). **(D)** Schematic depiction of the final constructs used for evaluating BiFC. Dlg1 was tagged at two different positions surrounding the binding region for the C-terminal 4 amino acids of Kv1.3, namely the PDZ1-2 domain tandem. Kv1.3-V_F was generated by exchanging EGFP of Kv1.3-EGFP for V_F. Each of the three V_F-variants (V_N155, V_N173, V_C156) was ligated into every variant of Dlg1 and Kv1.3 shown here.

orescent Protein (YFP)), various pairs of tagged Kv1.3 and Dlg1 were tested for reconstituted yellow fluorescence upon co-transfection into COS-7 cells. Fragments (V_F: Venus fragment) were inserted at position '555' in Kv1.3 and right before or after the PDZ1-2 tandem in Dlg (see Section 2.3.11). Myc- or HA-epitopes conjugated to the V_N or V_C fragments allowed for control stainings to validate expression. Each combination of the Kv1.3- and Dlg1-constructs was co-transfected into COS-7 cells.

A panel with representative fluorescent images of the screen for reconstituted Venus-signal is depicted in Fig. 8. All Dlg1-V_F constructs were expressed efficiently as indicated by strong HA- or Myc-antibody stainings. In contrast, only Kv1.3-V_C but not Kv1.3-V_N variants were clearly detectable by antibody staining.

Several combinations yielded a YFP-signal, yet with clearly different intensities. A particularly robust Venus-signal was obtained when Kv1.3-V_C was combined with expression of Dlg1[825-V_N155] (Fig.9, red frame). Notably, YFP-signal there is also present at the plasma
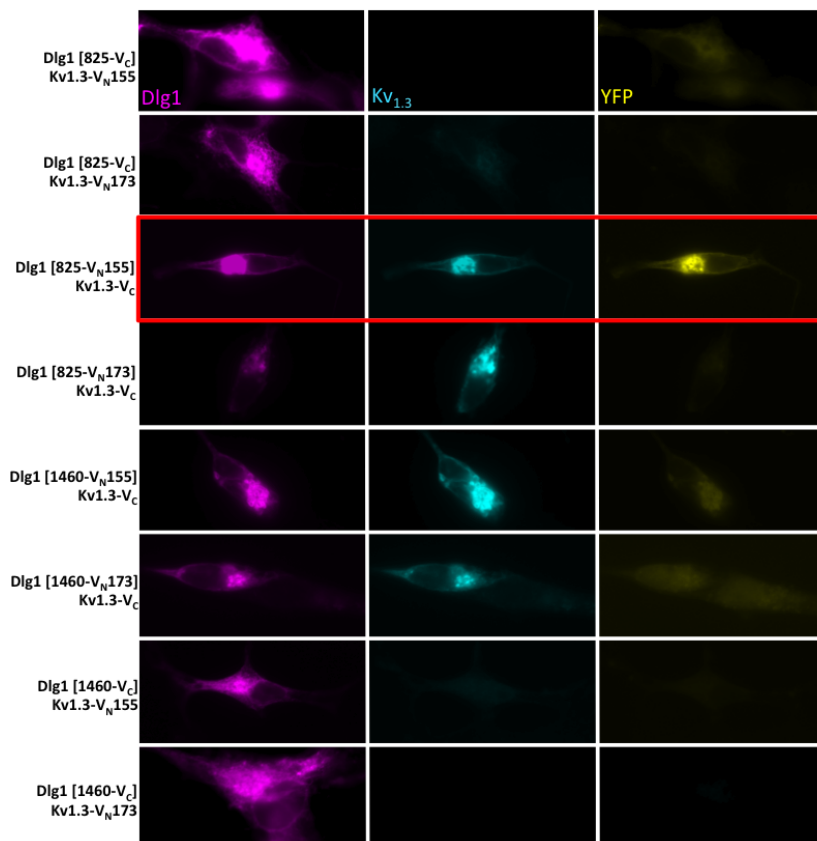
Figure 9: **Screen for Bimolecular Fluorescent Complementation of the FP Venus.** Coexpressed COS-7 cells with each variant of a V_F-tagged Kv1.3 and Dlg1. Cells were stained for Myc (V_C-) or HA (V_N-constructs) as a control for transfection and proper expression of the proteins. For the sake of convenience, color codes of the stainings were kept according to the interacting protein expressed, not the epitope-tag stained: Dlg1 constructs and Kv1.3-constructs, respectively. YFP-signal is only visible when the combination of the two V_F-tagged interacting proteins was sufficient for the FP to be complemented. The red frame indicates the combination of Kv1.3-V_F− and Dlg1-V-$_F$- co-expression that presented with the best possible YFP-signal.

membrane. Two YFP-yielding combinations displayed a rather high YFP-signal within the perinuclear region, where much of Kv1.3 and Dlg1 co-localize when stainings for both proteins are present within the cell. It is not necessarily expected that Kv1.3 recruits Dlg1. Hence, I speculated for this strong co-localization to be due to the inability of the two interacting proteins to dissociate once YFP has been reassembled [Morell et al., 2007]. However, co-expression of the proteins, each tagged with an individual FP (Kv1.3^{HA}-mRFP and EGFP-Dlg1), also displayed strong co-localization within the perinuclear region along with moderate co-localization in other parts of the cell, e.g. the plasma membrane (Fig. 10(A)). Eliminating Kv1.3's interaction with PDZ domains diminishes co-localization of the proteins anywhere in the cell (Fig. 10(B)). Moreover, enrichment of EGFP-Dlg1 in perinuclear regions is absent, yet plasma membrane insertion of Kv1.3 remains intact.

In summary, I successfully employed the BiFC-approach for validation of the *in vivo* interaction between Kv1.3-FP and Dlg1 in a mammalian system. Furthermore, there is evidence for a role of Kv1.3 in retaining Dlg1 in perinuclear regions.
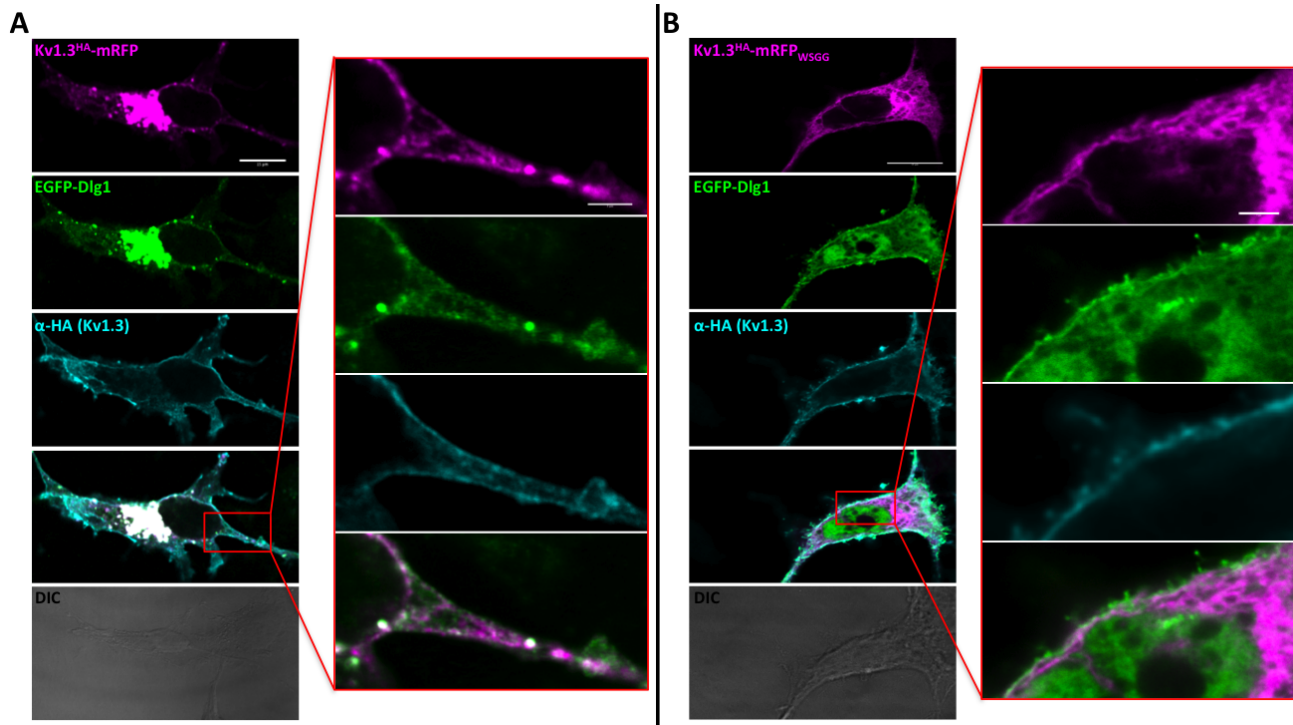
Figure 10: **Co-localization Studies in COS-7 Cells.(A)** The left panel (scale bar 50μm) illustrates representative pictures of Kv1.3^{HA}-mRFP (1st row) co-transfected with EGFP-Dlg1 (2nd row). To determine the transport of Kv1.3 to the plasma membrane, living cells were labeled for the extracellular HA-tag of Kv1.3^{HA}-mRFP before fixation(3rd row). Overlay of the three acquired channels is depicted in row four, DIC picture in row five. The right panel (scale bar 10 μm) details a zoomed fraction of this cell. It shows in a downward order: Kv1.3^{HA}-mRFP, EGFP-Dlg1, HA-labeling of Kv1.3^{HA}-mRFP and an overlay of the first two acquired channels (Kv1.3^{HA}-mRFP and EGFP-Dlg1) **(B)** The left panel displays a representative cell of Kv1.3-^{HA}-mRFP-$_{WSGG}$ co-transfected with EGFP-Dlg1 in matching order with (A), with the right panel depicting its respective zoomed fraction .

3.4 shRNA-mediated Knock-Down of Dlg1 and PSD-95

For assessing the role of the Kv1.3-Dlg1-interaction on Kv1.3's localization, mobility and function it was planned to interfere with this interaction by (I) mutating the PDZ binding motif in Kv1.3. (section 3.2.3) and (II) reducing the expression of Dlg by shRNA. Moreover, PSD-95 was later included in this type of analyses as [Szílagyi et al., 2013] reported a robust expression of this Dlg-like MAGUK in Jurkat T cells.

To select suitable target sites, online supporting programs of Ambion$^{®}$ (Dlg1, no link available, because inactive by now) and InvivoGen$^{®}$(PSD-95, SiRNA Wizard, `http://www.invivogen.com/sirnawizard/`) were employed. For both Dlg1 and PSD-95 three target sites distributed along the entire mRNAs of Dlg1 or PSD-95, respectively (Fig.11 (A) and (E), upper panels), were selected after ruling out the presence of OFF-target sequences with =16 bp matches (see Section 2.3.11).
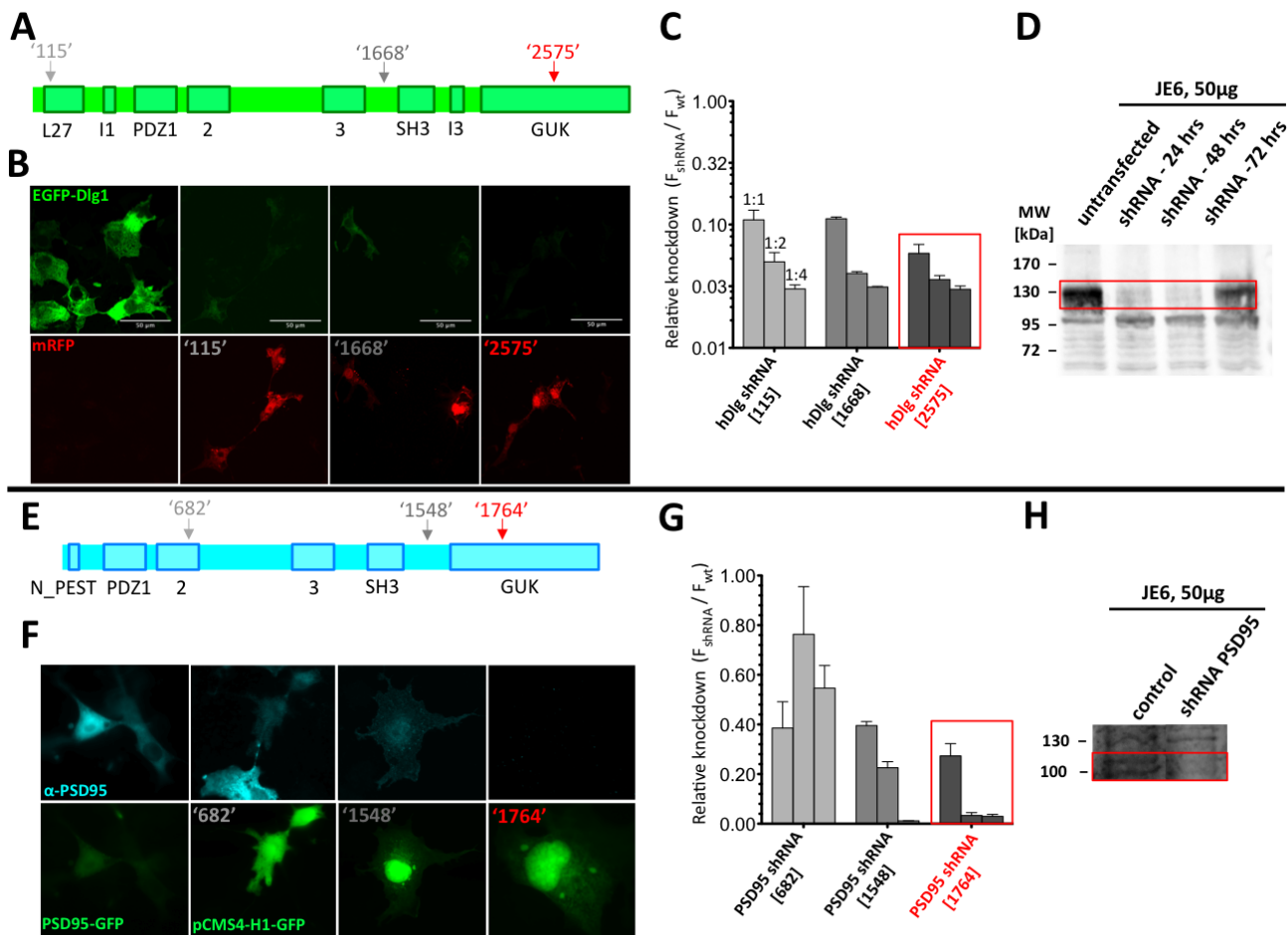
Figure 11: **shRNA-mediated Knock-Down of Dlg1 and PSD-95(A)-(D)** shRNA-mediated knock-down of Dlg1 and **(E)-(H)** PSD-95. **(A)** Full length mRNA of Dlg1 including noted protein domains. Numbers with arrows indicate the positions of the selected targets for shRNA-mediated knock-down. **(B)** Exemplary pictures from the assessment of transfection and knock-down of Dlg1 in COS-7 cells via co-transfecting EGFP-tagged Dlg1 with pZoff Dlg1 shRNA-constructs in a 1:2 ratio. EGFP-Dlg1 expression in absence of knock-down vector (first row) represents the positive control, whose average fluorescence value was set to value 1 for assessment of relative knock-down. Scale bars 50μm. **(C)** Summary of the quantification analysis of the relative knock-down of EGFP-Dlg1 in COS-7 cells. Equal amounts of EGFP-Dlg1 were co-transfected with three different amounts of each of the shRNA-pZoff constructs (1:1, 1:2, 1:4). The shRNA that was used for further verification of knock-down is framed in red. **(D)** Further validation of shRNA-mediated knock-down of Dlg1 in Jurkat T cells using αDlg1-labeled Western Blot of equal protein amounts of cell lysates of untransfected control and 24h, 48h and 72h after electroporation with Dlg1-shRNA$_{2575}$-pCMS4. The red frame highlights the band corresponding to Dlg1 at $\sim$130 kDa. **(E)** Full length mRNA of PSD-95 including noted protein domains, numbers with arrows indicating the positions of the chosen targets for shRNA-mediated knock-down. **(F)** Exemplary pictures of the assessment of transfection and knock-down of PSD-95, where PSD-95 and pCMS4 PSD-95 shRNA are co-transfected in a 1:2 ratio. α-PSD-95 in absence of the knock-down control EGFP represents the positive control, whose average fluorescence value was set to value 1 for assessment of relative knock-down. **(G)** Summary of the quantification of the relative knock-down of PSD-95 in COS-7 cells. Equal amounts of PSD-95 were co-transfected with three different amounts of each of the shRNA-pCMS4 constructs (1:1, 1:2, 1:4). The shRNA that was used for further verification of knock-down is framed in red. **(H)** Further verification shRNA-mediated knock-down of PSD-95 in Jurkat T cells using Western Blot of equal protein amounts of lysates of uninfected control or PSD-95-shRNA$_{1764}$. The red frame highlights the band corresponding to PSD-95 at $\sim$ 105 kDa.

The respective shRNA sequences were expressed from the H1 promoter in the pZoff- or pCMS4-H1 vectors, which simultaneously express mRFP or EGFP to identify transfected cells. The shRNA constructs were co-transfected with plasmids encoding EGFP-Dlg1 or PSD-95 (Fig.11 (B) and (F), upper panels) and the intensity of EGFP-Dlg1 or PSD-95 immunofluorescence was determined as a read-out for the efficacy of shRNA-mediated knock-down. Except for one PSD-95-specific shRNA construct, all others were found to efficiently suppress overexpression of the respective Dlg1- or PSD-95 constructs (Fig. 11(C), (G)). Dlg1-shRNA[2575] and PSD-95-shRNA[1764] were selected for further experiments. Both shRNAs were tested for its effect on endogeneously expressed protein in Jurkat T cells. As depicted in Figure 11 D, Dlg1 was strongly reduced within 24h in Jurkat T cells transiently expressing the respective shRNA. PSD-95 was decreased in Jurkat T cells stably expressing its shRNA.

Thus, I was able to design and clone shRNAs effectively targeting the expression of Dlg1 and PSD-95 in both COS-7 cells and Jurkat T cells.

3.5   Towards Functional Approaches Regarding the Interaction

Several studies have suggested a role for Kv1.3 within the IS [Cahalan and Chandy, 2009], and a study by the Conforti group provided evidence that the channel enters the IS primarily through lateral movement in the plasma membrane [Nicolaou et al., 2009]. Diminished localization in the IS as observed in T cells from SLE patients [Nicolaou et al., 2007b] led to altered Ca^{2+} signaling including Ca^{2+} amplitudes upon antigen stimulation [Nicolaou et al., 2009, Nicolaou et al., 2010]. the exact mechanism by which Kv1.3 is localized to this site has yet to be elucidated. A recent study by [Szílagyi et al., 2013] points to the involvement of Dlg-MAGUKs in the enrichment of Kv1.3 at the IS and, interestingly, PSD-95 appeared to be more crucial than Dlg1 in this context. So far, however, it is not known whether an enrichment of channels by Dlg-like MAGUKs is based on regulation of its movement within the plasma membrane and/ or trapping of the channel at synaptic sites as it is most likely the case at the *Drosophila* NMJs (3.1.2). Moreover, localization dependency may be bidirectional as suggested by the recruitment of Dlg1 by Kv1.3. to intracellular compartments (3.3.1).

3.5.1   Single-Molecule Tracking of Kv1.3 Channels Extracellularly Tagged with Quantum Dots®

Recent studies have implicated protein-protein interactions to be a major determinant of the mobility of membrane-anchored proteins, like Neurexins [Neupert et al., 2015] or immunological Lck [Douglass and Vale, 2005], which may also account for their trapping within synaptic sites.

Hence, I reasoned that the surface mobility of Kv1.3 might be controlled through its binding to Dlg-like MAGUKs.

To address this hypothesis, I performed single molecule tracking of HA-labeled Kv1.3 with the Quantum Dot® (QD®) technique in COS-7 cells, since this system allows for easy genetic manipulation and measurement of mobility in adherent cells.

COS-7 cells were transfected with wild type or binding mutant Kv1.3$_{HA}$-constructs (Kv1.3$_{HA}$, Kv1.3$_{HA}$-EGFP or Kv1.3$_{HA}$-EGFP-$_{WSGG}$). Specific labeling of the HA-tag within the first extracellular loop of Kv1.3 with QDs allowed for imaging and subsequent analysis of the channel's movement (Fig.12 (A) and (B)). Further co-transfection with EGFP-Dlg1 or PSD-95-EGFP, or their respective shRNAs allowed for monitoring direct effects of each protein on the channel's mobility.
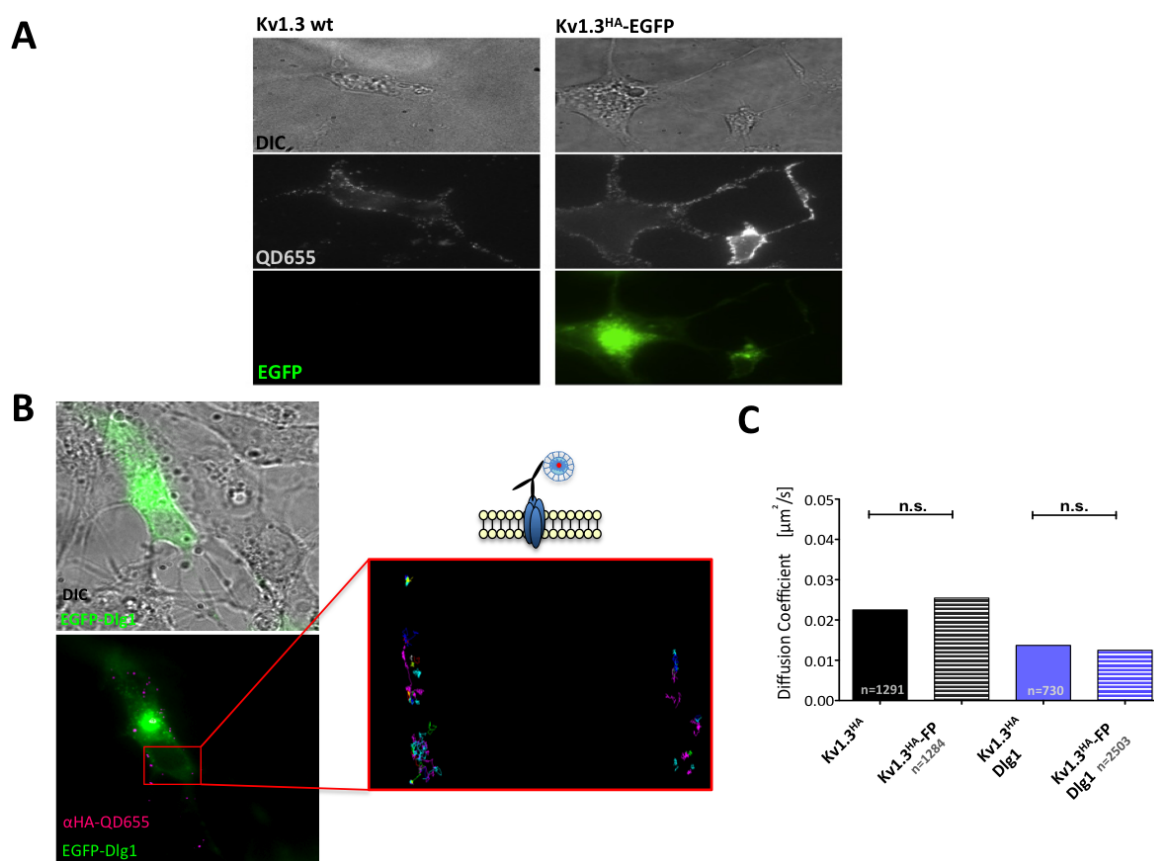
Figure 12: **Single Molecule Tracking of HA-tagged Kv1.3 with Quantum Dots®. (A)** Representative QD®-labeling of Kv1.3^{HA} constructs expressed in COS-7 cells. Upper row: DIC-images, middle row: images of QD®-labeled cells, lower row: expression of EGFP-constructs. **(B)** Illustration of specific labeling of transfected cells with QD®s, as indicated by presence of labeling of only one (Kv1.3-EGFP-expressing) cell in the field of view. The inset (red frame) shows the trajectories of single QDs, the upper scheme depicts the mode of Kv1.3^{HA}-labeling with primary antibody against the HA-tag of the channel and subsequent labeling with QD$^{®655}$-Fc. **(C)** Median diffusion coefficients (D [μm^2/s]) of single QDs of Kv1.3^{HA} vs Kv1.3^{HA}-EGFP alone or co-transfected with EGFP-Dlg1. Kruskall-Wallis Test (ANOVA) p < 0.0001

At first, it was of general interest whether the internal EGFP of Kv1.3$^{\text{HA}}$-EGFP interferes with the mobility of the channel. The median Diffusion Coefficients of QD-trajectories revealed no significant differences in the area touched per time between Kv1.3$^{\text{HA}}$ and Kv1.3$^{\text{HA}}$-EGFP alone (Fig. 12(C), black bars; 0.0225 μm^2/s vs. 0.0254 μm^2/s, respectively). Co-expressed with EGFP-Dlg1, both variants behaved virtually the same (blue bars; 0.0137 μm^2/s and 0.0125 μm^2/s for Kv1.3$^{\text{HA}}$ / Dlg1 and Kv1.3$^{\text{HA}}$-FP/Dlg1, respectively). Hence, values for Kv1.3$^{\text{HA}}$ and Kv1.3$^{\text{HA}}$-FP were pooled for future analysis, collectively referred to as Kv1.3$^{\text{HA}}$.

The impact of Dlg1 and PSD-95 on channel mobility is illustrated in Fig. 13 (A)-(C) and (D)-(F), respectively, showing analyses of the mean square displacement (MSD [μm^2], Fig. 13 (A)/(D)), median of diffusion coefficient (D [μm^2/s] Fig. 13 (B)/(E)) and populations for D (Fig. 13 (C)/(F)). The mean square displacement depicts the spatial dimension of channel movement over time, whereas the diffusion coefficient describes the general mobility of channels.

The MSD (Fig. 13(A)) over a period of 1s revealed that, compared to control, co-expression of Dlg1 led to a decreased averaged explored area (final values at 1.05s: 0.121 μm^2 $\pm$ 0.004 μm^2 vs. 0.077 μm^2 $\pm$ 0.004 μm^2, respectively), whereas expression of the Kv1.3 binding mutant (Kv1.3$^{\text{HA}}$-$_{\text{WSGG}}$) resulted in a larger exploited area (0.163 μm^2 $\pm$ 0.011 μm^2). Importantly, Kv1.3$^{\text{HA}}$ combined with Dlg1-shRNA yielded values very similar to those of the binding mutant (0.164 μm^2 $\pm$ 0.009 μm^2).

These results were mirrored in the calculated median of D (Fig. 13(B)). Kv1.3$^{\text{HA}}$ co-expressed with Dlg1, compared to control, yielded a significantly lower mean value for D (0.0132 μm^2/s versus 0.0236 μm^2/s), whereas expression of the mutant channel and wild type channel combined with Dlg1-shRNA resulted in significantly higher Ds (0.0452 μm^2/s and 0.0349 μm^2/s, respectively, vs. control 0.0236 μm^2/s). The higher value for the mobility of the binding mutant compared to wild type channel combined with Dlg1-shRNA was not significant, but there remained a tendency for a more mobile mutant.

Normalizing the diffusion coefficient distribution revealed three distinct populations, indicated by three occurring peaks (Fig. 13(C); immobile -, less mobile -, mobile fraction; from left to right). Compared to control, channels co-transfected with Dlg1 are shifted towards the immobile fraction, whereas the PDZ-binding mutant and Kv1.3 in combination with Dlg1-shRNA tended to be mobile. Particularly, a high peak in the mobile fraction for Dlg1-shRNA stood out, whereas the PDZ-binding mutant channel's less mobile population shifted toward a mobile fraction as a whole.

The effects of PSD-95 co-expression on channel mobility were highly similar to those of Dlg1 (Fig. 13(D)-(F)). Compared to control, co-expressing the channel with PSD-95 showed a de-
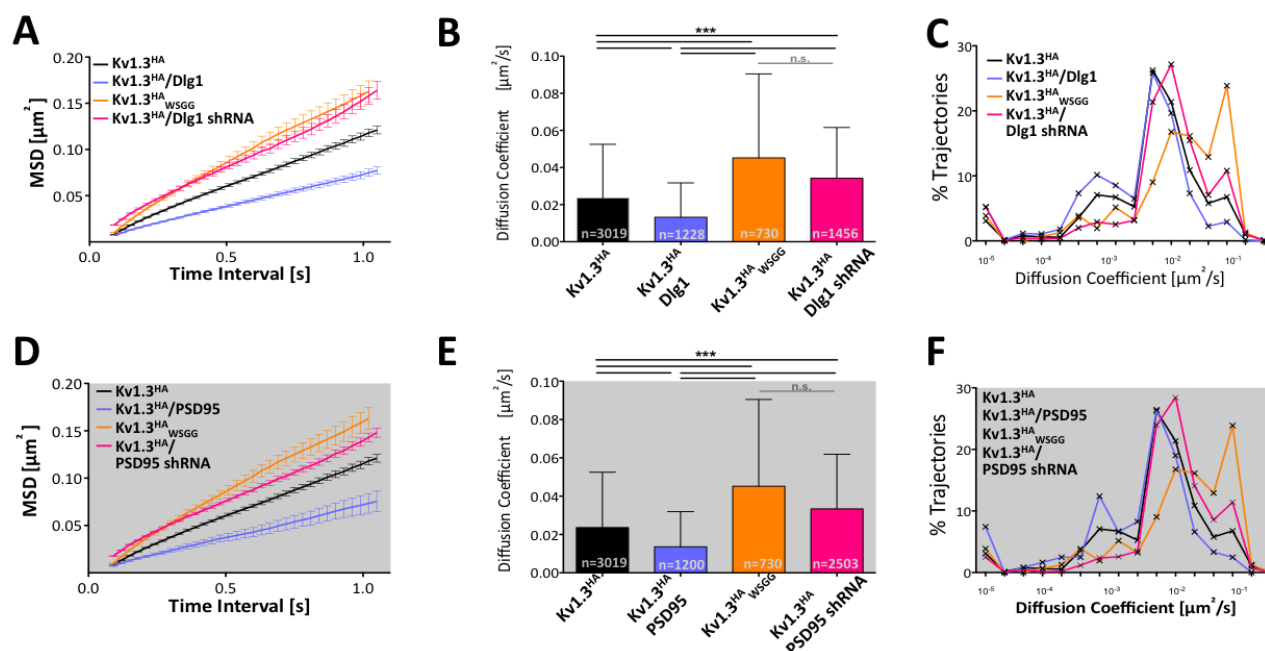
Figure 13: **Single Molecule Tracking of HA-tagged Kv1.3 in COS-7 cells - Dependency of its Mobility on Dlg1 and PSD-95. (A)-(C)** The effects of Dlg1 and **(D)-(F)** PSD-95 on the mobility of Kv1.3. **(A)/(D)** MSD of Kv1.3 alone and the impact of the presence of absence of Dlg1 or PSD-95, respectively. **(B)/(E)** Medians and interquartile ranges of Kv1.3's D under the influence of the presence or absence of Dlg1 or PSD-95, respectively. Kruskall-Wallis Test (ANOVA): P< 0.0001, Dunn's multiple comparison test: *** p < 0.001 **(C)/(F)** The distribution of D for Kv1.3.

creased exploited area (final values at 1.05s: 0.121 μm^2 $\pm$ 0.004 μm^2 vs. 0.075 μm^2 $\pm$ 0.01 μm^2), whereas the binding mutant channel and wild type channel combination with PSD-95 shRNA resulted in a channel showing similarly high MSDs (0.163 μm^2 $\pm$ 0.011 μm^2 and 0.148 μm^2 $\pm$ 0.004 μm^2, respectively)). Kv1.3^{HA} co-expressed with PSD-95 led to significantly lower median D values than control (0.0136 μm^2/s vs. 0.0236 μm^2/s, respectively), whereas the mutant channel or wild type channel and PSD-95 shRNA co-expression cause significantly higher Ds (0.0452 μm^2/s and 0.0334 μm^2/s, respectively). Like Dlg1, presence of PSD-95 led to a shift towards the immobile fraction when monitoring the normalized distribution of diffusion coefficients (Fig. 13 (F)).

In summary, the impact of both Dlg1 and PSD-95 on the mobility of Kv1.3 is of a restrictive nature.

3.5.2 Functional, Constitutively Expressing Jurkat T Cell Lines

The approach to electroporate Jurkat T cells with plasmid vector-based Kv1.3-constructs rendered to be ineffective in terms of transfection efficacy and expression. Hence, I cloned constructs
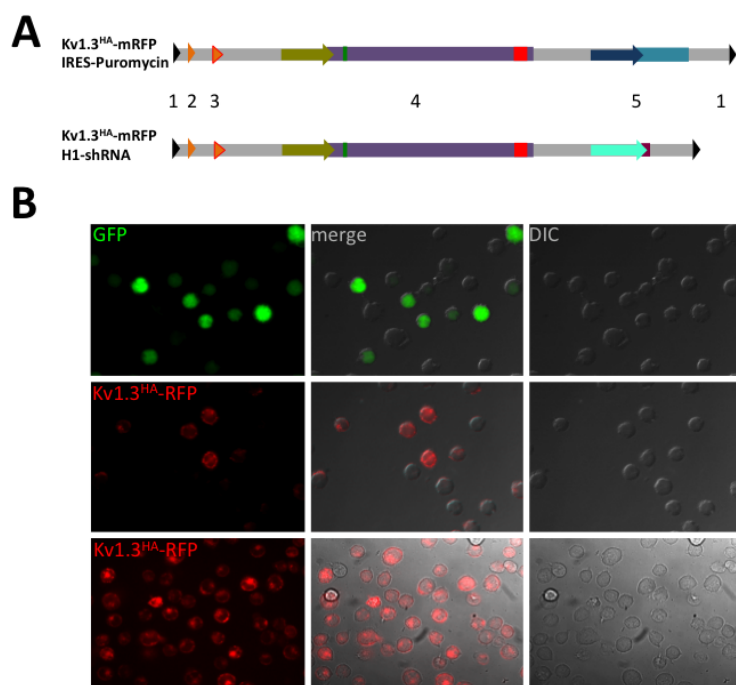
Figure 14: **Establishing Jurkat T Cell Lines Stably Expressing Kv1.3-Constructs with a HIV-Based Retroviral System.** **(A)** Exemplary scheme of HIV-based retroviral constructs harboring an expression cassette for Kv1.3^{HA}-mRFP-variants (4) under the control of the human Ubiquitin-Promoter (hUbc) combined with (5) either an IRES-Puromycin- or H1 promoter-[Dlg1/PSD-95] shRNA expression cassette. The genome-inserted fragment is flanked by a LTR-sequence (1) on either side and additionally harbors a psi packaging element (2) and a Rev response element (RRE, 3). **(B)** Representative depiction of Jurkat T cells after retroviral infection with supernatant of virus-producing HEK293T cultures via spinoculation for 30min. at 37°C(upper panel: EGFP control, middle panel: Kv1.3^{HA}-mRFP) and Jurkat T cell lines stably expressing the construct Kv1.3^{HA}-mRFP due to puromycin-selection (lower panel).

of the retroviral HIV-based FUGW-vector for wild type Kv1.3^{HA}-mRFP or binding mutant Kv1.3^{HA}-mRFP-$_{WSGG}$, which were combined with an IRES-Puromycin cassette or H1-shRNA-cassette for Dlg1 or PSD-95 (Fig.14(A), see Section 2.3.11). Combining Kv1.3$_{WSGG}$-expression with shRNA-mediated knock-down of Dlg1 or PSD-95, I aimed at accomplishing a complete lack of Kv1.3-binding to either one of the MAGUKs, since endogenous channels are still present and will be in mixed complexes with overexpressed mutant channel. This may enable the unfolding of specific roles for each MAGUK when compared to Kv1.3^{HA}-mRFP-$_{WSGG}$ alone. Virus-containing supernatant of Kv1.3-FUGW-transfected HEK 293T cells was used for spinoculation of Jurkat T cells. Subsequently, stable cell lines were generated by Puromycin-selection of cells containing the FUGW-vector-IRES-Puromycin expression cassette or magnetic-bead selection for the extracellular HA-tag of Kv1.3^{HA} / H1-shRNA-expressing cells. Each type of selection was highly efficient, leading to stably expressing Jurkat T cells lines (for examples, see Fig.14(B)).

The expression pattern of Kv1.3-mRFP constructs resembles that of Kv1.3-FP-expression in COS-7 cells: next to membrane localization of the channel, a strong FP-signal was detected in the perinuclear region (Fig.14(B)).

3.5.3 Localization Studies for Kv1.3 in Jurkat T Cells

Previous experiments in COS-7 cells have pointed to an impact of the interaction between Kv1.3 and Dlg1 on the localization of both proteins 3.3.1. Furthermore, Kv1.3 surface mobility was negatively influenced by presence of either Dlg1 or PSD-95 (3.5.1). However, a previous study demonstrated that enrichment of Kv1.3 at the IS of activated Jurkat T cells depends on the presence of PSD-95 but not Dlg1 [Szílagyi et al., 2013].

In order to elucidate the MAGUK-dependency of Kv1.3-IS-localization and vice versa, I de-
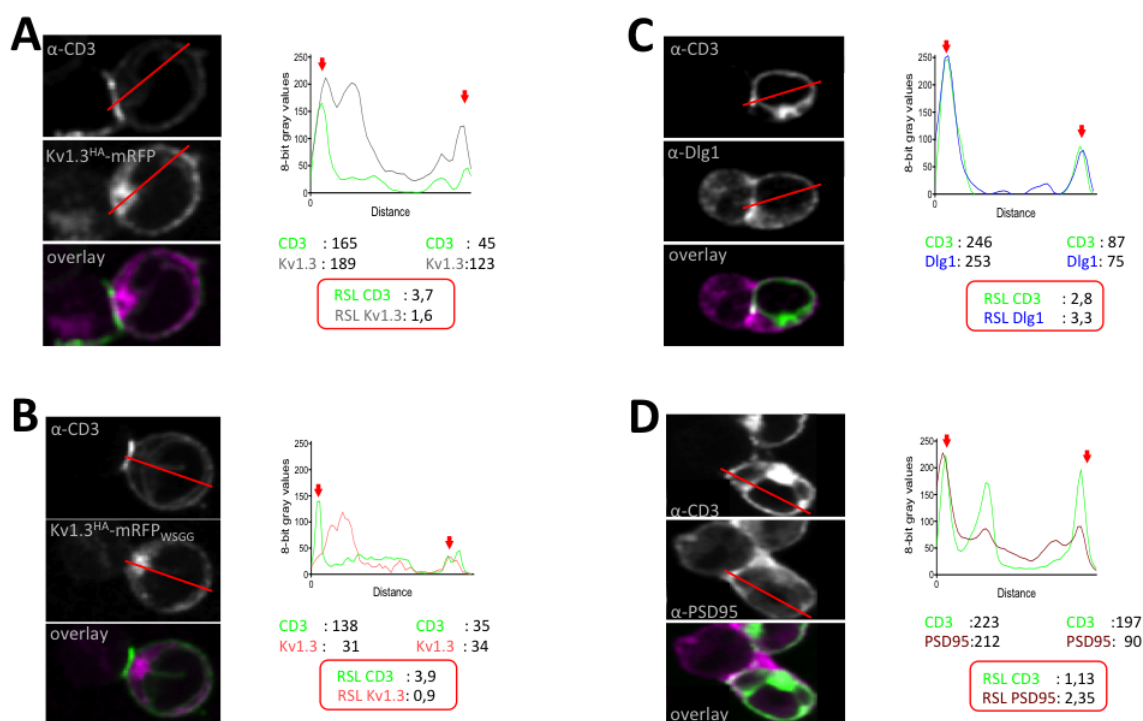
Figure 15: **Relative Synapse Localization of Kv1.3, Dlg1 and PSD-95 – Examples.** Representative fluorescent pictures of **(A)** overexpressed wild type Kv1.3, **(B)** binding mutant Kv1.3, **(C)** antibody-labeled endogenous Dlg1 and **(D)** PSD-95. Left upper panel: synapse control labeling for CD3, middle panel: respective protein (Kv1.3, Dlg1 or PSD-95), lower panel: merged images of the upper two. Right: plot of the grey values of both synapse control CD3 and respective protein along the red line of the left picture, red arrows indicating the grey values taken for synapse and the opposing plasma membrane as noted and exemplified below the plot. Respective RSLs are framed in red.

termined the Relative Synapse Localization (RSL) of Kv1.3^{HA}-mRFP, Kv1.3^{HA}-mRFP$_{WSGG}$, Dlg1 and PSD-95 to the IS formed between stably expressing Jurkat T cells (Kv1.3^{HA}-mRFP, Kv1.3^{HA}-mRFP$_{WSGG}$ either alone or combined with shRNA for Dlg1 or PSD-95) and SEE-loaded Raji B-Cells (Fig.15). In order to calculate the RSL, grey values were measured along an axis of Jurkat T cells crossing the IS (as indicated by CD3 control staining) as well as the opposing plasma membrane (Fig 18, right plots). IS grey values were divided by plasma membrane

grey values, yielding the amount of protein that is localized to the IS compared to the opposing plasma membrane. Hence, a calculated RSL value above 1 (a.u., artificial unit) for a protein of interest would indicate its accumulation at the IS relative to its presence at the opposing plasma membrane, whereas a value of 1 represents an equal distribution of the proteins and values below 1 point to an exclusion of the respective protein from the IS. Notably, both wild type and binding mutant Kv1.3 displayed a rather strong accumulation of the mRFP-signal just underneath the immunesynaptic membrane. It should be noted that this entity caused a discernible peak as exemplified in the grey value plot along the red line in Fig. 15 (A),(B) and therefore could be excluded from the analysis of Kv1.3 at the IS (for further interpretation of this phenomenon, see section 4.3).
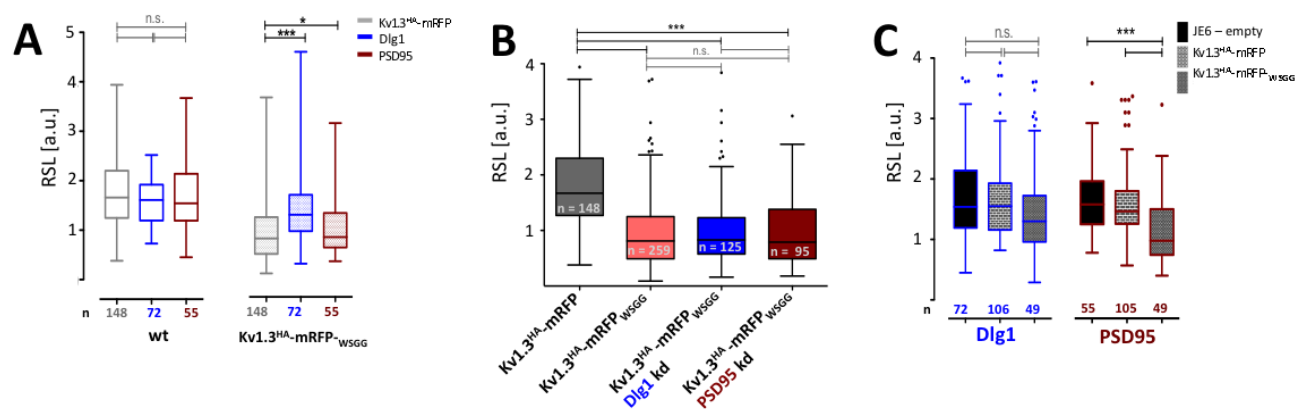
Figure 16: **Relative Synapse Localization of Kv1.3, Dlg1 and PSD-95 – Results (A)** Comparison of RSLs of Kv1.3^{HA}-mRFP, Dlg1 and PSD-95 in corresponding wild type (left) and Kv1.3^{HA}-mRFP$_{WSGG}$ cells (right), respectively. **(B)** Effect of Kv1.3-MAGUK-binding on Kv1.3's RSL, which was analyzed in Jurkat T cells stably expressing Kv1.3^{HA}-mRFP, Kv1.3^{HA}-mRFP$_{WSGG}$ and Kv1.3^{HA}-mRFP$_{WSGG}$ combined with Dlg1 or PSD-95 shRNA, respectively. **(C)** Correlation of the RSLs of Dlg1 (left) and PSD-95 (right) in wild type, Kv1.3^{HA}-mRFP- and Kv1.3^{HA}-mRFP$_{WSGG}$-expressing cells. Whiskers (A) and Tukey (B,C) Boxes; one-way analysis of variance (ANOVA): $p < 0.0001$, Bonferroni's multiple comparison test: * $p > 0.05$, *** $p < 0.001$

The median RSL of Kv1.3^{HA}-mRFP, Dlg1 and PSD-95 in their respective wild type situations, i.e. stably expressing Kv1.3^{HA}-mRFP for Kv1.3 or uninfected Jurkat T cells for antibody-labeled Dlg1 and PSD-95 were similar, indicating an about 1.6-fold enrichment at the Is for either protein (Fig. 16 (A); Kv1.3 1.66, Dlg1 1.61, PSD-95 1.54). In a Kv1.3 binding mutant expressing background, the RSL for the mutated channel and both MAGUKs was clearly reduced resulting in diminished enrichment for Dlg1 (1.30), and even in depleted for PSD-95 (0.84) and binding mutant Kv1.3 (0.81) at the IS (Fig. 16 (A)). No further decrease was observed when combining binding mutant Kv1.3 with shRNA-mediated knockdown for Dlg1 or PSD-95 (Fig. 16(B); RSL 1.67, 0.81, 0.83 and 0.79, respectively). On the other hand, overexpression of wild type Kv1.3 did not increase the IS enrichment of Dlg1 or PSD-95 compared to non-infected Jurkat T cells.

In summary, it is likely that Kv1.3 and its binding partners PSD-95 and Dlg1 show a localization interdepency.

3.5.4   Kv1.3 Mobility in Jurkat T Cells

Given the accessibility of HA-tagged Kv1.3 in the above-described single particle tracking experiments in COS-7 cells, I aimed at using this technique to study the mobility of the channel in Jurkat cells, in particular its dynamics and enrichment in the IS. Since trajectories of individual channels are difficult to monitor in non-adherent Jurkat cells and the plane of the IS is more or less perpendicular to the light axis on a conventional set-up, I employed TIRF microscopy. In this approach, Jurkat T cells expressing HA-tagged wild type or binding mutant Kv1.3 were pre-incubated with QD-coupled anti-HA antibody and then allowed to settle onto a αCD3/αCD28-coated glass cover slips to form IS-like specializations. Cells settled on non-coated cover slips were imaged to obtain baseline controls.

Compared to baseline control, the MSD (Fig. 17(A)) for QD®-labeled Kv1.3^{HA} over a period of 1s on activated cells revealed a tendency towards slightly increased explored area (final values at 0.9 s: $0.026\mu m^2$, $\pm$ 0.005 vs. $0.036\mu m^2$, $\pm$ 0.008, respectively; not significant).

In line with data from COS-7 cells (see section 3.5.1), binding mutant channels displayed significantly increased baseline explored area when compared to wild type ($0.050\mu m^2$, $\pm$ 0.006). As for wild type, compared to their respective baseline,, mutant channels display significantly elevated MSD upon activation ($0.050\mu m^2$, $\pm$ 0.006 vs. $0.068\mu m^2$, $\pm$ 0.010, respectively). Al-
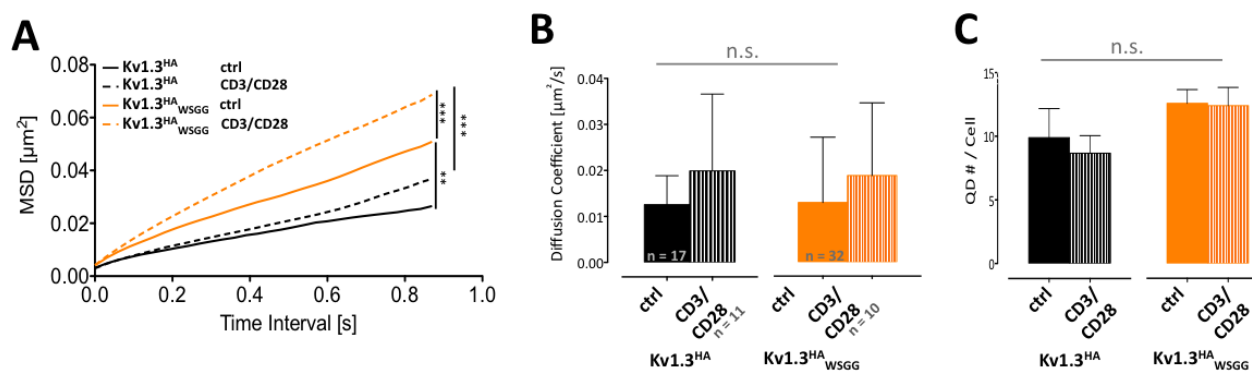
Figure 17: **Single Molecule Tracking of HA-tagged Kv1.3 in Jurkat T Cells - Dependency of its Mobility on the Activation Status of the Cell and its Binding to Endogenous MAGUKs.** **(A)** MSD of wild type and binding mutant Kv1.3 channels in baseline or αCD3/αCD28–stimulated conditions. One-way analysis of variance (ANOVA) of endpoints at 0.9 s $p < 0.0001$, Bonferoni's multiple comparison test: *** $p < 0.001$, ** $p < 0.01$ **(B)** Medians with interquartile range of Kv1.3's D depending on their binding status to endogenous MAGUKs and the activation status of the cell. T-test Kv1.3^{HA} ctrl vs CD3/CD28 $p = 0.0632$, Kv1.3^{HA}$_{WSGG}$ ctrl vs. CD3/CD28 $p = 0.1912$ **(C)** The mean number of QD®s (with SEM) present within the TIRF-interface for both, wild type and binding mutant Kv1.3 under control and αCD3/αCD28-stimulated conditions. T-test Kv1.3^{HA} ctrl vs CD3/CD28 $p = 0.6941$, Kv1.3^{HA}$_{WSGG}$ ctrl vs. CD3/CD28 $p = 0.9315$

though not statistically significant, similar trends may be observed for the calculated median of the diffusion coefficient (Kv1.3^{HA}: 0.0125 μm^2/s control vs. 0.199 μm^2/s αCD3/αCD28; Kv1.3^{HA}-mRFP$_{WSGG}$: 0.0137 μm^2/s control vs. 0.0199 μm^2/s αCD3/αCD28). A striking observation is that, in contrast to their respective MSD values, Kv1.3^{HA}-mRFP and Kv1.3^{HA}-mRFP$_{WSGG}$ reach the same D values within the IS (0.0199 μm^2/s) and display very similar diffusion coefficients in their control situation.

Noteworthy, the averageBPD number of QD$^{®}$s dwelling within the imaging focus did not increase upon αCD3/αCD28-stimulation in both, wild type and mutant channels. This indicates that QD$^{®}$-labeled channels were not able to enter or leave the contact site.

3.5.5 Functional Signaling Consequences of Eliminated Kv1.3-MAGUK-binding

Diminished accumulation of Kv1.3 at the IS leads to higher amplitude and prolongation of Ca^{2+} signals in Jurkat T cells and primary human T cells from SLE patients [Nicolaou et al., 2007a, Nicolaou et al., 2009, Nicolaou et al., 2010]. Lack of its binding partner Dlg1, however, had no consequences on Ca^{2+}-signaling in mice primary T cells [Stephenson et al., 2007]. In the course of my work, I observed that absence of Kv1.3-binding to MAGUKs leads to a significant decrease of the channel's accumulation at the IS in Jurkat T cells (Fig. 16 (B)). Hence, I aimed at unraveling the role of MAGUK-binding and MAGUKs itself on the Ca^{2+}-signal.

To this end, I performed calcium imaging experiments on Jurkat T cells expressing wild type or binding mutant Kv1.3, further combined with shRNA-mediated knock-down of Dlg1 or PSD-95, during activation with αCD3/αCD28-coated Dynabeads$^{®}$. In order to monitor [Ca^{2+}]$_i$, I loaded cells with Fura-2 and measured its emission at 510 nm after excitation at 360 nm and 380 nm (Fig.18(A)). Calculating the emission ratio of 360 nm, which signifies the dyes' "isosbestic point" and hence serves as loading control, and 380 nm, which decreases in fluorescence upon increasing [Ca^{2+}]$_i$, yields the relative [Ca^{2+}]$_i$ level (Fig.18(B)). The resulting traces were analyzed for non-activated baseline levels, baseline-peak-difference (BPD) – characterizing the relative initial influx of calcium across the membrane – , rise time and decay time of αCD3/αCD28-induced peaks (Fig.18(C) and (D)).

Normalized baselines of non-activated cells displayed significantly higher [Ca^{2+}]$_i$ levels in cells expressing Kv1.3-constructs compared to uninfected control cells (Fig.19(A)/(B): Kv1.3^{HA}-mRFP 1.139 $\pm$ 0.030; Kv1.3^{HA}-mRFP-$_{WSGG}$ 1.176 $\pm$ 0.034; Kv1.3^{HA}-mRFP-$_{WSGG}$ Dlg1 shRNA 1.164 $\pm$ 0.042; Kv1.3^{HA}-mRFP-$_{WSGG}$ shRNA PSD-95 1.173 $\pm$ 0.049 vs. control 0.9842 $\pm$ 0.029). However, no difference was observed between wild type Kv1.3 and the C-terminal binding mutant or its combination with Dlg1- or PSD-95-shRNA (1.139 $\pm$ 0.030; 1.176 $\pm$ 0.034; 1.164 $\pm$
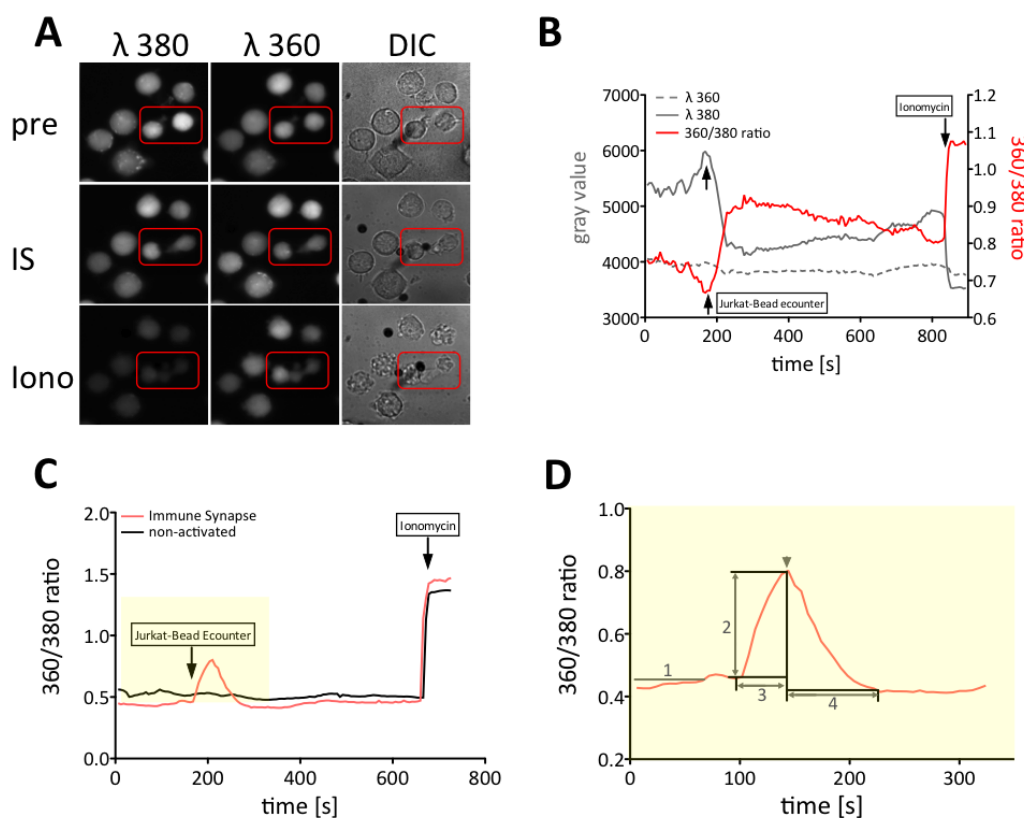
Figure 18: **Fura-2 Based Calcium Imaging in T Cells. (A)** Representative fluorescent pictures of Fura-2-loaded Jurkat T cells before (pre) and during stimulation (IS) with CD3/D28-coated Dynabeads, as well as after adding ionomycin. The red frame marks cells forming IS with beads. Surrounding cells, not encountering, served as baseline controls. **(B)** Demonstration of the calculation of the relative $[Ca^{2+}]_i$ of an IS-forming Jurkat T cell by calculating the 360nm/380nm ratio [a.u.]. **(C)** Representative $[Ca^{2+}]_i$ traces of a non-activated (black) and an activated, IS-forming Jurkat T cell. **(D)** Illustration of the parameters analysed from $[Ca^{2+}]_i$-traces, which are: **1** baseline **2** baseline-peak-difference (BPD), which is calculated via subtraction of the baseline value from the peak of one respective cell, yielding the normalized peak value, **3** rise time, which is the time passed between the first encounter of a αCD3/αCD28-coated bead and the peak and **4** decay time, which is the time passed between the peak and complete return to baseline level.

0.042; 1.173 $\pm$ 0.049; respectively).

Notably, cells expressing binding mutant Kv1.3 exhibited a significantly elevated BPD when compared to wild type Kv1.3, which does not further increase upon its combination with shRNA-mediated knock-down of Dlg1 or PSD-95 (Kv1.3^{HA}-mRFP-$_{WSGG}$ BPD 0.60 $\pm$ 0.03; Kv1.3^{HA}-mRFP-$_{WSGG}$ shRNA Dlg1 BPD 0.55, $\pm$ 0.016; Kv1.3^{HA}-mRFP-$_{WSGG}$ shRNA PSD-95 BPD 0.55, $\pm$ 0.019 vs. Kv1.3^{HA}-mRFP BPD 0.45, $\pm$ 0.012). The BPD of cells expressing wild type Kv1.3 was slightly, though not significantly lower from that of control cells (Fig.19(C); BPD 0.45, $\pm$ 0.019 vs. BPD 0.49, $\pm$ 0.012 , respectively).

Alternatively, main differences for the peak's rise and decay time were found between un-infected control versus overexpressing cell lines. Rise times for Kv1.3 overexpressing cells were
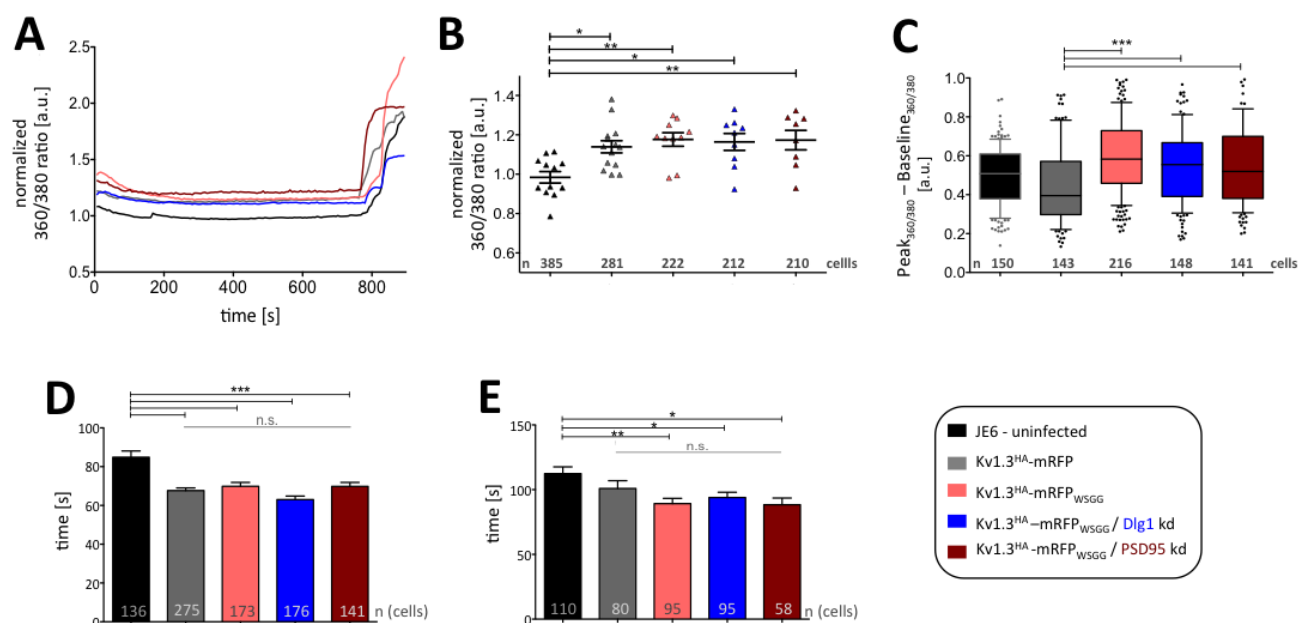
Figure 19: **Calcium Imaging in T Cells - Results. (A)** Mean baseline $[Ca^{2+}]_i$ traces of non-activated T cells of the employed Jurkat T cell lines (control, Kv1.3^{HA}-mRFP, Kv1.3^{HA}-mRFP-$_{WSGG}$, Kv1.3^{HA}-mRFP-$_{WSGG}$ Dlg1 shRNA and Kv1.3^{HA}-mRFP-$_{WSGG}$ PSD-95 shRNA. **(B)** Dotplot of mean baseline values with $\pm$ of non-activated T cells of the employed Jurkat T-cell lines. Each datapoint itself represents the mean baseline values of all cells measured within one stream (approximately 50 - 60 cells). **(C)** Comparison of BPDs (10-90 percentile Whiskers Box), **(D)** rise times (means with $\pm$), **(E)** decay times(means with $\pm$). One-way analysis of variance (ANOVA) $p < 0.0001$, Bonferroni's multiple comparison test: $^* p < 0.05$, $^{**} p < 0.01$, $^{***} p < 0.001$

significantly shorter than controls, displaying no significant differences among the Kv1.3 over-expressing cell lines (Fig.19(D): Kv1.3^{HA}-mRFP 67.64 s, $\pm$ 1.38 s; Kv1.3^{HA}-mRFP-$_{WSGG}$ 67.64 s $\pm$ 1.386 s; Kv1.3^{HA}-mRFP-$_{WSGG}$ Dlg1 shRNA 63.00 s $\pm$ 0.84 s; Kv1.3^{HA}-mRFP-$_{WSGG}$ shRNA PSD-95 69.81 s $\pm$ 2.06 s vs. control 84.86 s $\pm$ 3.22 sec). Likewise, decay times of Kv1.3 ex-pressing cells displayed generally lower values compared to controls. Wildtype Kv1.3's decay times tended to be shorter, and those of binding mutant Kv1.3 with or without shRNA for one of the MAGUKs were significantly shorter.

In summary, stable overexpression of Kv1.3 constructs in Jurkat T cells led to elevated $[Ca^{2+}]_i$ baseline levels. Most importantly, though, αCD3/αCD28-activated cells displayed elevated peak amplitudes when Kv1.3 was not able to bind MAGUKs. Furthermore, calcium kinetics were changed towards a faster and seemingly more efficient Ca^{2+} signaling in cells that overexpressed Kv1.3, as indicated by shorter rise and decay times. However, kinetics were not further changed for channels with compromised MAGUK binding with or without Dlg1 or PSD-95 shRNAs.

4 Discussion

During my PhD work, I aimed at: (1) validating the physical interaction between Kv1.3 and Dlg1 along with determining the impact of this interaction on the subcellular distribution of either protein with particular emphasis on the immune synapse, (2) assessing the surface mobility of Kv1.3 and its modulation by Dlg-like MAGUKs and (3) evaluating the Kv1.3-Dlg-like MAGUK interaction for its role in the control of Ca^{2+} signaling during TCA.

These aims were approached by (1) interaction studies in Y2H, (2) assessment of Dlg-dependent recruitment of a Kv1.3-reporter construct to *Drosophila* NMJs, (3) co-overexpression studies of wild type and binding mutant Kv1.3-mRFP with EGFP-Dlg1 in heterologous COS-7 cells, (4) localization studies of stably expressed wild type and binding mutant Kv1.3-mRFP as well as endogenous Dlg1 and PSD-95 at the IS of activated Jurkat T cells, (5) assessment of the impact of Dlg-like MAGUKs on Kv1.3's mobility via QD®-based single particle tracking of wild type and binding mutant Kv1.3 in both COS-7 cells and Jurkat T cells, (6) monitoring calcium signals in Jurkat T cells stably expressing wild type and binding mutant Kv1.3 along with knock-down of Dlg1 or PSD-95.

In summary, the data acquired during the course of my work support a role of the interaction in T cell calcium signaling.

4.1 Functional Expression of Tagged Kv1.3 Constructs

In this work, I generated a number of internally tagged Kv1.3 constructs (see Table 14) for imaging purposes such as localization, single molecule tracking and functional calcium studies.

Tagging highly sophisticated proteins like ion channels is demanding, as their cellular function or biochemical and electrophysiological properties may be disrupted easily [Zheng J., 2015, Park et al., 2009]. It was therefore important to carefully test for membrane localization, electrophysiological properties and interactions, particularly with MAGUKs.

Two modes of internal tagging were validated: (1) insertion of a HA-epitope within the first extracellular loop and (2) introduction of a FP 24 aa upstream of the PDZ binding C-terminus.

Intact surface expression was unambiguously demonstrated by immunoreaction against the extracellular HA-epitope on non-permeabilized cells and further affirmed by electrophysiological recordings (Figs. 6, 7).

HA-tagging had no effect on electrophysiological properties, even when antibody was bound to the epitope (Fig. 7). This finding is in line with [Nicolaou et al., 2009], who demonstrated unimpaired potassium currents when labeling the first extracellular loop with an commercially available antibody available from Sigma directed against the respective extracellular loop of

Kv1.3 itself. Also, FP positioning within the C-terminus did not render any differences. Several evidences from the literature suggest that PDZ binding of the C-terminal tail of membrane proteins depends on more than the canonical binding motif of 4 amino acids [Magidovich et al., 2006, Tonikian et al., 2008]. However, results from bimolecular fluorescence complementation experiments indicated that FP-tagging of the channel does not disturb its binding to Dlg1 (Fig. 9). Additionally, interaction was still detectable at the plasma membrane. Furthermore, a recent study implicated Kv1.3's binding to cortactin, an actin-polymerization factor, via a PXXP-motif (PQTP) within its C-terminus [Hajdu et al., 2015]. However, the FP tagging site is 74 aa downstream of the PQTP-motif, and therefore appears unlikely to interfere with cortactin binding.

Overexpression of transmembrane proteins often results in a profound enrichment at the ER and Golgi compartments [Kim et al., 1995, Waheed et al., 1997]. In fact, despite routinely co-expressing the β-subunit, next to discernible membrane localization, large amounts of Kv1.3 were found enriched at intracellular compartments, mostly within a perinuclear region (Fig. 6). This region, by comparison to published data, represents the Golgi apparatus [Spear et al., 2015].

4.2 Kv1.3-MAGUK-Interaction

Members of the MAGUK family constitute a submembranous scaffolding structure [Sakarya et al., 2007], harboring multiple protein-protein interaction domains, which enable them to bind several proteins at a time [Hanada et al., 2003, Kuriyan and Cowburn, 1997, Wu et al., 2000]. With their PDZ domains, they bind the 4 C-terminal amino acids (S/T-X-V) of transmembrane proteins like NMDA-receptor subunits 2A and B (ESDV) or the Shaker-type potassium channel Kv1.4 (ETDV) [Kim et al., 1995, Kornau et al., 1995, Niethammer et al., 1996, Hanada et al., 1997].

The actual interaction of the C-terminus (FTDV) of another member of the Kv family, Kv1.3, with the MAGUK Dlg1 was initially questionable due to an amino acid deviation within the proposed C-terminal binding motif. I was able to demonstrate an *in vivo* interaction of Kv1.3 with Dlg1 and map the interaction to the PDZ1-2 tandem of Dlg1 in *Drosophila* NMJ localization experiments and Yeast-two-Hybrid assays, with further validation in COS-7 cells employing the BiFC assay and co-expression of FP-tagged Kv1.3 and Dlg1 (Figs. 4, 5, 9, 10).

4.3 The Effects of Interaction on Subcellular Localization of Both Kv1.3 and MAGUKs

Dlg1 and PSD-95 have been proposed to exert distinct subcellular targeting and clustering behaviors on the Kv1 family members 1, 2 and 4 in COS-7 cells [Tiffany et al., 2000]. Co-expression studies had uncovered PSD-95-dependent trafficking and clustering of those channels to the plasma membrane, while Dlg1 completely retained them intracellularly. In the current work, however, upon co-expression with Dlg1, wild type as well as binding mutant Kv1.3 is trafficked to the plasma membrane in COS-7 cells (Fig. 9, Fig. fig:Fig8). Therefore, a distinct, PDZ binding-independent mechanism of membrane trafficking within the family of Kv channels is likely. Several candidates for intracellular motifs acting as tracking determinants have been discussed for channels of the Kv family [Vacher and Trimmer, 2012]. For example, a domain within the cytoplasmic N-terminus binds subunits of the microtubule motor kinesin 1 or 2, or the $Kv\beta$ subunits – also binding to the N-terminal fraction of the channels – can promote cell surface expression via effects on ER export.

On the other hand, the sub-cellular distribution of MAGUKs itself appears to be dependent on the presence of Kv1.3. Co-expression with wild type, but not mutant Kv1.3 in COS-7-cells strongly retains Dlg1 in the Golgi compartment, decreasing its plasma membrane localization (Fig. 10(A)). Expressed alone or together with binding mutant Kv1.3 (Figs. 11(B), 10(A)), it exerts a rather uniform distribution along the cell with stronger accumulation at the site of cellular membranes. This, along with demonstrating a role for Kv1.3 in retaining Dlg1 in subcellular compartments, also proves the absence of endogenous Kv1.3 in these cells. Concerning Kv1.3-dependent localization of MAGUKs, a similar observation has been made when co-expressing PSD-95 with the voltage-gated potassium channel Kv4.2 in heterologous cells. Here, the channel serves as shuttling device for PSD-95 to the plasma membrane [Wong et al., 2002]. The data presented herein advocate a sub-cellular localization dependency of both MAGUKs on the C-terminal binding motif of Kv1.3.

Regarding Kv1.3 enrichment at synaptic sites, I initially observed that Kv1.3's interaction with Dlg1 is responsible for its localization to the synaptic site of the *Drosophila* NMJ (Fig. 5). Additional localization studies at the IS of Jurkat T cells demonstrated that a lack of the ability of Kv1.3 to bind to MAGUKs does not only reduce, but exclude the channel from synapses (Figs. 15(B), 16(B)). [Hajdu et al., 2015] recently performed a similar experiment employing a Kv1.3 construct carrying a deletion of the C-terminus (Kv1.3ΔC), suggesting synaptic recruitment of Kv1.3ΔC. This obviously contrasts with the here presented finding. A possible explanation for this discrepancy is that their categorization of synaptic recruitment might indeed include an

accumulation of the channel protein at subsynaptic compartments such as the Golgi apparatus as discussed above. The Golgi apparatus is known to move to the IS [Allan et al., 2002]. Since a synaptic marker like CD3 was not included in their experiment, it is hardly possible to distinguish both regions from each other.

The accumulation of signaling-relevant proteins at the IS has been attributed to both the presence of lipid rafts and protein-protein interactions [Xavier et al., 1998, Douglass and Vale, 2005]. [Douglass and Vale, 2005] could show that proteins interacting with the costimulatory CD2, such as Lck, are trapped within the cSMAC, whereas absent interaction excludes certain molecules, such as CD45, from this site. Taking into account that Kv1.3 localizes to the IS under normal conditions and interacts with Dlg1, which is also linked to Lck [Hanada et al., 1997], the lack of interaction with the scaffolding molecule may be the reason for its exclusion from the synapse. Even though wild type endogenous α-subunits are present in Jurkat T cells, expression of the mutant subunit leads to exclusion of the channel from synapses, without additional effects upon its combination shRNA-mediated knock-down of Dlg1 or PSD-95 (Fig. 16(B)). The average number of endogenous Kv1.3 molecules within one Jurkat T Cell is 400 [Nicolaou et al., 2009]. Overexpressing the mutant α-subunit may by far exceed the number of its endogenous counterpart, resulting in Kv1.3 molecules that entail a ratio of mutant vs. wild type subunits larger than 1:1. Binding of Kv1.3 to the underlying MAGUKs may require multiple intact C-termini in order for it to be integrated into the scaffold's synaptic structure. Furthermore, I observed a decrease in Dlg1 and, even more so, PSD-95 at the IS in cells expressing the mutant Kv1.3 (16 (A)), which pointed to a localization interdependency of Kv1.3 and its binding partners. It may be speculated that converging mechanisms in T cells keep the two proteins in place only upon their interaction. For example, actin-based reorganization of the synapse plays a role in the formation of the IS. Indeed, studies have shown an actin-dependent localization at synaptic junctions for both Kv1.3 and Dlg1, which is mediated by the cytoskeleton-associated proteins cortactin and protein 4.1R, respectively [Hajdu et al., 2015, Hanada et al., 2003]. Disrupting the balance of Kv1.3-MAGUK interaction may interfere with such actin-based mechanismss, resulting in exclusion or decrease of both interaction partners. A recent study demonstrated an interaction of overexpressed Kv1.3 with caveolin in HEK293 cells [Pérez-Verdaguer et al., 2016]. This interaction is held responsible for targeting the channel to lipid rafts. Nevertheless, an interaction with submembranous proteins appears to be indispensible for Kv1.3 trapping at the IS.

In summary, my findings point towards a role for PDZ-binding in trapping the channel at the IS. Recently, [Szílagyi et al., 2013] demonstrated that only PSD-95 is responsible for enriching Kv1.3 at the IS. Due to the unexpected interplay in Kv1.3 and MAGUK enrichment at the IS, the experimental setup I chose can not really discern between the two MAGUKs in their role in

governing Kv1.3 accumulation at the IS. However, one should not rule out that Dlg1 take part in localizing Kv1.3 at the IS, since it interacts with and is able to localize Kv1.3 in at the NMJ of *Drosophila*.

In conclusion, a bilateral dependency of Kv1.3 and MAGUK proteins is likely. This finding strengthens a rather unattended view on transmembrane protein trafficking and localization, which until now was thought to rely on submembranous scaffolding molecules without by themselves exerting an impact on their interaction partners.

4.4   The Surface Mobility of Kv1.3

Recent single molecule tracking studies report an interplay between single membrane protein mobility within specific cellular compartments – like immune and neuronal synapses – and ambient circumstances, e.g. their binding to interaction partners or extracellular ion concentration [Douglass and Vale, 2005, Haggie et al., 2006, Heine et al., 2008, Neupert et al., 2015, Schneider et al., 2015]. For example, the lateral mobility of pre-synaptic αNeurexin is restricted by the presence of its secreted extracellular binding partner Neurexophilin in cultured mouse and rat neurons [Neupert et al., 2015]. Moreover, a study in Jurkat T cells revealed that immunesynaptic co-clustering of the proteins CD2, LAT and Lck in microdomains requires protein-protein interactions [Douglass and Vale, 2005]. However, studies on Kv1.3 demonstrated a dependency of its mobility on cholesterol composition of the plasma membrane as well as its association with caveolin of lipid rafts in HEK293 cells [O'Connell and Tamkun, 2005, Pérez-Verdaguer et al., 2016]

In the current work, I was able to prove a restrictive effect of the MAGUKs Dlg1 and PSD-95 on Kv1.3's lateral mobility in heterologous COS-7 cells (Fig. 13), validated in part in Jurkat T cells (Fig. 17 (A), (B)).

My results of single particle tracking indicate that both Dlg1 and PSD-95 are expressed in COS-7 cells and exert a role in regulating the channel's surface mobility. Furthermore, they appear to regulate channel mobility in a dose-dependent manner. Elevated spatial movement and mobility of overexpressed binding mutant compared to overexpressed wild type Kv1.3 in COS-7 cells (Fig. 13 (A), (B)) speak for the presence of endogenous PDZ-containing proteins in these cells, possibly of the MAGUK family. Endogenous Dlg1 is known to be present in COS-7 cells [Peiretti et al., 2003], but no such finding has been made for PSD-95. However, combining wild type Kv1.3 with shRNA for either Dlg1 or PSD-95 results in a channel that is significantly more mobile than wild type channel alone, but less mobile than the binding mutant

Kv1.3. Compensation by the respective other MAGUK may account for this effect in knock down of Dlg1 or PSD-95, each of which I showed to be efficient in COS-7 cells and Jurkat T cells. Nevertheless, poor Western Blot quality on samples from PSD-95 shRNA-infected Jurkat T cells - i.e. high background signal - leaves room for doubting PSD-95 knock down-efficiency. Moreover, PDZ domains of other proteins likely to be expressed in COS-7 cells – like MAGI1-4 – are also candidates, according the C-terminal motifs they are able to bind [Tonikian et al., 2008].

The effects on wild type Kv1.3 seen in combination with overexpression or shRNA-mediated knock-down of either Dlg1 or PSD-95 in COS-7 cells imply a role for both in exerting a role in controlling the mobility of the channel in a dose-dependent manner. (Fig. 13 (A), (B)). Comparing single molecule tracking results from COS-7 cells with RSL data from Jurkat T cells, it is not plausible that MAGUKS regulate Kv1.3 mobility in a dose dependent manner(Fig. 13), yet combining the binding mutant channel with shRNAs of either MAGUK does not increase its exclusion from the synapse (Fig. 16(B)). However, [Schneider et al., 2015] offer a valid explanation for this phenomenon by showing that general mobility and subcellular confinement of a transmembrane protein do not need to be congruent.

Data of populations of channels sorted according to their diffusion coefficients underline a shift among the fractions, which depends on the amount of scaffolding protein within the cell (shRNA mediated knockdown vs. endogenous and over-expression of both Dlg1 and PSD-95; Fig. 13 (C) and (F)). These findings are in line with mobility data for another PDZ-binding protein, cystic fibrosis transmembrane conductance regulator (CFTR), which is highly immobile when moderately expressed in several cell lines, but becomes more mobile when diminishing its ability to interact with PDZ domains or increasing its abundance at the surface [Haggie et al., 2006].

In this work, I successfully established single molecule tracking of QD®-labeled Kv1.3^{HA} in stably expressing Jurkat T cells while performing TIRF microscopy (Fig. 17(A) and (B)). Thereby, the mobility of molecules moving within the proximity of the glass cover slip was acquired, which enabled me to trace single surface molecules on usually non-adherent cells under control conditions (uncoated coverslips) and during the formation of the IS (αCD3/αCD28– coated coverslips). Compared to similar experiments in heterologous COS-7 cells expressing Kv1.3^{HA} constructs, the measured parameters were smaller. This may be assigned to both the smaller size of the observed cells and Kv1.3's entanglement within its actual molecular network in Jurkat T cells, which in turn may have a restrictive effect on its mobility (e.g. see [Heine et al., 2008, Schneider et al., 2015] for mobility differences in extra-synaptic versus synaptic calcium channel mobility) .

In general, Kv1.3's binding to MAGUKs in Jurkat T cells appears to regulate the area it explores, but not its general mobility (Fig. 17 (A), (B)). Kv1.3 holds a specific function within T cells and its association within molecular frameworks is most likely to be more elaborated than when expressed in heterologous cell lines [Sewing et al., 1996, Hanada et al., 1997, Szílagyi et al., 2013, Hajdu et al., 2015]. I therefore conclude that, in T cells, binding to MAGUKs mostly regulates its spatial movement, whereas its general mobility is governed by distinct molecular complexes, e.g. its association with the accessory β-subunit [Gulbis et al., 1999, McCormack et al., 1999].

Notably, the channel's spatial movement and general mobility are elevated during the formation of the IS for both the wild type and binding mutant (Fig. 17 (A), (B)). This effect may be assigned to changes in membrane characteristics – e.g. elevated membrane fluidity – during self-organization of protein-complexes towards the site of the IS. This concept has been reported repeatedly in the literature for immune synapses of T- and B cells [Qi et al., 2001, Lee et al., 2002, Tsourkas et al., 2008, Owen et al., 2010]. Nevertheless, an actin-dependent elevation of mobility of transmembrane proteins may be a another valid explanation. Although the actin cytoskeleton within the central part of the synapse is rather loose and has been assumed to not be involved in synaptic pattern formation in T cells [Qi et al., 2001, Beemiller and Krummel, 2013], Kv1.3 itself has been shown to be immobilized via actin-mediated mechanisms in the mature IS [Hajdu et al., 2015]. Since the mobility measurements in this work were only carried out for the first 3-4 minutes of synapse formation, an actin-mediated regulation appears less likely than regulation by sole membrane fluidity. A lack of significant differences (Fig. 17 (B) ctrl vs. CD3/CD28) may be due to relatively low sample numbers (¡ 40 QD®s / condition), which are caused by low availability of QD®s to be measured (see below).

Noteworthy, an expected increase of the average number of channels residing within the imaging field during the formation of an IS did not occur for both wild type or binding mutant Kv1.3 (Fig. 17(C)). This finding may constitute the main restriction of combining the tracking of QD®-labeled Kv1.3^{HA} with TIRF: the relatively large size of QD®s may prevent its access to the interface between the cell and glass coverslip [Groc et al., 2007, Alakoskela et al., 2011]. Thus, it is possible I only imaged the molecules residing in the field of interest when the cells were settling onto the glass surface whereas QD®-labeled channels were withheld from entering as well as leaving the synaptic site. Hence, kinetic parameters of movement, like dwell time of channels, can not be evaluated under these conditions. The outcome of approaching this method was not necessarily expected, since imaging of QD®-labeled transmembrane molecules in the synaptic cleft of neurons is feasible [Heine et al., 2008, Schneider et al., 2015]. Although general differences in mobility between wild type and binding mutant may be analyzed applying

this method, it is expedient to avert from the use of large QD®s in combination with TIRF imaging. For example, relatively smaller nano-particles, which have become available for labeling extracellularly EGFP-tagged membrane proteins may be employed instead. Alternatively, glass cover slips covered with lipid bi-layers comprising a more natural activation machinery for T cells may provide for more room [Crites et al., 2012]. Also, direct imaging of Kv1.3 tagged with mRFP or photoconvertible mEos [Schneider et al., 2015] may give better results. However, the close vicinity of the IS to the Golgi apparatus, which harbors large numbers of Kv1.3, may be a mayor disadvantage for this approach. Consequently, one may not the able to distinguish between intracellular – Golgi-residing – and surface Kv1.3 molecules unless an extracellular portion thereof is antibody-labeled.

4.5 Functional Signaling Consequences of Kv1.3 Expression and Exclusion from the IS

Employing the Fura-2 calcium-sensitive fluorescent dye to measure changes in $[Ca^{2+}]_i$, two methodological approaches are known to yield relative levels and changes of $[Ca^{2+}]_i$. Being a "ratiometric indicator", its fluorescence is excited at two wavelengths, while emission is recorded at 510 nm. The excitation wavelength pair may vary, being either 340 nm and 380 nm (340/380 ratio) or 360 nm and 380 nm (360/380 ratio) [Grynkiewicz et al., 1985, Li et al., 2012]. At 380 nm, one measures an inverse response to calcium-binding, i.e. the signal decreases with rising $[Ca^{2+}]_i$. 340 nm values, most commonly serving as nominator, positively correlate with increasing $[Ca^{2+}]_i$, i.e. fluorescence increases with elevated $[Ca^{2+}]_i$. 360 nm signifies the "isosbestic point" or Ca^{2+}-insensitive wavelength, at which fluorescence does not change, rather constituting the dye's loading control. Furthermore, altered fluorescence at 360 nm indicates a contribution of some non-Ca^{2+} divalent cation [Limke and Atchison, 2009]. Due to limitations given by the microscope used for Fura-2 measurements, I acquired fluorescence for 360/380 excitation wavelengths, which yielded suitable relative intracellular Ca^{2+} changes (Fig. 18(B)). Hence, the specific method used for monitoring intracellular Ca^{2+} changes during the activation of Jurkat T cells has proven to be valid.

Stable expression of Kv1.3 in Jurkat T cells leads to a significant elevation of the normalized baseline $[Ca^{2+}]_i$ level, which is not further enhanced when cells express binding mutant Kv1.3 alone or combined with shRNAs targeting Dlg1 or PSD-95 expression (Fig. 19(A) and (B)). These data are in line with two independent studies [Hou et al., 2014, Stephenson et al., 2007].

[Hou et al., 2014] showed that the number of active Kv1.3 channels on the cell surface regu-

lates membrane potential and intracellular calcium concentrations in native T cells. Their data were based on initial current-clamp measurements, followed by kinetic modeling of membrane potential and intracellular calcium concentrations. Larger amounts of Kv1.3 lead to elevated total membrane K^+ conductance, hence higher membrane potential, as well as baseline and activation-induced peak $[Ca^{2+}]_i$ levels. The data presented in the current work give experimental validation for the values calculated in Hou's model (Fig. 19(A),(B)).

A lack of further changes in baseline $[Ca^{2+}]_i$ levels in cells expressing shRNAs targeting Dlg1 or PSD-95 in combination with Kv1.3 binding mutant (Fig. 19(A) and (B)) may be explained by a recent publication by [Stephenson et al., 2007]. In their study, Dlg$^{-/-}$ T lymphocytes from chimeric mice did not display elevated baseline $[Ca^{2+}]_i$ levels. Dlg's binding partner – Kv1.3 – is voltage-gated, thus it opens via conformational change upon positive changes in membrane potential, which usually occurs during activation of the T cell [Chandy et al., 1984]. Therefore, it is conceivable that lack of either MAGUK binding to Kv1.3 in the periphery of the cell does not lead to any changes in intracellular baseline $[Ca^{2+}]_i$ levels. Furthermore, these data leave room for the speculation that MAGUKs do not by default act as a linker for the channel to inactivating enzymes, like protein kinases [Holmes et al., 1996, Dellis et al., 1999, Fadool et al., 1997, Matsushita et al., 2009, Tóth et al., 2009, Kuras et al., 2012], but only do so during its enrichment at the IS [Tóth et al., 2009, Nicolaou et al., 2009]. If MAGUKs were actively mediating a steady-state modulation of the channel's activity , i.e. phosphorylation level, changes in baseline $[Ca^{2+}]_i$ levels would be seen upon mutation of Kv1.3's binding motif or deletion of either MAGUK.

Observing the initial calcium transfer across the cell membrane during activation of cells, as indicated by the baseline-peak-difference (BDP), renders the most important result of this work: significantly more calcium enters the cell when expressing the binding mutant of Kv1.3 but not wild type Kv1.3 (Fig. 19 (C)).

With due regard to lack of IS enrichment of the first (Fig. 16 (B)), the findings are conforming to data presented by [Nicolaou et al., 2009], who demonstrated an increase of the calcium amplitude when Kv1.3's translocation to the IS was obstructed by crosslinking them on the surface. The approach used in my work gives a possible explanation as to why Kv1.3 may not enter the IS under more biological conditions: lack of intracellular binding partners moving them along the membrane and trapping them within the IS-network. Kv1.3 current is inactivated upon the channel's entrance to the IS [DeCoursey et al., 1984, Tóth et al., 2009], which is likely due to modulation of opening properties of the channel by phosphorylation [Holmes et al., 1996, Dellis et al., 1999, Fadool et al., 1997, Matsushita et al., 2009, Tóth et al., 2009, Kuras et al., 2012]. Obstructing the channel from entering the synapse may prevent its association

with kinases residing within the IS. Consequently, this would lead to elevated open probability of the channels, resulting in a bigger driving force for Ca^{2+}. Hence, excessive amounts of calcium would enter the cell within a short period of time. Further studies found that primary memory T cells of patients suffering from systemic lupus erythematosus (SLE), upon focal activation with αCD3/αCD28-coated Dynabeads, display altered Kv1.3 recruitment kinetics, leading to a short-lived localization of Kv1.3 in the IS [Nicolaou et al., 2007b, Nicolaou et al., 2010]. Furthermore, these cells displayed sustained calcium influx but no higher amplitude. Differences in calcium responses in these studies may be explained by differential distribution mechanisms of Kv1.3. Sustained calcium responses seen by [Nicolaou et al., 2007b, Nicolaou et al., 2010] could be due to transient inactivation of the channel only while it resides within the IS. The phosphatase CD45 has been shown to be a critical regulator of signaling thresholds during TCA by dephosphorylation of signaling proteins (reviewed in [Hermiston et al., 2003]). Channels being only transiently located – and phosphorylated – within the IS, may be dephosphorylated by passing the CD45-containing dSMAC [Freiberg et al., 2002]. Kv1.3 channels are thereby again susceptible to conformational changes, leading to an altered open probability. The reason for only transient increase in calcium influx in binding mutant Kv1.3 remains yet to be elucidated. A possible scenario may be that absence of Kv1.3 may ultimately be sensed within the IS, leading to compensatory mechanisms by mitochondria present within the IS. Mitochondria function as valid Ca^{2+} buffers, contributing to the driving force at the plasma membrane [Quintana et al., 2011].

Although the calcium responses seen in the different studies are not completely congruent with those presented in the current work, some links may be drawn between the MAGUK-dependent localization of Kv1.3 and the generation of autoimmune diseases. Several studies have revealed relations between $[Ca^{2+}]_i$ levels and the extent of nuclear factor of activated T cells (NFAT)-mediated gene expression [Timmerman et al., 1996, Hannanta-anan and Chow, 2016], as well as increased levels of NFAT in T cells of SLE patients [Kyttaris et al., 2007]. MAGUKs have not yet been implicated in the determination of the disease. Moreover, their role in NFAT signaling appears to be ambivalent for certain T cell subsets [Humphries et al., 2012]. However, several studies could prove a positive impact of Dlg1 on NFAT signaling [Round et al., 2007, Zanin-Zhorov et al., 2012]. Nevertheless, [Stephenson et al., 2007] were not able to report changes in $[Ca^{2+}]_i$ signaling in mice lacking Dlg1, which may be due to compensatory mechanisms of remaining MAGUKs. In order to completely decode the coherence of Kv1.3 localization to the IS, the role of MAGUKs therein and subsequent $[Ca^{2+}]$-defects within SLE patients, a study will have to be designed, in which (1) expression of MAGUKs in T cells from SLE patients and (2) $[Ca^{2+}]_i$–signals and Kv1.3 localization in cells carrying double knock-down of Dlg1 and PSD-95 are monitored.

Further characterization of the kinetics of the $[Ca^{2+}]_i$–levels in Jurkat T cells speak for a dependency of both initiation and clearance of the signal on the numbers of Kv1.3, indicated by significantly lower rise and decay times in all cells overexpressing the channel when compared to uninfected control cells (Fig. 19 (D),(E)).

This finding is particularly intriguing in light of a model presented by [Wulff et al., 2003], in which Kv1.3 channels become highly abundant during conversion from naïve T cells to effector memory T cells (T_{EM}). Furthermore, a recent study demonstrated that selective suppression of Kv1.3 expression in primary human T_{EM}s was able to induce a developmental switch to naïve T cells [Chimote et al., 2016]. T_{EM}s, as reviewed by [Beeton and Chandy, 2005], migrate rapidly to sites of inflammation and produce large amounts of pro-inflammatory cytokines. Rapid and synchronized activation of T cells requires the intracellular signaling machinery to be highly economical [Farber, 2009, Adachi and Davis, 2011], which may be achieved by generating an efficient $[Ca^{2+}]_i$–signal. Calcium signaling in memory T cells appears to be distinct when compared to that of naïve T cells [Arrol et al., 2008]. To my knowledge, however, kinetics of calcium signals in memory T cells has not been studied so far. The data presented in the current work may provide an explanation for the mechanism behind signaling efficiency in memory T cells, in which the reported higher number of Kv1.3 could be of high relevance.

Autoreactive T cells always constitute the fraction of memory T cells and are able to cause autoimmune disease in healthy animals [Beeton and Chandy, 2005]. Usually, autoreactive cells are suppressed by regulatory T cells (Tregs). Consequently, the lack of this suppression may play a role in the generation of autoimmune diseases, such as SLE or rheumatoid arthritis. Interestingly, a recent paper demonstrated 4-fold elevated Dlg1 recruitment to the IS in Tregs compared to other T cells. Tregs isolated from patients suffering from rheumatoid arthritis display a diminished recruitment and reduced function of Dlg1. Furthermore, Dlg1-silencing abrogated Treg function via impaired NFAT activation [Zanin-Zhorov et al., 2012]. Along this line, [Round et al., 2005] and [Round et al., 2007] were able to demonstrate that Dlg1 coordinates an alternative p38 kinase activation, which directs TCR signals specifically towards NFAT, but not NF-κB. Furthermore, this pathway is specifically elicited in T cells that previously encountered antigen [Adachi and Davis, 2011]. These results not being in line with [Xavier et al., 2004] may be justified by a study revealing that Dlg1 may both, facilitate or attenuate discrete TCR signals in different T cell subsets [Humphries et al., 2012].

Thus far, a function for PSD-95 in directing signals has not been investigated in immune cells. Studies in neurons revealed distinct cellular roles for Dlg1 and PSD-95, which relate to their function as scaffolding proteins (as reviewed by [Dimitratos et al., 1999]). Hence, the aspect of MAGUK proteins in directing TCR signals towards the nucleus may be operationally distinct

from that of enriching Kv1.3 within the IS, although both may be attributed to their scaffolding function. Theoretically, in regard to signal distribution, Dlg1 and PSD-95 may perform discrete tasks towards different cellular outcomes, e.g. via activation of distinct transcription factors in the nucleus, while both act in accumulating Kv1.3 at the IS.

Consequently, both proteins may regulate autoimmunity on a molecular level in several cell types. Loss of MAGUKs leads to diminished enrichment of Kv1.3 at the IS, which in turn may result in changes in calcium signaling, especially in Kv1.3^{high} T$_{EM}$s [Wulff et al., 2003, Feske et al., 2015]. Along this line, lack of Dlg1 results in reduced NFAT signaling in Tregs [Zanin-Zhorov et al., 2012], which may bring forward autoimmune symptoms. Therefore, the close functional interplay between Kv1.3 and Dlg-like MAGUKs may lead to autoimmune diseases if this tightly regulated system of interaction, localization and signaling is out of balance.

4.6 Conclusion and Outlook

My work lends strong support to the idea that Dlg-like MAGUKs control the surface dynamics of Kv1.3 and that this interaction is relevant for proper T cell activation.

Specifically, I provided evidence that, apart from solely interacting, Kv1.3 and Dlg-like MAGUKs together, via subcellular co-recruitment, modulate the calcium signaling of activated T cells. Furthermore, I found a possible link between elevated expression of Kv1.3 in memory T cells and the characteristic signaling phenotype associated with this cell type.

Whether – and if so, why – Dlg1 and PSD-95 play distinct roles in regulating Kv1.3 localization at the IS, as recently proposed by [Szílagyi et al., 2013], remains to be addressed in further detail. To this end, further studies should include expression of wild type Kv1.3 along with acute knock down of either MAGUK by shRNA or CRISPR. Moreover, structure-function analyses on the basis of naturally occurring variants of Dlg1 and PSD-95 or mutated versions thereof may be envisaged to unravel the engagement of domains other than the PDZ domains in regulating the IS localization of Kv1.3.

Eventually, it will be of particular importance to further substantiate the here reported findings on Jurkat T cells for Kv1.3's relevance in different subpopulations of primary T cells. For instance, the proposed involvement of Kv1.3 and Dlg-MAGUKs in generating a specific calcium signaling pattern in memory T cells may be addressed by measuring calcium kinetics using an optimized strategy for siRNA [Chimote et al., 2016] to achieve knock down of either component in primary T cells.

References

[Adachi and Davis, 2011] Adachi, K. and Davis, M. (2011). T-cell receptor ligation induces distinct signaling pathways in naïve vs. antigen-experienced t cells. *Proc Natl Acad Sci U S A*, 108(4):1549–1554.

[Alakoskela et al., 2011] Alakoskela, J.-M., Koner, A., Rudnicka, D., Köhler, K., Howarth, M., and Davis, D. (2011). Mechanisms for size-dependent protein segregation at immune synapses assessed with molecular rulers. *Biophys. J.*, 100(12):2865–2874.

[Allan et al., 2002] Allan, V. J., Thompson, H., and McNiven, M. A. (2002). Motoring around the golgi. *Nat Cell Biol*, 4(10):E236–E242.

[Altier et al., 2002] Altier, C., Dubel, S. J., Barrre, C., Jarvis, S. E., Stotz, S. C., Spaetgens, R. L., Scott, J. D., Cornet, V., De Waard, M., Zamponi, G. W., Nargeot, J., and Bourinet, E. (2002). Trafficking of l-type calcium channels mediated by the postsynaptic scaffolding protein akap79. *J. Biol. Chem.*, 277(37):33598–33603.

[Arrol et al., 2008] Arrol, H. P., Church, L. D., Bacon, P. A., and Young, S. P. (2008). Intracellular calcium signalling patterns reflect the differentiation status of human t cells. *Clin. Exp. Immunol.*, 153(1):86–95.

[Ashburner et al., 2005] Ashburner, M., Golic, K., and Hawley, R. (2005). *Drosophila: A Laboratory Handbook and Manual.*

[Attali et al., 1992] Attali, B., Romey, G., Honor, E., Schmid-Alliana, A., Matti, M. G., Lesage, F., Ricard, P., Barhanin, J., and Lazdunski, M. (1992). Cloning, functional expression, and regulation of two k^+ channels in human t lymphocytes. *J. Biol. Chem.*, 267(12):8650–8657.

[Badour et al., 2004] Badour, K., Zhang, J., and Siminovitch, K. (2004). Involvement of the wiskott-aldrich syndrome protein and other actin regulatory adaptors in t cell activation. *Semin. Immunol.*, 16(6):395–407.

[Bautista et al., 2002] Bautista, D. M., Hoth, M., and Lewis, R. S. (2002). Enhancement of calcium signalling dynamics and stability by delayed modulation of the plasma-membrane calcium-atpase in human t cells. *The Journal of Physiology*, 541(3):877–894.

[Beemiller and Krummel, 2013] Beemiller, P. and Krummel, M. F. (2013). Regulation of t-cell receptor signaling by the actin cytoskeleton and poroelastic cytoplasm. *Immunol. Rev.*, 256(1):148–159.

[Beeton and Chandy, 2005] Beeton, C. and Chandy, K. (2005). Potassium channels, memory t cells, and multiple sclerosis. *Neuroscientist*, 11(6):550–562.

[Benslimane et al., 2012] Benslimane, N., Hassan, G. S., Yacoub, D., and Mourad, W. (2012). Requirement of transmembrane domain for cd154 association to lipid rafts and subsequent biological events. *PLoS ONE*, 7(8):e43070–.

[Berg et al., 2002] Berg, J., J., T., and L., S. (2002). *Immune Responses Against Self-Antigens Are Suppressed*, chapter 33.6. W.H. Freeman, 5 edition.

[Berridge, 1993] Berridge, M. J. (1993). Inositol trisphosphate and calcium signalling. *Nature*, 361(6410):315–325.

[Bhakta et al., 2005] Bhakta, N. R., Oh, D. Y., and Lewis, R. S. (2005). Calcium oscillations regulate thymocyte motility during positive selection in the three-dimensional thymic environment. *Nat. Immunol.*, 6(2):143–151.

[Bohuslav et al., 1993] Bohuslav, J., Cinek, T., and Hoořejší, V. (1993). Large, detergent-resistant complexes containing murine antigens thy-1 and ly-6 and protein tyrosine kinase p56lck. *Eur. J. Immunol.*, 23(4):825–831.

[Bryant et al., 1993] Bryant, P. J., Watson, K., Justice, R., and Woods, D. (1993). Tumor suppressor genes encoding proteins required for cell interactions and signal transduction in drosophila. *Dev. Suppl.*, pages 239–249.

[Budnik et al., 2006] Budnik, V., Gorczyca, M., and Prokop, A. (2006). Selected methods for the anatomical study of drosophila embryonic and larval neuromuscular junctions. *Int. Rev. Neurobiol.*, 75:323–365.

[Cahalan and Chandy, 2009] Cahalan, M. and Chandy, K. (2009). The functional network of ion channels in t lymphocytes. *Immunol. Rev.*, 231(1):59–87.

[Cahalan and Lewis, 1990] Cahalan, M. and Lewis, R. (1990). Functional roles of ion channels in lymphocytes. *Semin. Immunol.*, 2(2):107–117.

[Chandy et al., 1984] Chandy, K., DeCoursey, T., Cahalan, M., McLaughlin, C., and Gupta, S. (1984). Voltage-gated potassium channels are required for human t lymphocyte activation. *J. Exp. Med.*, 160(2):369–385.

[Chimote et al., 2016] Chimote, A. A., Hajdu, P., Kottyan, L. C., Harley, J. B., Yun, Y., and Conforti, L. (2016). Nanovesicle-targeted kv1.3 knockdown in memory t cells suppresses cd40l expression and memory phenotype. *J. Autoimmun.*, 69:86–93.

[Cinek and Hoořejší, 1992] Cinek, T. and Hoořejší, V. (1992). The nature of large noncovalent compleces containing glycosyl-phosphatidylinositol-anchored membrane glycoproteins and protein tyrosine kinases. *J. Immunol.*, 149(7):2262–2270.

[Clapham, 1995] Clapham, D. E. (1995). Calcium signaling. *Cell*, 80(2):259–268.

[Conforti et al., 2003] Conforti, L., Petrovic, M., Mohammad, D., Lee, S., Ma, Q., Barone, S., and Filipovich, A. H. (2003). Hypoxia regulates expression and activity of kv1.3 channels in t lymphocytes: A possible role in t cell proliferation. *J. Immunol.*, 170(2):695–702.

[Conley et al., 2016] Conley, J. M., Gallagher, M. P., and Berg, L. J. (2016). T cells and gene regulation: The switching on and turning up of genes after t cell receptor stimulation in cd8 t cells. *Front. Immunol.*, 7:76.

[Craven et al., 1999] Craven, S. E., El-Husseini, A. E., and Bredt, D. S. (1999). Synaptic targeting of the postsynaptic density protein psd-95 mediated by lipid and protein motifs. *Neuron*, 22(3):497–509.

[Cristillo and Bierer, 2002] Cristillo, A. D. and Bierer, B. E. (2002). Identification of novel targets of immunosuppressive agents by cdna-based microarray analysis. *J. Biol. Chem.*, 277(6):4465–4476.

[Crites et al., 2012] Crites, T. J., Chen, L., and Varma, R. (2012). A tirf microscopy technique for real-time, simultaneous imaging of the tcr and its associated signaling proteins. *J. Vis. Exp.*, (61):3892.

[Dadsetan et al., 2008] Dadsetan, S., Zakharova, L., Molinski, T., and Fomina, A. (2008). Store-operated ca^{2+} influx causes ca^{2+} release from the intracellular ca^{2+} channels that is required for t cell activation. *J. Biol. Chem.*, 283(18):12512–12519.

[DeCoursey et al., 1984] DeCoursey, T., Chandy, K., Gupta, S., and Cahalan, M. (1984). Voltage-gated k^{+} channels in human t lymphocytes: a role in mitogenesis? *Nature*, 307(5950):465–468.

[Dellis et al., 1999] Dellis, O., Bouteau, F., Guenounou, M., and Rona, J.-P. (1999). Hiv-1 gp160 decreases the k^{+} voltage-gated current from jurkat e6.1 t cells by up-phosphorylation. *FEBS Lett.*, 443(2):187–191.

[Delves et al., 2011] Delves, P., Martin, S., Burton, D., and Roitt, I. (2011). *Roitt's Essential Immunology*. Wiley-Blackwell, 12 edition.

[Diehn et al., 2002] Diehn, M., Alizadeh, A. A., Rando, O. J., Liu, C. L., Stankunas, K., Botstein, D., Crabtree, G. R., and Brown, P. O. (2002). Genomic expression programs and the integration of the cd28 costimulatory signal in t cell activation. *Proc. Natl. Acad. Sci. U. S. A.*, 99(18):11796–11801.

[Dimitratos et al., 1999] Dimitratos, S. D., Woods, D. F., Stathakis, D. G., and Bryant, P. J. (1999). Signaling pathways are focused at specialized regions of the plasma membrane by scaffolding proteins of the maguk family. *Bioessays*, 21(11):912–921.

[Doerks et al., 2000] Doerks, T., Strauss, M., Brendel, M., and Bork, P. (2000). Gram, a novel domain in glucosyltransferases, myotubularins and other putative membrane-associated proteins. *Trends Biochem. Sci.*, 25(10):483–485.

[Dolmetsch et al., 1997] Dolmetsch, R. E., Lewis, R. S., Goodnow, C. C., and Healy, J. I. (1997). Differential activation of transcription factors induced by ca2+ response amplitude and duration. *Nature*, 386(6627):855–858.

[Douglass and Vale, 2005] Douglass, A. and Vale, R. (2005). Single-molecule microscopy reveals plasma membrane microdomains created by protein-protein networks that exclude or trap signaling molecules in t cells. *Cell*, 121(6):937–950.

[Doyle et al., 1996] Doyle, D., Lee, A., Lewis, J., Kim, E., Sheng, M., and MacKinnon, R. (1996). Crystal structures of a complexed and peptide-free membrane protein- binding domain: Molecular basis of peptide recognition by pdz. *Cell*, 85(7):1067–1076.

[Doyle et al., 1998] Doyle, D. A., Cabral, J. M., Pfuetzner, R. A., Kuo, A., Gulbis, J. M., Cohen, S. L., Chait, B. T., and MacKinnon, R. (1998). The structure of the potassium channel: Molecular basis of k$^+$ conduction and selectivity. *Science*, 280(5360):69–77.

[Dupré et al., 2002] Dupré, L., Aiuti, A., Trifari, S., Martino, S., Saracco, P., Bordignon, C., and Roncarolo, M.-G. (2002). Wiskott-aldrich syndrome protein regulates lipid raft dynamics during immunological synapse formation. *Immunity*, 17(2):157–166.

[Fadool, 1998] Fadool, D. (1998). Tyrosine phosphorylation downregulates a potassium current in rat olfactory bulb neurons and a cloned kv1.3 channela. *Ann. N. Y. Acad. Sci.*, 855(1):529–532.

[Fadool et al., 1997] Fadool, D., Holmes, T., Berman, K., Dagan, D., and Levitan, I. (1997). Tyrosine phosphorylation modulates current amplitude and kinetics of a neuronal voltage-gated potassium channel. *J. Neurophysiol.*, 78(3):1563–1573.

[Fadool et al., 2004] Fadool, D., Tucker, K., Perkins, R., Fasciani, G., Thompson, R., Parsons, A., Overton, J., Koni, P., Flavell, R., and Kaczmarek, L. (2004). Kv1.3 channel gene-targeted deletion produces super-smeller mice with altered glomeruli, interacting scaffolding proteins, and biophysics. *Neuron*, 41(3):389–404.

[Fanger et al., 1999] Fanger, C. M., Ghanshani, S., Logsdon, N. J., Rauer, H., Kalman, K., Zhou, J., Beckingham, K., Chandy, K. G., Cahalan, M. D., and Aiyar, J. (1999). Calmodulin mediates calcium-dependent activation of the intermediate conductance kca channel, ikca1. *J. Biol. Chem.*, 274(9):5746–5754.

[Fanger et al., 1995] Fanger, C. M., Hoth, M., Crabtree, G. R., and Lewis, C. (1995). Characterization of t cell mutants with defects in capacitative calcium entry: genetic evidence for the physiological toles of crac channels. *J. Cell Biol.*, 131(3):665–667.

[Fanning and Anderson, 1996] Fanning, A. S. and Anderson, J. M. (1996). Protein-protein interactions: Pdz domain networks. *Curr. Biol.*, 6(11):1385–1388.

[Farber, 2009] Farber, D. L. (2009). Biochemical signaling pathways for memory t cell recall. *Semin. Immunol.*, 21(2):84–91.

[Feske, 2007] Feske, S. (2007). Calcium signalling in lymphocyte activation and disease. *Nat. Rev. Immunol.*, 7(9):690–702.

[Feske et al., 2001] Feske, S., Giltnane, J., Dolmetsch, R., Staudt, L., and Rao, A. (2001). Gene regulation mediated by calcium signals in t lymphocytes. *Nat. Immunol.*, 2(4):316–324.

[Feske et al., 2006] Feske, S., Gwack, Y., Prakriya, M., Srikanth, S., Puppel, S.-H., Tanasa, B., Hogan, P. G., Lewis, R. S., Daly, M., and Rao, A. (2006). A mutation in orai1 causes immune deficiency by abrogating crac channel function. *Nature*, 441(7090):179–185.

[Feske et al., 2015] Feske, S., Wulff, H., and Skolnik, E. Y. (2015). Ion channels in innate and adaptive immunity. *Annu. Rev. Immunol.*, 33:291–353.

[Fields and Song, 1989] Fields, S. and Song, O.-K. (1989). A novel genetic system to detect protein-protein interactions. *Nature*, 340(6230):245–246.

[Fischer et al., 1998] Fischer, K.-D., Kong, Y.-Y., Nishina, H., Tedford, K., Marengre, L., Kozieradzki, I., Sasaki, T., Starr, M., Chan, G., Gardener, S., Nghiem, M., Bouchard, D., Barbacid, M., Bernstein, A., and Penninger, J. (1998). Vav is a regulator of cytoskeletal reorganization mediated by the t-cell receptor. *Curr. Biol.*, 8(10):554–562.

[Freedman et al., 1995] Freedman, B. D., Fleischmann, B. K., Punt, J. A., Gaulton, G., Hashimoto, Y., and Kotlikoff, M. I. (1995). Identification of kv1.1 expression by murine cd4cd8 thymocytes: A role for voltage-dependent k$^+$ channels in murine thymocyte development. *J. Biol. Chem.*, 270(38):22406–22411.

[Freiberg et al., 2002] Freiberg, B. A., Kupfer, H., Maslanik, W., Delli, J., Kappler, J., Zaller, D. M., and Kupfer, A. (2002). Staging and resetting t cell activation in smacs. *Nat. Immunol.*, 3(10):911–917.

[Funke et al., 2005] Funke, L., Dakoji, S., and Bredt, D. S. (2005). Membrane-associated guanylate kinases regulate adhesion and plasticity at cell junctions. *Annu. Rev. Biochem.*, 74(1):219–245.

[Gmyrek et al., 2013] Gmyrek, G. B., Graham, D. B., Sandoval, G., Blaufuss, G. S., Akilesh, H. M., Fujikawa, K., Xavier, R. J., and Swat, W. (2013). Polarity gene discs large homolog 1 regulates the generation of memory t cells. *Eur. J. Immunol.*, 43(5):1185–1194.

[Grakoui et al., 1999] Grakoui, A., Bromley, S. K., Sumen, C., Davis, M. M., Shaw, A. S., Allen, P. M., and Dustin, M. L. (1999). The immunological synapse: A molecular machine controlling t cell activation. *Science*, 285(5425):221–227.

[Groc et al., 2007] Groc, L., Lafourcade, M., Heine, M., Renner, M., Racine, V., Sibarita, J.-B., Lounis, B., Choquet, D., and Cognet, L. (2007). Surface trafficking of neurotransmitter receptor: Comparison between single-molecule/quantum dot strategies. *J. Neurosci.*, 27(46):12433–12437.

[Grynkiewicz et al., 1985] Grynkiewicz, G., Poenie, M., and Tsien, R. (1985). A new generagene of ca2+ indicators with greatly improved fluorescence properties. *J. Biol. Chem.*, 260(6):3440–3450.

[Gulbis et al., 1999] Gulbis, J., Mann, S., and MacKinnon, R. (1999). Structure of a voltage-dependent k+ channel subunit. *Cell*, 97(7):943–952.

[Haggie et al., 2006] Haggie, P., Kim, J., Lukacs, G., and Verkman, A. (2006). Tracking of quantum dot-labeled cftr shows near immobilization by c-terminal pdz interactions. *Mol. Biol. Cell*, 17(12):4937–4945.

[Hajdu et al., 2015] Hajdu, P., Martin, G., Chimote, A., Szilagyi, O., Takimoto, K., and Conforti, L. (2015). The c-terminus sh3-binding domain of kv1.3 is required for the actin-mediated immobilization of the channel via cortactin. *Mol. Biol. Cell*, 26(9):1640–1651.

[Hanada et al., 1997] Hanada, T., Lin, L., Chandy, K., Oh, S., and Chishti, A. (1997). Human homologue of the drosophila discs large tumor suppressor binds to p56(lck) tyrosine kinase and shaker type kv1.3 potassium channel in t lymphocytes. *J. Biol. Chem.*, 272(43):26899–26904.

[Hanada et al., 2000] Hanada, T., Lin, L., Tibaldi, E. V., Reinherz, E. L., and Chishti, A. H. (2000). Gakin, a novel kinesin-like protein associates with the human homologue of the drosophila discs large tumor suppressor in t lymphocytes. *J. Biol. Chem.*, 275(37):28774–28784.

[Hanada et al., 2003] Hanada, T., Takeuchi, A., Sondarva, G., and Chishti, A. (2003). Protein 4.1-mediated membrane targeting of human discs large in epithelial cells. *J. Biol. Chem.*, 278(36):34445–34450.

[Hannanta-anan and Chow, 2016] Hannanta-anan, P. and Chow, B. (2016). Optogenetic control of calcium oscillation waveform defines nfat as an integrator of calcium load. *Cell Systems*, 2(4):283–288.

[Hauser and Tsien, 2006] Hauser, C. T. and Tsien, R. Y. (2006). A hexahistidine-zn^{2+}-dye label reveals stim1 surface exposure. *Proc. Natl. Acad. Sci. U. S. A.*, 104(10):3693–3697.

[Heine et al., 2008] Heine, M., Groc, L., Frischknecht, R., Bque, J.-C., Lounis, B., Rumbaugh, G., Huganir, R., Cognet, L., and Choquet, D. (2008). Surface mobility of postsynaptic ampars tunes synaptic transmission. *Science*, 320(5873):201–205.

[Heinemann et al., 1994] Heinemann, S., Rettig, J., Scott, V., Parcej, D., Lorra, C., Dolly, J., and Pongs, O. (1994). The inactivation behaviour of voltage-gated k-channels may be determined by association of - and -subunits. *J. Physiol. (Paris)*, 88(3):173–180.

[Hermiston et al., 2003] Hermiston, M. L., Xu, Z., and Weiss, A. (2003). Cd45: A critical regulator of signaling thresholds in immune cells. *Annu. Rev. Immunol.*, 21(1):107–137.

[Holmes et al., 1996] Holmes, T., Fadool, D., and Levitan, I. (1996). Tyrosine phosphorylation of the kv1.3 potassium channel. *J. Neurosci.*, 76(5):1581–1590.

[Hoshi et al., 1990] Hoshi, T., Zagotta, W., and Aldrich, R. (1990). Biophysical and molecular mechanisms of shaker potassium channel inactivation. *Science*, 250(4980):533–538.

[Hoth et al., 1997] Hoth, M., Fanger, C. M., and Lewis, R. S. (1997). Mitochondrial regulation of store-operated calcium signaling in t lymphocytes. *J. Cell Biol.*, 137(3):633–648.

[Hou et al., 2014] Hou, P., Zhang, R., Liu, Y., Feng, J., Wang, W., Wu, Y., and Ding, J. (2014). Physiological role of kv1.3 channel in t lymphocyte cell investigated quantitatively by kinetic modeling. *PLoS ONE*, 9(3):E89975.

[Hough et al., 1997] Hough, C. D., Woods, D. F., Park, S., and Bryant, P. J. (1997). Organizing a functional junctional complex requires specific domains of the drosophila maguk discslarge. *Genes Dev.*, 11(23):3242–3253.

[Hradsky et al., 2011] Hradsky, J., Raghuram, V., Reddy, P., Navarro, G., Hupe, M., Casado, V., McCormick, P., Sharma, Y., Kreutz, M., and Mikhaylova, M. (2011). Post-translational membrane insertion of tail-anchored transmembrane ef-hand ca^{2+} sensor calneurons requires the trc40/asna1 protein chaperone. *J. Biol. Chem.*, 286(42):36762–36776.

[Humphries et al., 2012] Humphries, L., Shaffer, M., Sacirbegovic, F., Tomassian, T., McMahon, K.-A., Humbert, P., Silva, O., Round, J., Takamiya, K., Huganir, R., Burkhardt, J., Russell, S., and Miceli, M. (2012). Characterization of in vivo dlg1 deletion on t cell development and function. *PLoS ONE*, 7(9):E45276.

[Ishii et al., 1997] Ishii, T., Silvia, C., Hirschberg, B., Bond, C., Adelman, J., and MAylie, J. (1997). A human intermediate conductance calcium-activated potassium channel. *Proc. Natl. Acad. Sci. U. S. A.*, 94(21):11651–11656.

[Joiner et al., 1997] Joiner, W. J., Wang, L.-Y., Tang, M. D., and Kaczmarek, L. K. (1997). hsk4, a member of a novel subfamily of calcium-activated potassiumchannels. *Proc. Natl. Acad. Sci. U. S. A.*, 94(20):11013–11018.

[Kane et al., 2000] Kane, L. P., Lin, J., and Weiss, A. (2000). Signal transduction by the tcr for antigen. *Curr. Opin. Immunol.*, 12(3):242–249.

[Kaplan and Trout, 1968] Kaplan, W. D. and Trout, W. E. (1968). The behavior of four neurological mutants of drosophila. *Genetics*, 61(2):399–409.

[Kerppola, 2008] Kerppola, T. (2008). Bimolecular fluorescence complementation (bifc) analysis as a probe of protein interactions in living cells. *Methods Cell Biol.*, 85:431–470.

[Kim et al., 1995] Kim, E., Niethammer, M., Rothschild, A., Jan, Y., and Sheng, M. (1995). Clustering of shaker-type k^+ channels by interaction with a family of membrane-associated guanylate kinases. *Nature*, 378(6552):85–88.

[Kim and Sheng, 1996] Kim, E. and Sheng, M. (1996). Differential k$^+$ channel clustering activity of psd-95 and sap97, two related membrane-associated putative guanylate kinases. *Neuropharmacology*, 35(7):993–1000.

[Kornau et al., 1995] Kornau, H.-C., Schenker, L., Kennedy, M., and Seeburg, P. (1995). Domain interaction between nmda receptor subunits and the postsynaptic density protein psd-95. *Science*, 269(5231):1737–1740.

[Kuras et al., 2012] Kuras, Z., Kucher, V., Gordon, S., Neumeier, L., Chimote, A., Filipovich, A., and Conforti, L. (2012). Modulation of kv1.3 channels by protein kinase a i in t lymphocytes is mediated by the disc large 1-tyrosine kinase lck complex. *Am. J. Physiol. Cell Physiol.*, 302(10):C1504–C1512.

[Kuriyan and Cowburn, 1997] Kuriyan, J. and Cowburn, D. (1997). Modular peptide recognition domains in eukaryotic signaling. *Annu. Rev. Biophys. Biomol. Struct.*, 26:259–288.

[Kyttaris et al., 2007] Kyttaris, V., Wang, Y., Juang, Y., Weinstein, A., and Tsokos, G. (2007). Increased levels of nf-atc2 differentially regulate cd154 and il-2 gene in t cells from patients with systemic lupus erythematosus. *J. Immunol.*, 178(3):1960–1966.

[Laemmli, 1970] Laemmli, U. (1970). Cleavage of structural proteins during the assembly of the head of bacteriophage t4. *Nature*, 227(5259):680–685.

[Lee et al., 2002] Lee, S., Hori, Y., Groves, J., Dustin, M., and Chakraborty, A. (2002). Correlation of a dynamic model for immunological synapse formation with effector functions: two pathways to synapse formation. *Trends Immunol.*, 23(10):492–499.

[Li et al., 2012] Li, W., Calfa, G., Larimore, J., and Pozzo-Miller, L. (2012). Activity-dependent bdnf release and trpc signaling is impaired in hippocampal neurons of mecp2 mutant mice. *Proc. Natl. Acad. Sci. U. S. A.*, 109(42):17087–17092.

[Lim et al., 2002] Lim, I., Hall, D., and Hell, J. (2002). Selectivity and promiscuity of the first and second pdz domains of psd-95 and synapse-associated protein 102. *J. Biol. Chem.*, 277(24):21697–21711.

[Limke and Atchison, 2009] Limke, T. L. and Atchison, W. D. (2009). Application of single-cell microfluorimetry to mechanistic toxicology. *Current protocols in toxicology*, CHAPTER:Unit–12.15.

[Liou et al., 2005] Liou, J., Kim, M. L., Heo, W. D., Jones, J. T., Myers, J. W., Ferrell, J. E., and Meyer, T. (2005). Stim is a ca^{2+} sensor essential for ca^{2+}-store-depletion-triggered ca^{2+} influx. *Curr. Biol.*, 15(13):1235–1241.

[Lioudyno et al., 2007] Lioudyno, M. I., Kozak, J. A., Penna, A., Safrina, O., Zhang, S. L., Sen, D., Roos, J., Stauderman, K. A., and Cahalan, M. D. (2007). Orai1 and stim1 move to the immunological synapse and are up-regulated during t cell activation. *Proc. Natl. Acad. Sci. U. S. A.*, 105(6):2011–2016.

[Liu et al., 2002] Liu, Q.-H., Fleischmann, B. K., Hondowicz, B., Maier, C. C., Turka, L. A., Yui, K., Kotlikoff, M. I., Wells, A. D., and Freedman, B. D. (2002). Modulation of kv channel expression and function by tcr and costimulatory signals during peripheral cd4$^+$ lymphocyte differentiation. *J. Exp. Med.*, 196(7):897–909.

[Logsdon et al., 1997] Logsdon, N. J., Kang, J., Togo, J. A., Christian, E. P., and Aiyar, J. (1997). A novel gene, hkca4, encodes the calcium-activated potassium channel in human t lymphocytes. *J. Biol. Chem.*, 272(52):32723–32726.

[Ludford-Menting et al., 2005] Ludford-Menting, M., Oliaro, J., Sacirbegovic, F., Cheah, E.-Y., Pedersen, N., Thomas, S., Pasam, A., Lazzolino, R., Dow, L., Waterhouse, N., Murphy, A., Ellis, S., Smyth, M., Kershaw, M., Darcy, P., Humbert, P., and Russell, S. (2005). A network of pdz-containing proteins regulates t cell polarity and morphology during migration and immunological synapse formation. *Immunity*, 22(6):737–748.

[Luik et al., 2006] Luik, R. M., Wu, M. M., Buchanan, J., and Lewis, R. S. (2006). The elementary unit of store-operated ca(2+) entry: local activation of crac channels by stim1 at er-plasma membrane junctions. *J. Cell Biol.*, 174(6):815–825.

[Macián et al., 2002] Macián, F., García-Cózar, F., Im, S.-H., Horton, H. F., Byrne, M. C., and Rao, A. (2002). Transcriptional mechanisms underlying lymphocyte tolerance. *Cell*, 109(6):719–731.

[Magidovich et al., 2006] Magidovich, E., Fleishman, S., and Yifrach, O. (2006). Intrinsically disordered c-terminal segments of voltage-activated potassium channels: A possible fishing rod-like mechanism for channel binding to scaffold proteins. *Bioinformatics*, 22(13):1546–1550.

[Marks and Fadool, 2007] Marks, D. and Fadool, D. (2007). Post-synaptic density perturbs insulin-induced kv1.3 channel modulation via a clustering mechanism involving the sh3 domain. *J. Neurochem.*, 103(4):1608–1627.

[Matheu et al., 2008] Matheu, M. P., Beeton, C., Garcia, A., Chi, V., Rangaraju, S., Safrina, O., Monaghan, K., Uemura, M. I., Li, D., Pal, S., de la Maza, L. M., Monuki, E., Flgel, A., Pennington, M. W., Parker, I., Chandy, K. G., and Cahalan, M. D. (2008). Imaging of effector memory t cells during a delayed-type hypersensitivity reaction and suppression by kv1.3 channel block. *Immunity*, 29(4):602–614.

[Matsushita et al., 2008] Matsushita, Y., Ohya, S., Itoda, H., Kimura, T., Suzuki, Y., Yamamura, H., and Imaizumi, Y. (2008). Molecular mechanisms for kv1.3 potassium channel current inhibition by cd3/cd28 stimulation in jurkat t cells. *Biochem. Biophys. Res. Commun.*, 374(1):152–157.

[Matsushita et al., 2009] Matsushita, Y., Ohya, S., Suzuki, Y., Itoda, H., Kimura, T., Yamamura, H., and Imaizumi, Y. (2009). Inhibition of kv1.3 potassium current by phosphoinositides and stromal-derived factor-1 in jurkat t cells. *Am. J. Physiol. Cell Physiol.*, 296(5):C1079–C1085.

[Matteson and Deutsch, 1984] Matteson, D. and Deutsch, C. (1984). K channels in t lymphocytes: A patch clamp study using monoclonal antibody adhesion. *Nature*, 307(5950):468–471.

[McCormack et al., 1999] McCormack, T., McCormack, K., Nadal, M., Vieira, E., Ozaita, A., and Rudy, B. (1999). The effects of shaker -subunits on the human lymphocyte k^+ channel kv1.3. *J. Biol. Chem.*, 274(29):20123–20126.

[Monks et al., 1998] Monks, C. R. F., Freiberg, B. A., Kupfer, H., Sciaky, N., and Kupfer, A. (1998). Three-dimensional segregation of supramolecular activation clusters in t cells. *Nature*, 395(6697):82–86.

[Moore et al., 2010] Moore, C., Guthrie, E., Huang, M., and Taxman, D. (2010). Short hairpin rna (shrna): design, delivery, and assessment of gene knockdown. *Methods Mol. Biol.*, 629:141–158.

[Morell et al., 2007] Morell, M., Espargar, A., Avils, F., and Ventura, S. (2007). Detection of transient protein-protein interactions by bimolecular fluorescence complementation: The abl-sh3 case. *Proteomics*, 7(7):1023–1036.

[Negulescu et al., 1996] Negulescu, P. A., Krasieva, T. B., Khan, A., Kerschbaum, H. H., and Cahalan, M. D. (1996). Polarity of t cell shape, motility, and sensitivity to antigen. *Immunity*, 4(5):421–430.

[Neupert et al., 2015] Neupert, C., Schneider, R., Klatt, O., Reissner, C., Repetto, D., Biermann, B., Niesmann, K., Missler, M., and Heine, M. (2015). Regulated dynamic trafficking of neurexins inside and outside of synaptic terminals. *J. Neurosci.*, 35(40):13629–13647.

[Nicolaou et al., 2007a] Nicolaou, S., Neumeier, L., Peng, Y., Devor, D., and Conforti, L. (2007a). The ca2+-activated k+ channel kca3.1 compartmentalizes in the immunological synapse of human t lymphocytes. *Am. J. Physiol. Cell Physiol.*, 292(4):C1431–C1439.

[Nicolaou et al., 2009] Nicolaou, S., Neumeier, L., Steckly, A., Kucher, V., Takimoto, K., and Conforti, L. (2009). Localization of kv1.3 channels in the immunological synapse modulates the calcium response to antigen stimulation in t lymphocytes. *J. Immunol.*, 183(10):6296–6302.

[Nicolaou et al., 2010] Nicolaou, S., Neumeier, L., Takimoto, K., Lee, S., Duncan, H., Kant, S., Mongey, A., Filipovich, A., and Conforti, L. (2010). Differential calcium signaling and kv1.3 trafficking to the immunological synapse in systemic lupus erythematosus. *Cell Calcium*, 47(1):19–28.

[Nicolaou et al., 2007b] Nicolaou, S., Szigligeti, P., Neumeier, L., Lee, S., Duncan, H., Kant, S., Mongey, A., Filipovich, A., and Conforti, L. (2007b). Altered dynamics of kv1.3 channel compartmentalization in the immunological synapse in systemic lupus erythematosus. *J. Immunol.*, 179(1):346–356.

[Niethammer et al., 1996] Niethammer, M., Kim, E., and Sheng, M. (1996). Interaction between the c terminus of nmda receptor subunits and multiple members of the psd-95 family of membrane-associated guanylate kinases. *J. Neurosci.*, 16(7):2157–2163.

[Norcross, 1984] Norcross, M. A. (1984). A synaptic basis for t-lymphocyte activation. *Annales d'immunologie*, 135D(2):113–134.

[O'Connell and Tamkun, 2005] O'Connell, K. M. S. and Tamkun, M. M. (2005). Targeting of voltage-gated potassium channel isoforms to distinct cell surface microdomains. *J. Cell Sci.*, 118(10):2155–2166.

[Ogawa et al., 2008] Ogawa, Y., Horresh, I., Trimmer, J., Bredt, D., Peles, E., and Rasband, M. (2008). Postsynaptic density-93 clusters kv1 channels at axon initial segments independently of caspr2. *J. Neurosci.*, 28(22):5731–5739.

[Oliva et al., 2012] Oliva, C., Escobedo, P., Astorga, C., Molina, C., and Sierralta, J. (2012). Role of the maguk protein family in synapse formation and function. *Devel. Neurobio.*, 72(1):57–72.

[Owen et al., 2010] Owen, D. M., Oddos, S., Kumar, S., Davis, D. M., Neil, M. A., French, P. M., Dustin, M. L., Magee, A. I., and Cebecauer, M. (2010). High plasma membrane lipid order imaged at the immunological synapse periphery in live t cells. *Mol. Membr. Biol.*, 27(0):10.3109/09687688.2010.495353–.

[Panyi et al., 2003] Panyi, G., Bagdny, M., Bodnr, A., Vmosi, G., Szentesi, G., Jenei, A., Mtyus, L., Varga, S., Waldmann, T., Gspr, R., and Damjanovich, S. (2003). Colocalization and non-random distribution of kv1.3 potassium channels and cd3 molecules in the plasma membrane of human t lymphocytes. *Proc. Natl. Acad. Sci. U. S. A.*, 100(5):2592–2597.

[Panyi et al., 2004] Panyi, G., Vmosi, G., Bacs, Z., Bagdny, M., Bodnr, A., Varga, Z., Gspr, R., Mtyus, L., and Damjanovich, S. (2004). Kv1.3 potassium channels are localized in the immunological synapse formed between cytotoxic and target cells. *Proc. Natl. Acad. Sci. U. S. A.*, 101(5):1285–1290.

[Park et al., 2009] Park, E.-J., Kim, B.-J., Kim, S.-H., Kim, S.-Y., Sung, T.-S., Chae, H.-G., Kim, S. J., Kim, J., Park, H. H., So, I., and Jeon, J.-H. (2009). Altered biochemical properties of transient receptor potential vanilloid 6 calcium channel by peptide tags:. *Biol. Pharm. Bull.*, 32(10):1790–1794.

[Pati, 1992] Pati, U. (1992). Novel vectors for expression of cdna encoding epitope-tagged proteins in mammalian cells. *Gene*, 114(2):285–288.

[Payet and Dupuis, 1992] Payet, M. D. and Dupuis, G. (1992). Dual regulation of the n type k^+ channel in jurkat t lymphocytes by protein kinases a and c. *J. Biol. Chem.*, 267(26):18270–18273.

[Peiretti et al., 2003] Peiretti, F., Deprez-Beauclair, P., Bonardo, B., Aubert, H., Juhan-Vague, I., and Nalbone, G. (2003). Identification of sap97 as an intracellular binding partner of tace. *J. Cell Sci.*, 116(10):1949–1957.

[Pérez-Verdaguer et al., 2016] Pérez-Verdaguer, M., Capera, J., Martnez-Mrmol, R., Camps, M., Comes, N., Tamkun, M. M., and Felipe, A. (2016). Caveolin interaction governs kv1.3 lipid raft targeting. *Scientific Reports*, 6:22453–.

[Perrimon, 1988] Perrimon, N. (1988). The maternal effect of lethal(1)discs-large-1: a recessive oncogene of drosophila melanogaster. *Dev. Biol.*, 127(2):392–407.

[Qi et al., 2001] Qi, S., Groves, J., and Chakraborty, A. (2001). Synaptic pattern formation during cellular recognition. *Proc. Natl. Acad. Sci.*, 98(12):6548–6553.

[Quintana and Hoth, 2004] Quintana, A. and Hoth, M. (2004). Apparent cytosolic calcium gradients in t-lymphocytes due to fura-2 accumulation in mitochondria. *Cell Calcium*, 36(2):99–109.

[Quintana et al., 2011] Quintana, A., Pasche, M., Junker, C., AlAnsary, D., Rieger, H., Kummerow, C., Nuez, L., Villalobos, C., Meraner, P., Becherer, U., Rettig, J., Niemeyer, B., and Hoth, M. (2011). Calcium microdomains at the immunological synapse: how orai channels, mitochondria and calcium pumps generate local calcium signals for efficient tcell activation. *EMBO Journal*, 30(19):3895–3912.

[Rangaraju et al., 2009] Rangaraju, S., Chi, V., Pennington, M., and Chandy, K. (2009). Kv1.3 potassium channels as a therapeutic target in multiple sclerosis. *Expert Opin. Ther. Targets*, 13(8):909–924.

[Rettig et al., 1994] Rettig, J., Helnemann, S., Wunder, F., Lorra, C., Parcej, D., Dolly, J., and Pongs, O. (1994). Inactivation properties of voltage-gated k^+ channels altered by presence of β-subunit. *Nature*, 369(6478):289–294.

[Robbins et al., 2005] Robbins, J. R., Lee, S. M., Filipovich, A. H., Szigligeti, P., Neumeier, L., Petrovic, M., and Conforti, L. (2005). Hypoxia modulates early events in t cell receptor-mediated activation in human t lymphocytes via kv1.3 channels. *J. Physiol.*, 564(Pt 1):131–143.

[Roufaiel et al., 2015] Roufaiel, M., Wells, J., and Stepstone, R. (2015). Impaired t-cell function in b-cell lymphoma: a direct consequence of events at the immunological synapse? *Front. Immunol..*, 6(258).

[Round et al., 2007] Round, J., Humphries, L., Tomassian, T., Mittelstadt, P., Zhang, M., and Miceli, M. (2007). Scaffold protein dlgh1 coordinates alternative p38 kinase activation, directing t cell receptor signals toward nfat but not nf-b transcription factors. *Nat. Immunol.*, 8(2):154–161.

[Round et al., 2005] Round, J., Tomassian, T., Zhang, M., Patel, V., Schoenberger, S., and Miceli, M. (2005). Dlgh1 coordinates actin polymerization, synaptic t cell receptor and lipid raft aggregation, and effector function in t cells. *J. Exp. Med.*, 201(3):419–430.

[Sakarya et al., 2007] Sakarya, O., Armstrong, K., Adamska, M., Adamski, M., Wang, I.-F., Tidor, B., Degnan, B., Oakley, T., and Kosik, K. (2007). A post-synaptic scaffold at the origin of the animal kingdom. *PLoS ONE*, 2(6):E506.

[Schlüter et al., 2006] Schlüter, O. M., Xu, W., and Malenka, R. C. (2006). Alternative n-terminal domains of psd-95 and sap97 govern activity-dependent regulation of synaptic ampa receptor function. *Neuron*, 51(1):99–111.

[Schneider et al., 2015] Schneider, R., Hosy, E., Kohl, J., Klueva, J., Choquet, D., Thomas, U., Voigt, A., and Heine, M. (2015). Mobility of calcium channels in the presynaptic membrane. *Neuron*, 86(3):672–680.

[Sewing et al., 1996] Sewing, S., Roeper, J., and Pongs, O. (1996). Kv1 subunit binding specific for shaker-related potassium channel subunits. *Neuron*, 16(2):455–463.

[Singleton et al., 2009] Singleton, K., Roybal, K., Sun, Y., Fu, G., Gascoigne, N., Van Oers, N., and Wlfing, C. (2009). Spatiotemporal patterning during t cell activation is highly diverse. *Sci. Signal.*, 2(65):ra15.

[Spear et al., 2015] Spear, J. M., Koborssy, D. A., Schwartz, A. B., Johnson, A. J., Audhya, A., Fadool, D. A., and Stagg, S. M. (2015). Kv1.3 contains an alternative c-terminal er exit motif and is recruited into copii vesicles by sec24a. *BMC Biochemistry*, 16:16.

[Stephenson et al., 2007] Stephenson, L., Sammut, B., Graham, D., Chan-Wang, J., Brim, K., Huett, A., Miletic, A., Kloeppel, T., Landry, A., Xavier, R., and Swat, W. (2007). Dlgh1 is a negative regulator of t-lymphocyte proliferation. *Mol. Cell. Biol.*, 27(21):7574–7581.

[Stewart et al., 1972] Stewart, M., Murphy, C., and Fristrom, J. (1972). The recovery and preliminary characterization of x chromosome mutants affecting imaginal discs of drosophila melanogaster. *Dev. Biol.*, 27:71–83.

[Szigligeti et al., 2006] Szigligeti, P., Neumeier, L., Duke, E., Chougnet, C., Takimoto, K., Lee, S. M., Filipovich, A. H., and Conforti, L. (2006). Signalling during hypoxia in human t lymphocytes - critical role of the src protein tyrosine kinase p56lck in the o(2) sensitivity of kv1.3 channels. *J. Physiol.*, 573(2):357–370.

[Szílagyi et al., 2013] Szílagyi, O., Boratkó, A., Panyi, G., and Hajdu, P. (2013). The role of psd-95 in the rearrangement of kv1.3 channels to the immunological synapse. *Pflugers Arch.*, 465(9):1341–1353.

[Tejedor et al., 1997] Tejedor, F., Bokhari, A., Rogero, O., Gorczyca, M., Zhang, J., Kim, E., Sheng, M., and Budnik, V. (1997). Essential role for dlg in synaptic clustering of shaker k$^+$ channels in vivo. *J. Neurosci.*, 17(1):152–159.

[Tempel et al., 1987] Tempel, B., Papazian, D., Schwarz, T., Jan, Y., and Jan, L. (1987). Sequence of a probable potassium channel component encoded at shaker locus of drosophila. *Science*, 237(4816):770–775.

[Thomas et al., 2000] Thomas, U., Ebitsch, S., Gorczyca, M., Koh, Y., Hough, C., Woods, D., Gundelfinger, E., and Budnik, V. (2000). Synaptic targeting and localization of discs-large is a stepwise process controlled by different domains of the protein. *Curr. Biol.*, 10(18):1108–1117.

[Thomas et al., 1997a] Thomas, U., Kim, E., Kuhlendahl, S., Koh, Y. H., Gundelfinger, E. D., Sheng, M., Garner, C. C., and Budnik, V. (1997a). Synaptic clustering of the cell adhesion molecule fasciclin ii by discs-large and its role in the regulation of presynaptic structure. *Neuron*, 19(4):787–799.

[Thomas et al., 1997b] Thomas, U., Phannavong, B., Müller, B., Garner, C. C., and Gundelfinger, E. D. (1997b). Functional expression of rat synapse-associated proteins sap97 and sap102 in drosophila dlg-1 mutants: effects on tumor suppression and synaptic bouton structure. *Mech. Dev.*, 62(2):161–174.

[Tiffany et al., 2000] Tiffany, A., Manganas, L., Kim, E., Hsueh, Y.-P., Sheng, M., and Trimmer, J. (2000). Psd-95 and sap97 exhibit distinct mechanisms for regulating k$^+$ channel surface expression and clustering. *J. Cell Biol.*, 148(1):147–157.

[Timmerman et al., 1996] Timmerman, L. A., Clipstone, N. A., Ho, S. N., Northrop, J. P., and Crabtree, G. R. (1996). Rapid shuttling of nf-at in discrimination of ca^{2+} signals and immunosuppression. *Nature*, 383(6603):837–840.

[Tonikian et al., 2008] Tonikian, R., Zhang, Y., Sazinsky, S., Currell, B., Yeh, J.-H., Reva, B., Held, H., Appleton, B., Evangelista, M., Wu, Y., Xin, X., Chan, A., Seshagiri, S., Lasky, L., Sander, C., Boone, C., Bader, G., and Sidhu, S. (2008). A specificity map for the pdz domain family. *PLoS Biol.*, 6(9):2043–2059.

[Tóth et al., 2009] Tóth, A., Szilágyi, O., Krasznai, Z., Panyi, G., and Hajdú, P. (2009). Functional consequences of kv1.3 ion channel rearrangement into the immunological synapse. *Immunol. Lett.*, 125(1):15–21.

[Tsourkas et al., 2008] Tsourkas, P. K., Longo, M. L., and Raychaudhuri, S. (2008). Monte carlo study of single molecule diffusion can elucidate the mechanism of b cell synapse formation. *Biophys. J.*, 95(3):1118–1125.

[Vacher and Trimmer, 2012] Vacher, H. and Trimmer, J. S. (2012). Trafficking mechanisms underlying neuronal voltage-gated ion channel localization at the axon initial segment. *Epilepsia*, 53(Suppl 9):21–31.

[Vig et al., 2006] Vig, M., Beck, A., Billingsley, J. M., Lis, A., Parvez, S., Peinelt, C., Koomoa, D. L., Soboloff, J., Gill, D. L., Fleig, A., Kinet, J.-P., and Penner, R. (2006). Cracm1 multimers form the ion-selective pore of the crac channel. *Curr. Biol.*, 16(20):2073–2079.

[Waheed et al., 1997] Waheed, A., Parkkila, S., Zhou, X. Y., Tomatsu, S., Tsuchihashi, Z., Feder, J. N., Schatzman, R. C., Britton, R. S., Bacon, B. R., and Sly, W. S. (1997). Hereditary hemochromatosis: Effects of c282y and h63d mutations on association with (2)-microglobulin, intracellular processing, and cell surface expression of the hfe protein in cos-7cells. *Proc. Natl. Acad. Sci. U. S. A.*, 94(23):12384–12389.

[Wang et al., 2010] Wang, H., Kadlecek, T. A., Au-Yeung, B. B., Goodfellow, H. E. S., Hsu, L.-Y., Freedman, T. S., and Weiss, A. (2010). Zap-70: An essential kinase in t-cell signaling. *Cold Spring Harb. Perspect. Biol.*, 2(5):a002279–.

[Weikl and Lipowsky, 2004] Weikl, T. R. and Lipowsky, R. (2004). Pattern formation during t-cell adhesion. *Biophys. J.*, 87(6):3665–3678.

[Wong et al., 2002] Wong, W., Newell, E., Jugloff, D., Owen, T., and Schlichter, L. (2002). Cell surface targeting and clustering interactions between heterologously expressed psd-95 and the shai voltage-gated potassium channel, kv4.2. *J. Biol. Chem.*, pages 20423–20430.

[Woods et al., 1996] Woods, D., Hough, C., Peel, D., Callaini, G., and Bryant, P. J. (1996). Dlg protein is required for junction structure, cell polarity, and proliferation control in drosophila epithelia. *J. Cell. Biol.*, 134(6):1469–1482.

[Wu et al., 2000] Wu, H., Reissner, C., Kuhlendahl, S., Coblentz, B., Reuver, S., Kindler, S., Gundelfinger, E., and Garner, C. (2000). Intramolecular interactions regulate sap97 binding to gkap. *EMBO Journal*, 19(21):5740–5751.

[Wu et al., 2006] Wu, M. M., Buchanan, J., Luik, R. M., and Lewis, R. S. (2006). Ca^{2+} store depletion causes stim1 to accumulate in er regions closely associated with the plasma membrane. *J. Cell Biol.*, 174(6):803–813.

[Wulff et al., 2003] Wulff, H., Calabresi, P., Allie, R., Yun, S., Pennington, M., Beeton, C., and Chandy, K. (2003). The voltage-gated kv1.3 k+ channel in effector memory t cells as new target for ms. *J. Clin. Invest.*, 112(2):298–.

[Wülfing and Davis, 1998] Wülfing, C. and Davis, M. M. (1998). A receptor/cytoskeletal movement triggered by costimulation during t cell activation. *Science*, 282(5397):2266–2269.

[Xavier et al., 1998] Xavier, R., Brennan, T., Li, Q., McCormack, C., and Seed, B. (1998). Membrane compartmentation is required for efficient t cell activation. *Immunity*, 8(6):723–732.

[Xavier et al., 2004] Xavier, R., Rabizadeh, S., Ishiguro, K., Andre, N., Ortiz, J., Wachtel, H., Morris, D., Lopez-Ilasaca, M., Shaw, A., Swat, W., and Seed, B. (2004). Discs large (dlg1) complexes in lymphocyte activation. *J. Cell Biol.*, 166(2):173–178.

[Yeromin et al., 2006] Yeromin, A., Zhang, S., Jiang, W., Yu, Y., Safrina, O., and Cahalan, M. (2006). Molecular identification of the crac channel by altered ion selectivity in a mutant of orai. *Nature*, 443(7108):226–229.

[Zanin-Zhorov et al., 2012] Zanin-Zhorov, A., Lin, J., Scher, J., Kumari, S., Blair, D., Hippen, K., Blazar, B., Abramson, S., Lafaille, J., and Dustin, M. (2012). Scaffold protein disc large homolog 1 is required for t-cell receptor-induced activation of regulatory t-cell function. *Proc. Natl. Acad. Sci. U. S. A.*, 109(5):1625–1630.

[Zhang et al., 2006] Zhang, S. L., Yeromin, A. V., Zhang, X. H.-F., Yu, Y., Safrina, O., Penna, A., Roos, J., Stauderman, K. A., and Cahalan, M. D. (2006). Genome-wide rnai screen of ca^{2+} influx identifies genes that regulate ca^{2+} release-activated ca^{2+} channel activity. *Proc. Natl. Acad. Sci. U. S. A.*, 103(24):9357–9362.

[Zhang et al., 2005] Zhang, S. L., Yu, Y., Roos, J., Kozak, J. A., Deerinck, T. J., Ellisman, M. H., Stauderman, K. A., and Cahalan, M. D. (2005). Stim1 is a ca^{2+} sensor that activates crac channels and migrates from the ca(2+) store to the plasma membrane. *Nature*, 437(7060):902–905.

[Zhang et al., 1999] Zhang, W., Irvin, B., Trible, B., Abraham, R., , and Samelson, L. (1999). Functional analysis of lat in tcr-mediated signaling pathways using a lat-deficient jurkat cell line. *Int. Immunol.*

[Zhang et al., 1998] Zhang, W., Sloan-Lancaster, J., Kitchen, J., Trible, R., and Samelson, L. (1998). Lat: the zap-70 tyrosine kinase substrate that links t cell receptor to cellular activation. *Cell*, 92(1):83–92.

[Zheng J., 2015] Zheng J., T. M. (2015). *Handbook of Ion Channels*. CRC Press.

[Zhou et al., 2008] Zhou, W., Zhang, L., Guoxiang, X., Mojsilovic-Petrovic, J., Takamaya, K., Sattler, R., Huganir, R., and Kalb, R. (2008). Glur1 controls dendrite growth through its binding partner, sap97. *J. Neurosci.*, 28(41):10220–10233.

[Zito et al., 1997] Zito, K., Fetter, R. D., Goodman, C. S., and Isacoff, E. Y. (1997). Synaptic clustering of fasciclin ii and shaker: Essential targeting sequences and role of dlg. *Neuron*, 19(5):1007–1016.

[Zweifach and Lewis, 1993] Zweifach, A. and Lewis, R. S. (1993). Mitogen-regulated ca2+ current of t lymphocytes is activated by depletion of intracellular ca2+ stores. *Proc. Natl. Acad. Sci. U. S. A.*, 90(13):6295–6299.

Appendix

Table 12: **List of Oligonucleotides used for shRNA-mediated Knock Down of Dlg1 and PSD95.**

Target Gene	#	Target Site [CDS] [Sequence]	Oligonucleotide Sequence
hDlg	1	[1668] 5'-aatacatgatttacgggagca-3'	**forward (1668BglIIfw):** gatct aatacatgatttacgggagca ttctcgag tgctcccgtaaatcatgtatt ttt gg a **reverse (1668HIIIrev):** agctt cc aaa aatacatgatttacgggagca ctcgagaa tgctcccgtaaatcatgtatt a
	2	[115] 5'-aacatatttcagagcaacctc-3'	**forward (115BglIIfw):** gatct aacatatttcagagcaacctc ttctcgag gaggttgctctgaaatatgtt ttt gg a **reverse (115HIIIrev):** agctt ccaaa aacatatttcagagcaacctc ctcgagaa gaggttgctctgaaatatgtt a
	3	[2575] 5'-aaactggaacaggagtttact-3'	**forward (2575BglIIfw):** gatct aaactggaacaggagtttact ttctcgag agtaaactcctgttccagttt tt gg a **reverse (2575HIIIrev):** agctt cc aa aaactggaacaggagtttact ctcgagaa agtaaactcctgttccagttt a
PSD95	1	[682] 5'-gccctgaagaacacgtatgat-3'	**forward (682BglIIfw):** gatcc gccctgaagaacacgtatgat ttctgaga tcatacgtgttcttcagggc ttttt gg a **reverse (682HIIIrev):** agctt cc aaaaa gccctgaagaacacgtatgat ctcagaa atcatacgtgttcttcagggc g
	2	[1548] 5'-ggttctgagctacgagacagt-3'	**forward (1548BglIIfw):** gatcc ggttctgagctacgagacagt ttctgag actgtctcgtagctcagaacc ttttt gg a **reverse (1548HIIIrev)** agctt cc aaaaa ggttctgagctacgagacagt ctcagaa actgtctcgtagctcagaacc g
	3	[1764] 5'-ggacattcaggcgcacaagtt-3'	**forward (1764BglIIfw)** gatcc ggacattcaggcgcacaagtt ttctgaga aacttgtgcgcctgaatgtcc ttttt gg a **reverse (1764HIIIrev)** agctt cc aaaaa ggacattcaggcgcacaagtt ctcagaa aacttgtgcgcctgaatgtcc g

```
gc gga ggc ggg cgc gcg ccc cgc agg gga ggg ggc gga gag cgc gag aag gag gga gga ggc gtc ccc gtg cgg gag ccc  <80
   G   G   R   A   P   R   R   G   G   G   G   E   R   E   K   E   G   G   V   P   V   R   E   P
cg cct ccg ccc gcg cgc ggg gcg tcc cct ccc ccg cct ctc gcg ctc ttc ctc cct cct ccg cag ggg cac gcc ctc ggg
          10          20          30          40          50          60          70

ggc tga ccg cgc cag acc cag aca gag cat cgc ggc ttt ggc tgc aac agg cgg tgg gct cgg ctc ggg ggg gga ggc gg  <160
   G   *   P   R   Q   T   Q   T   E   H   R   G   F   G   C   N   R   R   W   A   R   L   G   G   G   G
ccg act ggc gcg gtc tgg gtc tgt ctc gta gcg ccg aaa ccg acg ttg tcc gcc acc cga gcc gag ccc ccg cct ccg cc
          90         100         110         120         130         140         150

c gaa agg gcg ggg agc gcg agg agg agc gac ctg gcc tca ccg ctg ccg cct ctt ccc cgc cgc atg gac gag cgc ctc a  <240
   E   R   A   G   S   A   R   R   S   D   L   A   S   P   L   P   P   L   P   R   R   M   D   E   R   L   S
g ctt tcc cgc ccc tcg cgc tcc tca tcg ctg gac cgg agt ggc gac ggc gga gaa ggg gcg gcg tac ctg ctc gcg gag t
         170         180         190         200         210         220         230

gc ctt ctg cgc tcg ccg ccg ccg ccc tca gcc cgc cac cgc gcc cac cct cct cag cgc cca gcg agc agc ggc ggt gcc  <320
   L   L   R   S   P   P   P   P   S   A   R   H   R   A   H   P   P   Q   R   P   A   S   S   G   G   A
cg gaa gac gcg agc ggc ggc ggc agt cgg gcg gtg gcg cgg gtg gga gga gtc ggc ggt cgc tcg ccg cca cgg
         250         260         270         280         290         300         310

cac acg ctg gtg aac cac ggc tac gcg gag ccc gcc gca ggc cgc gag ctg ccg ccc gac atg acc gtg gtg ccc ggg ga  <400
   H   T   L   V   N   H   G   Y   A   E   P   A   A   G   R   E   L   P   P   D   M   T   V   V   P   G   D
gtg tgc gac cac ttg gtg ccg atg cgc ctc ggg cgg cgt ccg gcg ctc gac ggc ggg ctg tac tgg cac cac ggg ccc ct
         330         340         350         360         370         380         390

c cac ctg ctg gag ccg gag gtg gcc gat ggt gga ggg gcc ccg cct caa ggc ggc tgt ggc ggc ggc ggc tgc gac cgc t  <480
   H   L   L   E   P   E   V   A   D   G   G   A   P   P   Q   G   G   C   G   G   G   G   C   D   R   Y
g gtg gac gac ctc ggc ctc cac cgg cta cca cct ccc cgg ggc gga gtt ccg ccg aca ccg ccg ccg ccg acg ctg gcg a
         410         420         430         440         450         460         470

ac gag ccg ctg ccg ccc tca ctg ccg gcc ggc ggc gag gac tgc tgc ggg gag cgc gtg gtc atc aac atc tcc ggg  <560
   E   P   L   P   P   S   L   P   A   A   G   E   Q   D   C   C   G   E   R   V   V   I   N   I   S   G
tg ctc ggc gac ggc ggg agt gac ggc cgg cag ccg ctc gtc ctg acg acg ccc ctc gcg cac cag tag ttg tag agg ccc
         490         500         510         520         530         540         550

ctg cgc ttc gag acg cag ctg aag acc ctt tgc cag ttc ccc gag acg ctg ctg ggc gac ccc aag cgg cgc atg agg ta  <640
   L   R   F   E   T   Q   L   K   T   L   C   Q   F   P   E   T   L   L   G   D   P   K   R   R   M   R   Y
gac gcg aag ctc tgc gtc gac ttc tgg gaa acg gtc aag ggg ctc tgc gac gac ccg ctg ggg ttc gcc gcg tac tcc at
         570         580         590         600         610         620         630

c ttc gac ccg ctc cgc aac gag tac ttc ttc gac cgc aac cgg ccc agc ttc gac gcc atc ctc tac tac tat cag tcc g  <720
   F   D   P   L   R   N   E   Y   F   F   D   R   N   R   P   S   F   D   A   I   L   Y   Y   Y   Q   S   G
g aag ctg ggc gag gtg ttg ctc atg aag aag gtg ttg gcc ggg tcg aag ctg cgg tag atg atg atg atg gtc agg c
         650         660         670         680         690         700         710

gg ggc cgc atc cgc cgg ccg gtc aac gtg ccc atc gac att ttc tcc gag gag atc cgc ttc tac cag ctg ggc gag gag  <800
   G   R   I   R   R   P   V   N   V   P   I   D   I   F   S   E   E   I   R   F   Y   Q   L   G   E   E
cc ccg gcg tag gcg gcc ggc cag ttg cac ggg tag tta taa aag gac ctc ctc tag gcg aag atg gtc gac ccg ctc ctc
         730         740         750         760         770         780         790

gcc atg gag aag ttc cgc gag gac gag ggc ttc ctg cgg gag gag gag cgg ccc ttg ccc cgc cgc gac ttc cag cgc ca  <880
   A   M   E   K   F   R   E   D   E   G   F   L   R   E   E   E   R   P   L   P   R   R   D   F   Q   R   Q
cgg tac ctc ttc aag gcg ctc ctg ctc ccg aag gac gcc ctc ctc gcc ggg aac ggg gcg gcg tac aag ctg gcg gt
         810         820         830         840         850         860         870
                                                                          >S1 Transmembrane Domain
                                                                          |
g gtg tgg ctg ctc ttc gag tac ccc gag agc tcc ggg ccg gcc cgg ggc atc gcc atc gtg tcc gtg ctg gtc atc ctc a  <960
   V   W   L   L   F   E   Y   P   E   S   S   G   P   A   R   G   I   A   I   V   S   V   L   V   I   L   I
c cac acc gac gag aag ctc atg ggg ctc agg ccc ggc cgg ccg tag cgg tag cac agg cac cag tag gag t
         890         900         910         920         930         940         950

tc tcc att gtc atc ttc tgc ctg gag acg ctg ccg gag ttc cgc gac gag aag gac tac ccc gcc tcg acg tcg cag gac  <1040
   S   I   V   I   F   C   L   E   T   L   P   E   F   R   D   E   K   D   Y   P   A   S   T   S   Q   D
ag agg taa cag tag aag acg gac ctc tgc gac ggc ctc aag gcg ctg ctc ttc ctg atg ggg cgg agc tgc agc gtc ctg
         970         980         990        1000        1010        1020        1030
                                                      >CDS
                                                      |
tca ttc gaa gca gcc ggc aac agc acg tcg ggg tcc cgc gca gga gcc tcc agc ttc tcc gat ccc ttc ttc gtg gtg ga  <1120
   S   F   E   A   A   G   N   S   T   S   G   S   R   A   G   A   S   S   F   S   D   P   F   F   V   E
agt aag ctt cgt cgg ccg ttg tcg tgc agc ccc agg gcg cgt cct cgg agg tcg aag agg cta ggg aag aag cac cac ct
         1050        1060        1070        1080        1090        1100        1110
              >S2 Transmembrane Domain
              |
g acg ctg tgc atc atc tgg ttc tcc ttc gaa ctg ctg gtg cgg ttc ttc gct tgt cct agc aaa gcc acc ttc tcg cga a  <1200
   T   L   C   I   I   W   F   S   F   E   L   L   V   R   F   F   A   C   P   S   K   A   T   F   S   R   N
c tgc gac acg tag tag acc aag agg aag ctt gac gac cac gcc aag aag cga aca gga tcg ttt cgg tgg aag agc gct t
         1130        1140        1150        1160        1170        1180        1190
                                              >S3 Transmembrane Domain
                                              |
ac atc atg aac ctg atc gac att gtg gcc atc att cct tat ttt atc act ctg ggt acc gag ctg gcc gaa cga cag ggc  <1280
   I   M   N   L   I   D   I   V   A   I   I   P   Y   F   I   T   L   G   T   E   L   A   E   R   Q   G
tg tag tac ttg gac tag ctg taa cac cgg tag taa gga ata aaa tag tga gac cca tgg ctc gac cgg ctt gct gtc ccg
         1210        1220        1230        1240        1250        1260        1270
                                              >S4 Transmembrane Domain
                                              |
aat gga cag cag gcc atg tct ctg gcc atc ctg agg gtc atc cgc ctg gta agg gtc ttc cgc atc ttc aag ctg tcg cg  <1360
   N   G   Q   Q   A   M   S   L   A   I   L   R   V   I   R   L   V   R   V   F   R   I   F   K   L   S   R
tta cct gtc gtc cgg tac aga gac cgg tag gac tcc cag tag gcg gac cat tcc cag tag aag gcg tag aag ttc gac agc gc
         1290        1300        1310        1320        1330        1340        1350

c cac tcc aag ggg ctg cag atc ctc ggg caa acg ctg aag gcg tcc atg cgg gag ctg gga ttg ctc atc ttc ttc ctc t  <1440
   H   S   K   G   L   Q   I   L   G   Q   T   L   K   A   S   M   R   E   L   G   L   L   I   F   L   F
g gtg agg ttc ccc gac gtc tag gag ccc gtt tgc gac ttc cgc agg tac gcc ctc gac cct aac gag tag aag aag gag a
          1370        1380        1390        1400        1410        1420        1430
    >S5 Transmembrane Domain
    |
tt att ggg gtc atc ctt ttc tcc agc gcg gtc tac ttt gcc gag gca gac gac ccc act tca ggt ttc agc agc atc ccg  <1520
   I   G   V   I   L   F   S   S   A   V   Y   F   A   E   A   D   D   P   T   S   G   F   S   S   I   P
aa taa ccc cag tag gaa aag agg tcg cgc cag atg aaa cgg ctc cgt ctg ctg gga tga agt cca aag tcg tcg tag ggc
          1450        1460        1470        1480        1490        1500        1510
```

94

>Selectivity Filter
                                        |
gat gcc ttc tgg tgg gca gtg gta acc atg aca aca gtg ggt tac ggc gat atg cac cca gtg acc ata ggg ggc aag at <1600
 D   A   F   W   W   A   V   V   T   M   T   T   V   G   Y   G   D   M   H   P   V   T   I   G   G   K   I
cta cgg aag acc acc cgt cac cat tgg tac tgt tgt cac cca atg ccg cta tac gtg ggt cac tgg tat ccc ccg ttc ta
        1530   1540   1550   1560   1570   1580   1590

                                    >S6 Transmembrane Domain
                                        |
t gtg gga tct ctc tgt gcc atc gcc ggt gtc ttg acc atc gca ttg cca gtt ccc gtg att gtt tcc aac ttc aat tac t <1680
  V   G   S   L   C   A   I   A   G   V   L   T   I   A   L   P   V   P   V   I   V   S   N   F   N   Y   F
a cac cct aga gag aca cgg tag cgg cca cag aac tgg tag cgt aac ggt caa ggg cac taa caa agg ttg aag tta atg a
        1610   1620   1630   1640   1650   1660   1670

tc tac cac cgg gag aca gaa ggg gaa gag caa tcc cag tac atg cac gtg gga agt tgc cag cac ctc tcc tct tca gcc <1760
  Y   H   R   E   T   E   G   E   E   Q   S   Q   Y   M   H   V   G   S   C   Q   H   L   S   S   A
ag atg gtg gcc ctc tgt ctt ccc ctt ctc gtt agg gtc atg tac gtg cac cct tca acg gtc gtg gag agg aga agt cgg
        1690   1700   1710   1720   1730   1740   1750

gag gag ctc cga aaa gca agg agt aac tcg act ctg agt aag tcg gag tat atg gtg atc gaa gag ggg ggt atg aac ca <1840
 E   E   L   R   K   A   R   S   N   S   T   L   S   K   S   E   Y   M   V   I   E   G   G   M   N   H
ctc ctc gag gct ttt cgt tcc tca ttg agc tga gac tca ttc agc ctc ata tac cac tag ctt ctc ccc cca tac ttg gt
        1770   1780   1790   1800   1810   1820   1830

t agc gct ttc ccc cag acc cct ttc aaa acg ggc aat tcc act gcc acc tgc acc acg aac aat aat ccc aac tct tgt g <1920
  S   A   F   P   Q   T   P   F   K   T   G   N   S   T   A   T   C   T   T   N   N   N   P   N   S   C   V
a tcg cga aag ggg gtc tgg gga aag ttt tgc ccg tta agg tga ctg acg tgg tgc ttg tta ggg ttg aga aca c
        1850   1860   1870   1880   1890   1900   1910

                    >PDZ binding
                        |
tc aac atc aaa aag ata ttc acc gat gtt taa tat gtg ata caa gtg aca tgc tgt gct cag tat tgt gtg gaa cgt gcc <2000
  N   I   K   K   I   F   T   D   V   *   Y   V   I   Q   V   T   C   C   A   Q   Y   C   V   E   R   A
ag ttg tag ttt ttc tat aag tgg cta caa att ata cac tat gtt cac tgt acg aca cga gtc ata aca cac ctt gca cgg
        1930   1940   1950   1960   1970   1980   1990

ccc ttg gtc tgc cta tgc cct tgt ttt ata cat ttc cag acc att cat caa gga aag gac ctg aag aag tgg aaa gca ca <2080
 P   L   V   C   L   C   P   C   F   I   H   F   Q   T   I   H   Q   G   K   D   L   K   K   W   K   A   H
ggg aac cag acg gat acg gga aca aaa tat gta aag gtc tgg taa gta gtt cct ttc ctg gac ttc ttc acc ttt cgt gt
        2010   2020   2030   2040   2050   2060   2070

c ttc att ctc cct ctc cct gct gct tca tac tga aac agg tgc ctg ttt tgc aag tgg gct gca ttc tct cag ctc tcc t <2160
  F   I   L   P   L   P   A   A   S   Y   *   N   R   C   L   F   C   K   W   A   A   F   S   Q   L   S   F
g aag taa gag gga gag gga cga cga agt atg act ttg tcc acg gac aaa acg ttc acc cga cgt aag aga gtc gag agg a
        2090   2100   2110   2120   2130   2140   2150

tt tcc ctc tta ccc tct ctc tct taa cat tgt aaa caa cag act tac gtt aaa ctt cat ttc tag tac acg ccc tat tta <2240
  S   L   L   P   S   L   S   *   H   C   K   Q   Q   T   Y   V   K   L   H   F   *   Y   T   P   Y   L
aa agg gag aat ggg aga gag aga att gta aca ttt gtt gtc tga atg caa ttt gaa gta aag atc atg tgc ggg ata aat
        2170   2180   2190   2200   2210   2220   2230

aaa aag agc agt aca tcc tgg gag gaa atg aaa cta aag aac agt tag agt aac tgt tta acc tca gaa ttt taa agg ca <2320
 K   K   S   S   T   S   W   E   E   M   K   L   K   N   S   *   S   N   C   L   T   S   E   F   *   R   Q
ttt ttc tcg tca tgt agg acc ctc ctt tac ttt gat ttc ttg tca atc tca ttg aca aat tgg agt ctt aaa att tcc gt
        2250   2260   2270   2280   2290   2300   2310

g ttg ttt ctt tcc taa gca cat caa ttc gta gta aat gat gct tcg gtt tga tgg acc ttt caa cgt tat tta ttg aat a <2400
  L   F   L   S   *   A   H   Q   F   V   V   N   D   A   S   V   *   W   T   F   Q   R   Y   L   L   N   M
c aac aaa gaa agg att cgt gta gtt aag cat cat tta cta cga agc caa act acc tgg aaa gtt gca ata aat aac tta t
        2330   2340   2350   2360   2370   2380   2390

tg tat ttc ggt tgc cta ccc tgt aga tat gtg gat gaa gag tct aac tag aat aat gac ttg taa acc cac cat gag tta <2480
  Y   F   G   C   L   P   C   R   Y   V   D   E   E   S   N   *   N   N   D   L   *   T   H   E   L
ac ata aag cca acg gat ggg aca tct ata cac cta ctt ctc aga ttg atc tta tta ctg aac att tgg gtg gta ctc aat
        2410   2420   2430   2440   2450   2460   2470

ttt ggt ttt tga ctt aaa ttc cta ttt gaa tcc cct ttc ccg gaa ttt taa gtg tct cta caa ctt tga ata aag gga aa <2560
 F   G   F   *   L   K   F   L   F   E   S   P   F   P   E   F   *   V   S   L   Q   L   *   I   K   G   N
aaa cca aaa act gaa ttt aag gat aaa ctt agg gga aag ggc ctt aaa att cac aga gat gtt gaa act tat ttc cct tt
        2490   2500   2510   2520   2530   2540   2550

t gcc caa gat gtc ctg atc tga aaa aaa aaa aaa aaa aa < 2599
  A   Q   D   V   L   I   *   K   K   K   K   X
a cgg gtt cta cag gac tag act ttt ttt ttt ttt ttt tt
        2570   2580   2590

Features :
CDS   : [225 - 1952]
S1 Transmembrane Domain   : [927 - 983]
S2 Transmembrane Domain   : [1107 - 1172]
S3 Transmembrane Domain   : [1206 - 1268]
S4 Transmembrane Domain   : [1311 - 1367]
S5 Transmembrane Domain   : [1416 - 1475]
Selectivity Filter   : [1554 - 1571]
S6 Transmembrane Domain   : [1599 - 1667]
PDZ binding   : [1941 - 1949]

Figure A.1: **Kv1.3 CDS with Protein Translation and Domain Features.**

95

Table 13: List of Primers used in this Work

Name	Sequence	Application
GFPant_ERI_rev	ggaattcgccatgtgtaatcccagca	Cloning of hCD8-GFP from the template hCD8-GFP-shaker. Binds to the-terminus of GFPS65T-antique, introducing an EcoRI site.
hCD8(Nhe)_fw	tgctagcatggccttaccagtgaccg	Amplification of hCD8-GFP, binding upstream of the Start-Codon
hcd8_GFPseq	tgtacttcagccacttcgtgc	Sequencing of hCD8-GFP at the junction of hCD8 and GFP.
Kv1.3TM(NheI)_fw	tgctagccgcatgg	generating PCR product of Kv1.3TM$_{1470}$
Kv1.3TM(NheI)_rev	caagggcactaacaaaggctagcgtt	generating PCR product of Kv1.3TM $_{1470}$
Kv13_TMXbaI_fw	ttctagacgcatggacgagcgcct	Amplification of the n-terminal, transmembrane (TM) region of Kv1.3 for endogenously EGFP-tagged Kv1.3$_{1545/1670}$. Inserts a XbaI-site upstream of the Start-Codon, which is compatible with the NheI-site upstream of EGFP-C2.
Kv13_cyto_fw	cgaattcaattacttctaccac	Cloning of the c-terminal cytoplasmic tail for Kv1.3-GFP$_{1470}$.Begins at the init of the cytoplasmic tail, inserting an EcoRI-site.
Kv13_cyto_rev	tgtcgacatattaaacatcggtg	Cloning of the c-terminal cytoplasmic tail Kv1.3-GFP $_{1470}$ and the full length wildtype Kv1.3. Binds downstream the STOP-Codon, introducing a SalI-site.
Kv13_TMNheI1670_rev	agctagcgtggtgcaggtggcagtg	Amplification of the n-terminal TM of Kv1.3 for Kv1.3-GFP$_{1670}$, inserting an NheI-site at the 3' end.
Kv1.3_cyto(XhoI-1665)_fw	cctcgagcacgaacaataatccca	Amplification of the c-terminal cytoplasmic tail Kv1.3-GFP$_{1670}$, introducing a XhoI-site for the MCS of pEGFP-C2.
Kv1.3_TM(NheI-1545)_rev	gctagctcctcggctgaagaggag	Amplification of the n-terminal TM of Kv1.3 for Kv1.3-GFP$_{1545}$, inserting an NheI-Site at the 3' end of the PCR product.
Kv1.3_cyto(SI-1510)_fw	agctcgaggcacctctcctcttca	Amplification of the c-terminal cytoplasmic tail of Kv1.3 for Kv1.3-GFP$_{1510}$, introducing a SalI-site compatible with the multiple cloning site of pEGFP-C2.
Kv1.3-ATG_fw	cgaattccatggacgagcgcctcag	Amplification of full length wiltype Kv1.3 for cloning into pCDNA3.1
hdlg_PDZ1[RI]_fw	agaattcgttaatggcacagatg	Cloning of the PDZI-II tandem into the pGBKT7 vektor, inducing an EcoRI- site at the 5' end of the PCR product.
hdlg_PDZ2[Sal]_rev	gtcgactgcttcttcatgagtaac	Cloning of the PDZI-II tandem into the pGBKT7 vektor, inducing an SalI-site at the 3' end of the PCR product.
hdlg_PDZ3[RI]_fw	tgaattcttgggccagacaccag	Cloning of the PDZIII into the pGBKT7 vector, i nducing an EcoRI-site.
hdlg_PDZ3[Sal]_rev	ggtcgactgctcccgtaaatcatg	Cloning of the PDZIII into the pGBKT7 vector, inducing a SalI-site.
hdlg_PDZ2[Sal]_rev	agtcgactgcttcttcatgagtaac	Cloning of the PDZI-II tandem into the pGBKT7 vektor, inducing a SalI-Site at the 3' end of the PCR product.
hdlg_PDZ3[RI]_fw	tgaattcttgggccagacaccag	Cloning of the PDZIII into the pGBKT7 vector, inducing an EcoRI-site.
hKv.4_cyto[RI]_fw	cgaattctaccacagagagactg	Cloning of the cytoplasmic tail of Kv1.4 for Y2H, inducing an EcoRI-site.
hKv1.4_STOP[SalI]_rev	aagtcgactcacacatcagtctccac	Cloning of the cytoplasmic tail of Kv1.4 for Y2H, inducing a SalI-site.
mCherryNhefw	atccgctagcgctaccggtcg	Cloning of mCherry into the pZoff using NheI und XbaI
mCherryXbaIrev	ctctagatctgagtccggacttg	Cloning of mCherry into the pZoff vector. Inserts a XbaI-site downstream of mCherry for exchanging mCherry against EGFP in the pZoff.
pZoffH1rev	gtggcgccctgcaatatttgc	For sequencing of the pZoff knock-down constructs, binding within the H1-Promoter. Since H1 runs in 3' -5' -orientation, the primer has to be designed in reverse.

Name	Sequence	Application
Kv1.3RI1880fw	agaattcagcagcatcccggatgc	Cloning of the n-terminal part of Kv1.3-GFP $_{1670}$. Induces an EcoRI-site in the position into which an HA- and Dlg-epitope were successfully cloned into the Cav channel.
Kv1.3RI1880rev	tgaattctgaagtggggtcgtctg	Cloning of the c-terminal part of Kv1.3-GFP $_{1670}$. Induces an EcoRI-site in the position into which an HA- and Dlg-epitope were successfully cloned into the Cav channel.
Kv1.3RI1370fw	ggaattccgcgacgagaaggacta	Cloning of the n-terminal part of Kv.13 GFP $_{1670}$. For induction of an EcoRI-site within the Sigma-Antibody (P4497) epitope, in order to insert an HA-epitope.
Kv1.3RI1370rev	tgaattccggcagcgtctccag	Cloning of the c-terminal part of Kv.13 GFP$_{1670}$. For induction of an EcoRI-Site within the Sigma-Antibody (P4497) epitope, in order to insert an HA-epitope.
H1_fw	tcgctatgtgttctgggaaa	Sequencing primer for shRNA-inserts of the pCMS4 and other H1-promoter based vectors.
pEGFP_N_sense	ccaaaatgtcgtaacaactc	Sequencing primer for GFP-tagged constructs. Binds upstream of GFP within the pEGFP-N.
pEGFP C-sense	catggtcctgctggagttcgtg	Forward sequencing primer for GFP-tagged constructs. Binds towards the 3' end of EGFP.
hDlgNheI825_fw	agctagcagttaatggcacagatcag	Induction of a NheI-site at nucleotide 825 of hDlg for cloning of Split- Venus, to be combined with hDlg1750_rev.
hDlgNheI825_rev	agctagcgcgtaagttggtgtttcaag	Induction of an NheI-site at nucleotide 825 of hDlg for cloning of Split-Venus, to be comined with hDlg1750_rev pEGFP_N_sense
hDlg1750_rev	gtttaccgatataatacgatctcc	Binds to hDlg cDNA, amplifying an internal SacI-site that was used for further cloning.
hDlgNheI1460_fw	agctagctgataaccatgttagccc	Induction of an NheI-site at nucleotide 1460 of hDlg for cloning of Split- Venus, to be comined with hDlg1750_rev.
2hDlgNheI1460_rev	agctagctgagaagaagagttggtg	Induction of an NheI-site at nucleotide 1460 of hDlg for cloning of Split- Venus, to be comined with pEGFP_N_sense
VN_HA[NheI]_rev	gctagcttagcgtaatctggaaca	Induction of a NheI-site within the MCS of VN-construct for cloning into hDlg.
VC_Myc[NheI]_rev	gctagcttcagatcctcttcagag	Induction of a NheI-site within the MCS of VC-construct for cloning into hDlg.
VC_Myc[NheI]_rev	gctagcttcagatcctcttcagag	Induction of a NheI-site within the MCS of VC-construct for cloning into hDlg.
VN(NheI)_fw	gctagcaatggtgagcaaggg	Shifts reading frame of pre-existing VN-construct to be in-frame with Kv1.3-GFP $_{1670}$ and hDlg.
VN_HA[BGLII]_rev	agatcttagcgtaatctggaacatcg	Inserts a BglII-site into the MCS of VN-constructs for subsequent cloning into Kv1.3-GFP$_{1670}$.
VC_Myc[BGLII]_rev	agatcttcagatcctcttcagaga	Inserts a BglII-site into the MCS of VC-constructs for subsequent cloning into Kv1.3-GFP$_{1670}$.
2crKV13BglII	gagatctgcaccaccaacaataatcc	Amplifies ratKv1.3 cytoplasmic tail ("WSGG" mutant) for subsequent cloning into Kv1.3-GFP$_{1670}$. Inserts a BglII-site at 5' end of the PCR product.
Kv1.3-ERI814_fw	agaattcttcgaagcagccggcaac	Cloning of c-terminal part of Kv1.3for the induction of an EcoRI-Site within the area of the extra-cellular epitope used by the antibody P4497 (Sigma), into which a HA-tag can be cloned. To be combined with Kv1.3XbaI_rev or (full length Kv1.3) Kv13_TMNheI1670_rev (Kv1.3-EGFP).
Kv1.3-ERI814_rev	agaattcctgcgacgtcgaggcgg	Cloning of n-terminal part of Kv1.3 for the induction of an EcoRI-Site within the area of the extra-cellular epitope used by the antibody P4497 (Sigma), into which a HA-tag can be cloned. To be combined with Kv1.3STGBHIfw (Kv1.3full length) or pEGFP-NdeI_fw (Kv1.3-EGFP).

Name	Sequence	Application
pEGFP-NdeI_fw	atcatatgccaagtacgccccct	Binds at internal NdeI-site of the pEGFP vector. Together with Kv1.3-ERI814_rev, it amplifies the n-terminal part of Kv1.3.
Kv1.3-ATGBHI_fw	aGgatcccatggacgagcgcctca	Binds directly upstream of the ATG, inducing a BamHI-site.
Kv1.3XbaI_rev	agggccctctagactcgacata	Binds downstream of the Stop-codon of Kv1.3, herein inducing a XbaI-site
Kv13Sigma_fw	ttcgagtaccccgagagctc	Sequencing primer for the Kv1.3 area of the epitope recognized by P4497 (Sigma).
Kv13 170rev	cgcggtaccgtcgactgcagaattcta	Cloning of Kv1.3 untagged constructs, amplifying the internal SalI-site. For cloning of Kv1.3 into the FUGW vector.
Kv13BHI_fw	ggatccaatggacgagcgcctcag	Cloning of Kv1.3 constructs into FUGW, inserting a BamHI-site upstream of ATG.
Kv1.3SIrev	gcggtcgacatattaaacatcggtgaatat	Cloning of Kv1.3-GFP-based constructs into FUGW vector. Inserts a SalI-site downstream of STOP codon.
FUW UbiC fwd	gctcggggttggcgagtgtg	Sequencing of FUGW-constructs downstream of the hUbc-Promoter.
pEGFPC1NheI_fw	gctagccaccatggtgagcaag	Induces a NheI-site upstream of ATG of GFP for cloning into the Split-Venus insertion site of hDlg.
pEGFPC1NheI_rev	tgctagcttgtacagctcgtccatg	Induces a NheI-site at the 3' end of GFP for cloning into the Split-Venus insertion site of hDlg.
pTagRFPBglII2_rev	tagatctagagtccggaatta	Shifts the BglII-site at the 3' end of TagRFP in order to shift the open reading frame for cloning into Kv1.3.
CF_IRES_XhoI_fw	TCGATACCGTCGACCaattccgcccctctccctcc	ColdFusion cloning of IRES-PuroR-cassette into empty FUGW vector.
CF_PuroR_XhoI_rev	ttttctaggtctcgaaaactcaggcaccgggcttg	ColdFusion cloning of IRES-PuroR-cassette into empty FUGW vector.
CF_IRES_BspEI_fw	GCCCGAGAGCTGCATaattccgcccctctccctcc	ColdFusion cloning of IRES-PuroR-cassette into Kv1.3- FUGW constructs
CF_PuroR_BspEI_rev	cccagtacagtccggaaactcaggcaccgggcttg	ColdFusion cloning of IRES-PuroR-cassette into Kv1.3- FUGW constructs
CF_H1sh_BspEI_fw	gcccgagagctgcatcgaattcgaacgctgacgtc	ColdFusion cloning of H1-hDlg/PSD95 shRNA-cassette into Kv1.3- FUGW constructs
CF_H1sh_BspEI_rev	cccagtacagtccggtcgacagctcttaagct	ColdFusion cloning of H1-hDlg/PSD95 shRNA-cassette into Kv1.3-FUGW constructs

Table 14: List of Constructs used in this Work.

Construct Name Reference	Construct Token	Insert [Restriction Sites]	Vector Backbone / Type [Restriction Sites]
hDlg$_{\text{PDZI-II}}$-pGBKT7	JH99	hDlg$_{\text{PDZI-II}}$ [EcoRI/SalI]	pGBKT7 [EcoRI/SalI]
hDlg$_{\text{PDZIII}}$-pGBKT7	JH100	hDlg$_{\text{PDZIII}}$ [EcoRI/SalI]	pGBKT7 [EcoRI/SalI]
Kv1.4$_{\text{cyto}}$-pGBKT7	JH101	Kv1.4$_{\text{cyto}}$ [EcoRI/SalI]	pGBKT7 [EcoRI/SalI]
hDlg$_{\text{PDZI-II}}$-pGADT7	JH102	hDlg$_{\text{PDZI-II}}$ [EcoRI/SalI]	pGADT7 [EcoRI/XhoI]
hDlg$_{\text{PDZIII}}$-pGADT7	JH103	hDlg$_{\text{PDZIII}}$ [EcoRI/SalI]	pGADT7 [EcoRI/XhoI]
Kv1.4$_{\text{cyto}}$-pGADT7	JH104	Kv1.4$_{\text{cyto}}$ [EcoRI/SalI]	pGADT7 [EcoRI/XhoI]
Kv1.3$_{\text{cyto}}$-pGBKT7	JH105	Kv1.3$_{\text{cyto}}$ [EcoRI/SalI]	pGBKT7 [EcoRI/SalI]
Kv1.3$_{\text{cyto}}$-pGADT7	JH106	Kv1.3$_{\text{cyto}}$ [EcoRI/SalI]	pGADT7 [EcoRI/XhoI]
hCD8-GFP-Kv1.3cyto-pmhcP	JH77	hCD8-GFP-Kv1.3cyto [NheI, EcoRI, Xba]	pmhcP [NheI]
Kvβ2-pCMVSPORT6 (from imaGenes)	–	Kvβ2	pCMVSPORT6
Kv1.3-EGFP$_{485}$	JH73	Kv1.3$_{\text{TM}}$-EGFP-Kv1.3$_{\text{C-term}}$	[NheI/NheI–XhoI/SalI]
Kv1.3-EGFP$_{510}$	JH107	Kv1.3$_{\text{TM}}$-EGFP-Kv1.3$_{\text{C-term}}$	[XbaI/NheI–XhoI/SalI]
Kv1.3-EGFP$_{555}$ ('Kv1.3-EGFP')	JH111	Kv1.3$_{\text{TM}}$-EGFP-Kv1.3$_{\text{C-term}}$	[XbaI/NheI–XhoI/SalI]
Kv1.3-pCDNA3.1	JH119	full length Kv1.3 [BamHI / SalI]	pCDNA3.1 Mammalian Expression Vector [BamHI / XhoI]
Kv1.3-mRFP	RP25	Kv1.3-EGFP$_{1670}$ tagged with HA @ '814'	pEGFP-C2
Kv1.3-EGFP$_{\text{WSGG}}$	JH170	rKv1.3 c-terminus [BglII / SalI]	Kv1.3-EGFP [BglII / SalI]
Kv1.3$^{\text{HA}}$-pCDNA3.1	RP19	full length Kv1.3 tagged with HA @ '814'	pCDNA3.1
Kv1.3$^{\text{HA}}$-EGFP	RP21	Kv1.3-EGFP$_{1670}$ tagged with HA @ '814'	pEGFP-C2
Kv1.3$^{\text{HA}}$-EGFP$_{\text{WSGG}}$	RP23	Kv1.3-EGFP$_{1670}$ tagged with HA @ '814'	pEGFP-C2

Construct Name	Construct Token	Insert	Vector Backbone
Kv1.3$^{\text{HA}}$-mRFP	RP26	Kv1.3-EGFP$_{1670}$ tagged with HA @ '814'	pEGFP-C2
Kv1.3$^{\text{HA}}$-mRFP$_{\text{WSGG}}$	RP27	Kv1.3-EGFP$_{1670}$ tagged with HA @ '814'	pEGFP-C2
PSD-95 – EGFP [Craven et al., 1999]			
EGFP–Dlg1 (gift from Dr. T. Hanada)			
Kv1.3-V$_{\text{N}}$155-pCMV	JH158	V$_{\text{N}}$155-HA [NheI/BglII]	Kv1.3-pCMV [NheI/BglII]
Kv1.3-V$_{\text{N}}$173-pCMV	JH159	V$_{\text{N}}$173-HA [NheI/BglII]	Kv1.3-pCMV [NheI/BglII]
Kv1.3-V$_{\text{C}}$156-pCMV	JH160	V$_{\text{C}}$156-HA [NheI/BglII]	Kv1.3-pCMV [NheI/BglII]
hDlg[825-V$_{\text{N}}$155]	JH161	V$_{\text{N}}$155-HA [NheI/NheI]	pCMV [NheI/BglII]
hDlg[825-V$_{\text{N}}$173]	JH162	V$_{\text{N}}$173-HA [NheI/NheI]	pCMV [NheI/BglII]
hDlg[825-V$_{\text{C}}$156]	JH163	V$_{\text{C}}$156-Myc [NheI/NheI]	pCMV [NheI/NheI]
hDlg[1460-V$_{\text{N}}$155]	JH164	V$_{\text{C}}$155-Myc [NheI/NheI]	pCMV [NheI/NheI]
hDlg[1460-V$_{\text{N}}$173]	JH165	V$_{\text{N}}$155-Myc [NheI/NheI]	pCMV [NheI/NheI]
hDlg[1460-V$_{\text{C}}$156]	JH166	V$_{\text{C}}$155-Myc [NheI/NheI]	pCMV [NheI/NheI]
hDlgshRNA$_{1668}$-pZoffmCherry	JH129	annealed oligonucleotides 1668BglIIfw and 1668HindIIIrev [BglII/HindIII]	pZoffmCherry [BglII/HindIII]
hDlgshRNA$_{2757}$-pZoffmCherry	JH130	annealed oligonucleotides 2575BglIIfw and 2575HindIIIrev [BglII/HindIII]	pZoffmCherry [BglII/HindIII]
hDlgshRNA$_{115}$-pZoffmCherry	JH132	annealed oligonucleotides 115BglIIfw and 115HindIIIrev [BglII/HindIII]	pZoffmCherry [BglII/HindIII]
PSD95shRNA$_{682}$-pCMS4	JH178a	annealed oligonucleotides 682BglIIfw and 682HindIIIrev [BglII/HindIII]	pCMS4 [BglII/HindIII]
PSD95shRNA$_{1548}$-pCMS4	JH179a	annealed oligonucleotides 1548BglIIfw and 1548HindIIIrev [BglII/HindIII]	pCMS4 [BglII/HindIII]

Construct Name	Construct Token	Insert	Vector Backbone
PSD95shRNA$_{1764}$-pCMS4	JH182a	annealed oligonucleotides 1764BglIIfw and 1764HindIIIrev [BglII/HindIII]	pCMS4 [BglII/HindIII]
Kv1.3^{HA}-mRFP [IRESPuroR]-FUGW	JH206	Kv1.3^{HA}-mRFP [BamHI/SacII–XhoI] [IRESPuroR] (CF)	FUGW [BamHI/XhoI] [BspEI]
Kv1.3^{HA}-mRFP$_{WSGG}$ [IRESPuroR]-FUGW	JH207	Kv1.3^{HA}-mRFP$_{WSGG}$ [BamHI/SalI–XhoI] [IRESPuroR] (CF)	FUGW [BamHI/XhoI] [BspEI]
Kv1.3^{HA}-mRFP$_{WSGG}$ [Dlg1 shRNA-H1]-FUGW	JH212	Kv1.3^{HA}-mRFP$_{WSGG}$ [BamHI/SalI–XhoI] [Dlg1 shRNA-H1] (CF)	FUGW [BamHI/XhoI] [BspEI]
Kv1.3^{HA}-mRFP$_{WSGG}$ [PSD-95 shRNA-H1]-FUGW	JH215	Kv1.3^{HA}-mRFP$_{WSGG}$ [BamHI/SalI–XhoI]	FUGW [BamHI/XhoI] [BspEI]

Publications

Dopamine-modulated recurrent corticoefferent feedback in primary sensory cortex promotes detection of behaviorally relevant stimuli.
Max Happel, Matthias Deliano, **Juliane Handschuh**, Frank Ohl;
Journal of Neuroscience, January 2014, 34(4):1234-47

RSK-mediated nuclear accumulation of the cold shock Y-box protein-1 controls proliferation of T-cells and T-ALL blasts.
Steffi Gieseler-Halbach, Stefan Meltendorf, Mandy Pierau, Soenke Weinert, Florian H. Heidel, Thomas Fischer, **Juliane Handschuh**, Ruediger C. Braun-Dullaeus, Martin Schrappe, Jonathan A. Lindquist, Peter R. Mertens, Ulrich Thomas, and Monika C. Brunner-Weinzierl;
Cell Death & Differentation (*in revision*)

Curriculum Vitae

Personal Data

Name:	Juliane
Family name:	Handschuh
Familiy status:	married
Kids:	3 (1 daughter [3 Years], 2 step daughters [10 and 13 Years])
Date if birth:	October 25$^{\text{th}}$ 1984
Place of birth:	Merseburg, Germany
Nationality:	German

Education

seit 1/2010	PhD student at the Leibniz Institute for Neurobiology, Magdeburg, Germany
	June 2012 - March 2013 maternal leave
11/2009 - 12/2009	Scientific assistant at Leibniz Institute for Neurobiology, Magdeburg, Germany
11/2008 - 10/2009	Diploma Thesis at the Leibniz Institute for Neurobiology, Magdeburg, Germany
	Degree: Diploma Biology, Grade: very good (1,2)
10/2007 - 07/2008	Scientific assistant in the Group Neuroprosthetics at the Leibniz Institute for Neurobiology, Magdeburg, Germany
10/2006 - 07/2008	Graduate studies Neurobiology: Otto-von-Guericke University Magdeburg
10/2004 - 09/2006	Basic studies Biology: Martin-Luther University Halle
06/2004	University entrance diploma / Abitur: Novalis-Gymnasium Bad Dürrenberg (Grade: 1,7)

Declaration

Juliane Handschuh

Arndtstraße 11

39108 Magdeburg

Email: Juliane.Handschuh@gmail.com

I hereby declare that the dissertation entitled

The Interaction of Kv1.3 with Dlg-like MAGUKs and its Impact on Calcium Signaling in Activated T Cells

is my own unaided work. All direkt or indirect sources used are acknowledged as references.

I further declare that this work has not been used as a dissertation, nor did I submit this or another work to another institution for the award of the academic degree doctor rerum naturalium (Dr. rer. nat.).

Magdeburg, June 21 _____

Acknowledgements

During the course of my work, a number of people helped me in various ways. Therefore, I would like to thank:

First and foremost, my supervisor in the lab, Dr. Ulrich Thomas. Thank you for judging me to be capable of starting a whole new project in your *Drosophila melanogaster* neurogenetic lab. Sometimes I cursed you for that, but eventually I did learn a lot during that time. Who needs a project that has everything already laid out in front, right?! Thanks for always advising me during my many attempts to get the experiments in this project started. Also, I would like to thank you for the friendly atmosphere you generated in the lab (and office) and for keeping me well candied throughout the years.

Profs. Eckart Gundelfinger and Michael Naumann for letting me be part of the GRK1167, which allowed me not only to visit topic-related lectures and take part in annual retreats to discuss my project with the fellow students. It also allowed me to partake in certain aspects of scientific organization tasks, which lead me to pursue an occupation in that field.

Kathrin Gruss for careful and routine support in the lab, especially for following my special requests with heterologous cell cultures. Also a huge thank you for the other technicians in the department who kept this place running so well.

Isabel Herbert for sitting my Lab-Babies, i.e. stably expressing Jurkat T cell lines when I was not around. Also, the students in the lab who helped me with cloning work during their lab rotations or thesis work (Mehul Ghautam, Rebecca Pötzschke and Jonas Happel)

Dr. Martin Heine for introducing me to imaging methods like Quantum Dot and Fura-2 Calcium Imaging and discussing data, which now make up a great part of this work.

Dr. Stefanie Kliche et al. for giving me orientation in working with T cells and always giving me a good time while staying at your institute (especially Anke Ramonat).

Oliver Kobler for helping with everything that concerns imaging, be it confocal imaging or analysis of microscope pictures. Also, for being my partner in crime in handling Ulrich.

The former and current fellow students in the department of neurochemistry for the good atmosphere and help with methodological questions as well as motivational lows (you know who you are, but in case you don't: Ana Dinca, Carina Fürst (!!!!!!!), Rebecca Pötschke, Isabel Herbert, Barbara Schweitzer, Romy Schneider, Dani Ivanova, Maru Andres Alonso, Sandra Fienko and, since he is still a young student at heart, Renato Frischknecht).

Tea, for keeping me awake and concentrated (You drink coffee, I drink tea my dear; Sting 1987).

All of the musicians for making my daily lab life easier with your work, especially Kanye

West, Bon Iver, Michael Jackson, Amy Winehouse, Bill Withers, Sixto Rodriguez, Aloe Blacc, Coldplay, The Police, Common, Jack Garratt, AnnenMayKantereit, Marteria, Samy Deluxe, Max Herre, Joy Denalane, Jack Johnson, Jose Gonzales, Otis Redding, Ray Charles, and many more

My family. My (step-)parents for always supporting me in what I did even though it may have been hard to comprehend at times. My three kids, Johanna, Phili and Lina for positive distraction from my every day work life. I am looking forward to spending much more time with you once I am done with this.

Ultimately, the biggest piece of the thank-you-cake is dedicated to my very best friend, my lover and husband, Dr. Max Happel. Thanks for always putting up with my bullshit, and my stupid, below the beltline jokes. Music sounds better with you (Stardust, 1998) and love never felt so good (Jackson M., 1983).